

GEOSEISMIC MODELING STUDY OF
THE MORROW FORMATION IN
EASTERN DEWEY COUNTY,
OKLAHOMA

By

YUSUF BIYIKOGLU

Bachelor of Science
University of Istanbul
Istanbul, Turkey
1974

Master of Science
University of Istanbul
Istanbul, Turkey
1981

Submitted to the Faculty of the
Graduate College of the
Oklahoma State University
in partial fulfillment of
the requirement for
the Degree of
MASTER OF SCIENCE
May, 1988

Thesis
1988
B624g
Cop. 2

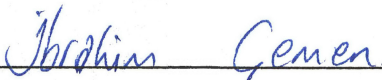


GEOSEISMIC MODELING STUDY OF
THE MORROW FORMATION IN
EASTERN DEWEY COUNTY,
OKLAHOMA

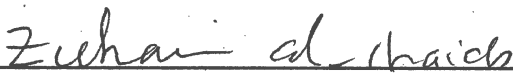
Thesis Approved:



Thesis Adviser



Ibrahim Cemen



Zuhair al-Haich



Dean of the Graduate College

ACKNOWLEDGMENTS

All praise is due to Allah, whose guidance and help made the realization of this work possible.

I wish to express my sincere appreciation to all the people who assisted me with this study. I am especially indebted to my major advisor, Dr. Douglas C. Kent, who suggested this topic, provided the software and the hardware used in this study, and offered his professional and personal guidance throughout this study and my entire graduate program. Special thanks is also extended to the other committee members, Dr. Ibrahim Cemen and Dr. Zuhair Al-Shaieb, for their advice and assistance in this study.

I would also like to thank my close friend Rajeev L. Dwivedi for his moral support. In addition, I extend my gratitude to Kimberly Gillette for her support and her help in editing and preparing the final manuscript.

I would like to express my sincere gratitude to my sponsor, the King Faisal Foundation in Riyadh, Saudi Arabia, for sending me to the U.S. to complete my higher education.

My wife, Sadiye, and daughters, Melek and Bilge, are especially appreciated for their encouragement, companionship, and help in my finding the time to write.

Finally, I wish to express my deepest gratitude and appreciation to my father, Kemal Biyikoglu, who died before seeing my graduation, my mother, Nadire Biyikoglu, my uncle, Gunduz Sevilgen, and my mother-in-law, Murvet Gocen, for their blessings, prayers, and encouragement during my studies abroad.

TABLE OF CONTENTS

Chapter	Page
I. INTRODUCTION.	1
II. SEISMIC MODELING.	6
III. GEOLOGIC OVERVIEW	18
IV. METHODOLOGY	26
Log Assist	26
Synthetics Plus.	27
Step	27
Seismic Modeling System II	28
Model Site Selection	30
Acoustic Stratigraphy.	30
Modeling Procedures.	31
V. MODEL APPLICATIONS.	34
Sensitivity Analysis	34
Geary Field Model.	40
Synthetic Seismograms.	40
Two-Dimensional Models	47
Eastern Dewey County Model	49
VI. SUMMARY & CONCLUSIONS	61
REFERENCES	65
APPENDIXES	69
APPENDIX A - GEOLOGIC MODEL FOR GEARY FIELD AND ITS SEISMIC RESPONSE FOR DIFFERENT FREQUENCIES.	70
APPENDIX B - LIST OF LOGS AND SYNTHETIC SEISMOGRAMS FOR EASTERN DEWEY COUNTY	75
APPENDIX C - INTERPOLATED LOG SECTIONS AND TWO-DIMENSIONAL SYNTHETIC SEISMIC MODELS FOR CROSS SECTIONS A1-A2 THROUGH F1-F2	79

APPENDIX D - OVERVIEW OF BASIC SEISMIC PRINCIPLES	86
--	----

LIST OF TABLES

Table	Page
<p>I. File, Company, and Well Names Used to Construct Geologic Cross Sections of Eastern Dewey County</p>	76
<p>II. Factors Affecting Seismic Amplitudes.</p>	99

LIST OF PLATES

Plate
<p>1. Stratigraphic Cross-Section A1-A2 Geary Field, Canadian County, Oklahoma . . . in pocket</p>
<p>2. Stratigraphic Cross-Section A1-A2 Eastern Dewey County, Oklahoma in pocket</p>
<p>3. Stratigraphic Cross-Section B1-B2 Eastern Dewey County, Oklahoma in pocket</p>
<p>4. Stratigraphic Cross-Section C1-C2 Eastern Dewey County, Oklahoma in pocket</p>
<p>5. Stratigraphic Cross-Section D1-D2 Eastern Dewey County, Oklahoma in pocket</p>
<p>6. Stratigraphic Cross-Section E1-E2 Eastern Dewey County, Oklahoma in pocket</p>
<p>7. Stratigraphic Cross-Section F1-F2 Eastern Dewey County, Oklahoma in pocket</p>

LIST OF FIGURES

Figure	Page
1. Two-dimensional Modeling Procedure.	2
2. Seismic Model Showing the Similarity Between Two Different Subsurface Features	3
3. Index Map of Oklahoma Showing Locations of the Study Areas.	5
4. Characteristics of Seismic Models	8
5. Construction of a Synthetic Seismogram.	9
6. Methodology for Generating a Two-dimensional Seismic Model	11
7. Ray Trace Modeling.	13
8. Schematic Relationship Between Wavefronts and Rays.	14
9. Wavefront Propagation and Huygens' Principle.	16
10. Total Morrow Isopach.	20
11. Computer-generated Isopach Map of the Morrow Formation Based on Bentkowski, 1985	21
12. Impact of Changing Geology on Reflections	23
13. Principal Major Pennsylvanian Structural Features of the Southern Midcontinent	24
14. Type Log of the Morrow Formation in the Study Area.	25
15. Flow Chart Utilized in this Modeling Study.	29
16. a) Geologic Model for Tuning Thickness.	35
b) Seismic Response of the Geologic Model for Gas Saturated Sand Wedge	36
c) Seismic Response of the Geologic Model for Oil Saturated Sand Wedge	37
d) Seismic Response of the Geologic Model for Brine Saturated Sand Wedge	38

17.	Reference Map Showing Cross Section A1-A2, Seismic Lines, and Wells Used to Construct the Cross Section in Geary Field	41
18.	Synthetic Seismogram for Well Cruse #1, Geary Field.	42
19.	Synthetic Seismogram for Well Leck #1, Geary Field.	43
20.	Comparison of Synthetic Seismogram for Well Cruse #1 with Seismic Line 383, Going Through the Well	45
21.	Comparison of Synthetic Seismogram for Well Leck #1 with Seismic Line 383, Going Through the Well	46
22.	For Geary Field : a) Two-dimensional synthetic seismogram, b) Interpolated log section	48
23.	Comparison of Two-dimensional Synthetic Seismic Section and Line 383 Between Wells Cruse #1 and Robinson.	50
24.	Reference Map Showing Cross Sections from A1-A2 to F1-F2, and Wells Used to Construct the Cross Sections in Eastern Dewey County	51
25.	Synthetic Seismogram for Well Blain Simon #1	52
26.	Geologic Model for Cross Section A1-A2, and its Seismic Response, Eastern Dewey County	55
27.	Geologic Model for Cross Section B1-B2, and its Seismic Response, Eastern Dewey County	56
28.	Geologic Model for Cross Section C1-C2, and its Seismic Response, Eastern Dewey County	57
29.	Geologic Model for Cross Section D1-D2, and its Seismic Response, Eastern Dewey County	58
30.	Geologic Model for Cross Section E1-E2, and its Seismic Response, Eastern Dewey County	59
31.	Geologic Model for Cross Section F1-F2, and its Seismic Response, Eastern Dewey County	60
32.	The Geologic Model in Geary Field.	71
33.	Seismic Response of the Geologic Model for Frequency 40 Hz.	72

34.	Seismic Response of the Geologic Model for Frequency 60 Hz.	73
35.	Seismic Response of the Geologic Model for Frequency 80 Hz.	74
36.	Synthetic Seismogram for Well Addis #1	77
37.	Synthetic Seismogram for Well Prophet #1	78
38.	Interpolated Log Section and Two-dimensional Synthetic Seismic Model for Cross Section A1-A2 of Eastern Dewey County.	80
39.	Interpolated Log Section and Two-dimensional Synthetic Seismic Model for Cross Section B1-B2 of Eastern Dewey County.	81
40.	Interpolated Log Section and Two-dimensional Synthetic Seismic Model for Cross Section C1-C2 of Eastern Dewey County.	82
41.	Interpolated Log Section and Two-dimensional Synthetic Seismic Model for Cross Section D1-D2 of Eastern Dewey County.	83
42.	Interpolated Log Section and Two-dimensional Synthetic Seismic Model for Cross Section E1-E2 of Eastern Dewey County.	84
43.	Interpolated Log Section and Two-dimensional Synthetic Seismic Model for Cross Section F1-F2 of Eastern Dewey County.	85
44.	Particle Motion of Waves	88
45.	Snell's Law and Numerical Examples of Acoustic Impedance and the Reflection Coefficient	90
46.	Density-Velocity Relationship in Rocks of Different Lithology and Acoustic Impedance Graph.	93
47.	Schematic Graph Showing Seismic Visibility of a Unit	95
48.	Relationship Between Lithology Propagating Wavelet and Seismic Response	96
49.	Factors Which Affect Amplitude	98
50.	Variations in Amplitude Response Due to Changes in Pore Fluid	101

51.	a) Absorption b) Spherical Divergence	102
52.	Fresnel Zone	104
53.	a) Nomogram for Fresnel Zone Radii.	105
	b) Nomogram; Relationship Between Velocity, Frequency, and Wavelet	106
54.	Reflections from Sandstone Bodies of Varying Widths Expressed in Terms of the Width of the Fresnel Zone	108
55.	Zero-phase (Symmetrical) Normal (Positive), and Reverse (Negative) Wavelets.	109
56.	Widess Diagram Illustrating Limit of Vertical Resolution for a High Velocity Layer	111
57.	Limit of Vertical Resolution	112
58.	The Limit of Vertical Resolution for a Thin Bed Using Two Different Wavelets	113
59.	Seismic Response for Different Types of Bed Contacts	114
60.	Seismic Response of Sandstone with Gas Cap Using Three Different Wavelets	116
61.	Importance of Choosing the Wavelet	118
62.	Amplitude and Gain Control Sections.	119
63.	Major Groups of Reflection Configurations.	122

CHAPTER I

INTRODUCTION

Field seismic sections are not simple images of the subsurface geometry due to the complex behavior of the seismic sections. Interpretation can be very difficult, especially when the geology is complicated. One method to gain an understanding of the complex behavior of the seismic reflections is modeling, which consists of mathematical efforts to match the seismic responses that result from geological changes. Seismic modeling tests a geologic concept, analyzes the seismic response of the geologic concept, and produces synthetic seismic sections (May and Hron, 1978). Figure 1 shows a procedure for two-dimensional seismic modeling.

Over-simplified assumptions can lead to erroneous interpretations. If the geologic model does not fit real conditions, a computer model with the correct assumptions does not give the same or similar response. Obtaining identical seismic responses from highly different subsurface configurations is the other possibility (Figure 2) (McQuillin and others, 1984).

The index map of Oklahoma (Figure 3) shows the locations of the areas which were modeled. The first model

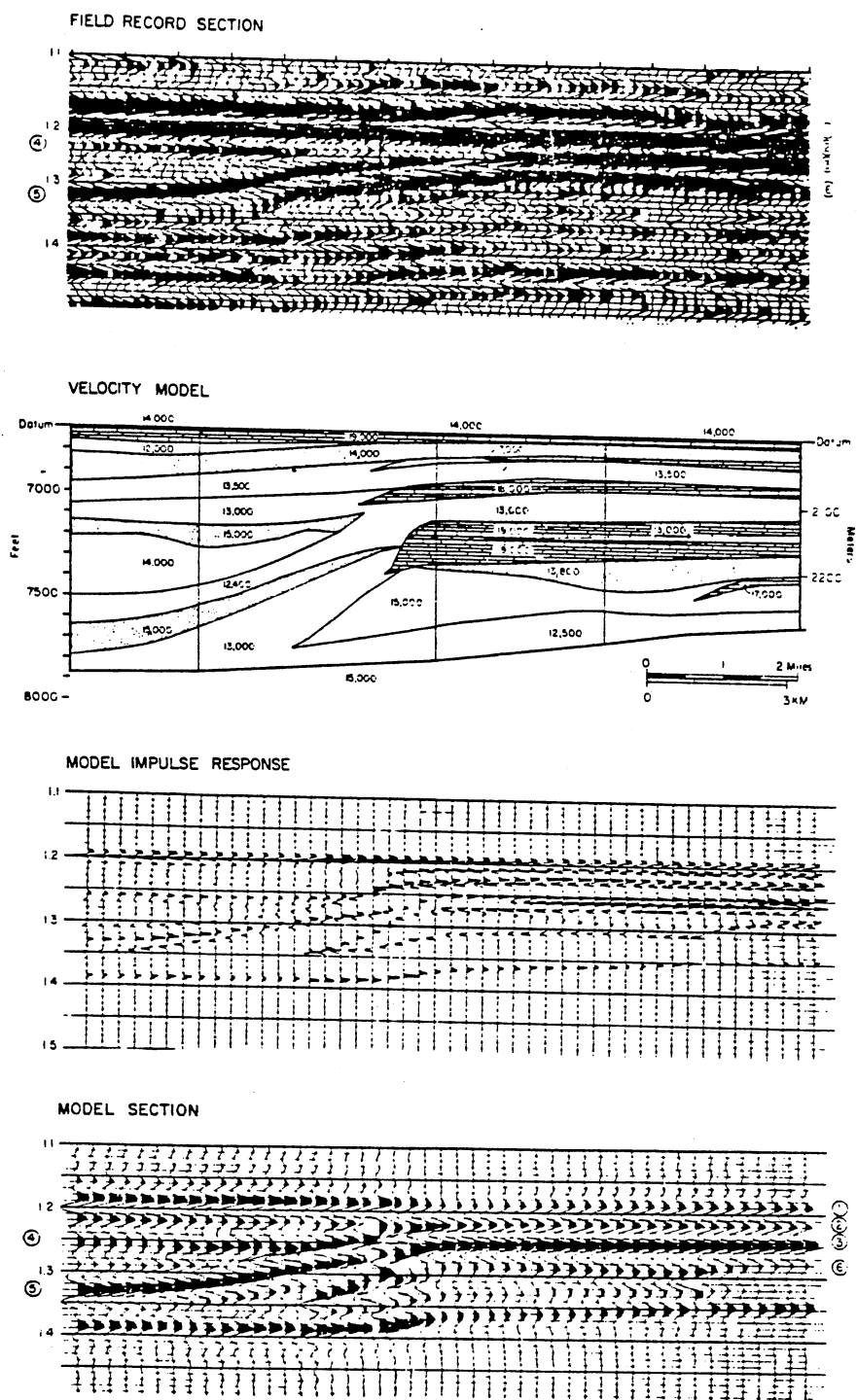


Figure 1. Two-dimensional Modeling Procedure:

- (1) Field record section
- (2) Development of geologic model
- (3) Calculation of impulse-response model
- (4) Convolution of the impulse-response model with the wavelet to obtain synthetic seismic section.

(After Galloway et. al. 1977)

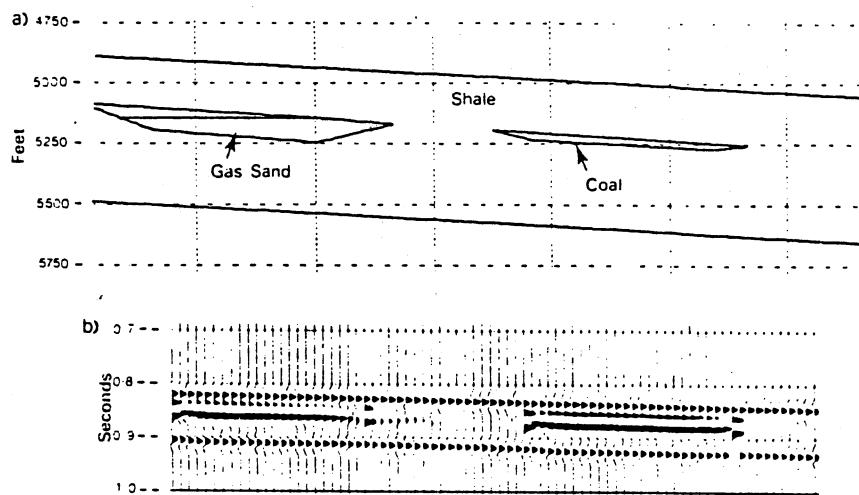


Figure 2. Seismic Model Showing the Similarity
Between Two Different Subsurface Features
(From McQuillin and others, 1984)

is of Geary Field, T13N-R10W, Canadian County, Oklahoma. The entire seismic stratigraphic investigation for this field is already completed (Clement, 1977). The reason for doing a modeling study in this field is to enable the calibration of the program and the choosing of the correct model parameters for the second model, Eastern Dewey County, Oklahoma. The second modeled area, Eastern Dewey County, contains sixteen adjacent townships T16N to T19N, R14W to R17W.

The objectives of this study are to investigate the Morrow Formation seismically and to present the results of seismic modeling study of the Morrow Formation in the eastern portion of Dewey County, Oklahoma. More specifically, the following has been determined: 1) Whether or not the Morrow Formation geometry produces a seismic anomaly, 2) The limit of vertical resolution for the Morrow Formation, 3) Whether or not the geologic models match the seismic sections. This will be accomplished using the Geosim Seismic Modeling programs package. The geologic data from which the seismic model is derived, Eastern Dewey County, has been very well documented by Bentkowski, 1985.

OKLAHOMA



Figure 3. Index Map of Oklahoma Showing Locations of the Study Areas

CHAPTER II

SEISMIC MODELING

Seismic modeling is a computational procedure which simulates seismic response of assumed subsurface geologic features. These features are defined in terms of all available geophysical and geological assumptions and information including interval properties such as density, velocity, and attenuation and other acoustically important parameters as well as interface geometry (Neidell, 1975).

Modeling is classified into two groups: 1) stratigraphic and 2) structural. Stratigraphic models are mathematical efforts to fit the seismic responses that would be generated from facies changes. In structural modeling the primary objective is subsurface geometry. Although many problems consist of members of both types of modeling, experience indicates that most modeling applications can be commonly regarded in one of these groups (Lindsey and Dedman, 1975-a).

Modeling is also divided into three classes, depending on the number of dimensions used: 1) one-dimensional, 2) two-dimensional, and 3) three-dimensional modeling. The one-dimensional model

(Figure 4-a) concerns vertical, straight ray paths, and assumes that each layer is horizontal and flat. A seismic wave penetrates the layers and returns to the geophone along the same vertical straight ray path. In order to obtain reflection character, the thickness, density, and velocity values of the layers are used. Synthetic seismograms are the most common example of one-dimensional modeling. To generate a synthetic seismogram, velocity and density values obtained from well logs and a propagating wavelet shape are used (Figure 5). One-dimensional synthetic seismograms obtained from one borehole log data set are used in distinguishing primary reflections from multiple reflections and in determining reflections with a particular interface. If the generated synthetic seismogram does not fit the real seismic section, the propagating wavelet shape can be changed until the best fit of the seismogram and the seismic section is achieved. Both the two and the three-dimensional models are used when geometric characteristics of the geologic section are of primary interest. If the stratigraphy does not change significantly in the horizontal direction, perpendicular to the spread, the two-dimensional model is used (Fig. 4-b) (Angona, 1960). Seismic ray paths are refracted across dipping boundaries. For the purpose of obtaining reflection character, the two-dimensional model uses thickness, density, velocity, and lateral distribution of the layers. Two-dimensional modeling requires the

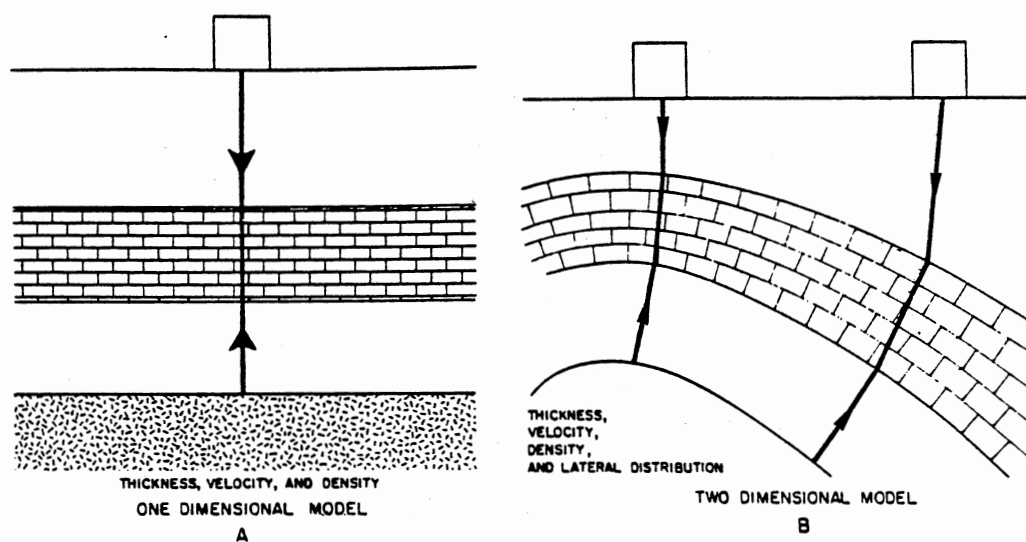


Figure 4. Characteristics of Seismic Models:
a) One-dimensional, b) Two-dimensional
(From Galloway and others, 1977)

LITHOLOGY

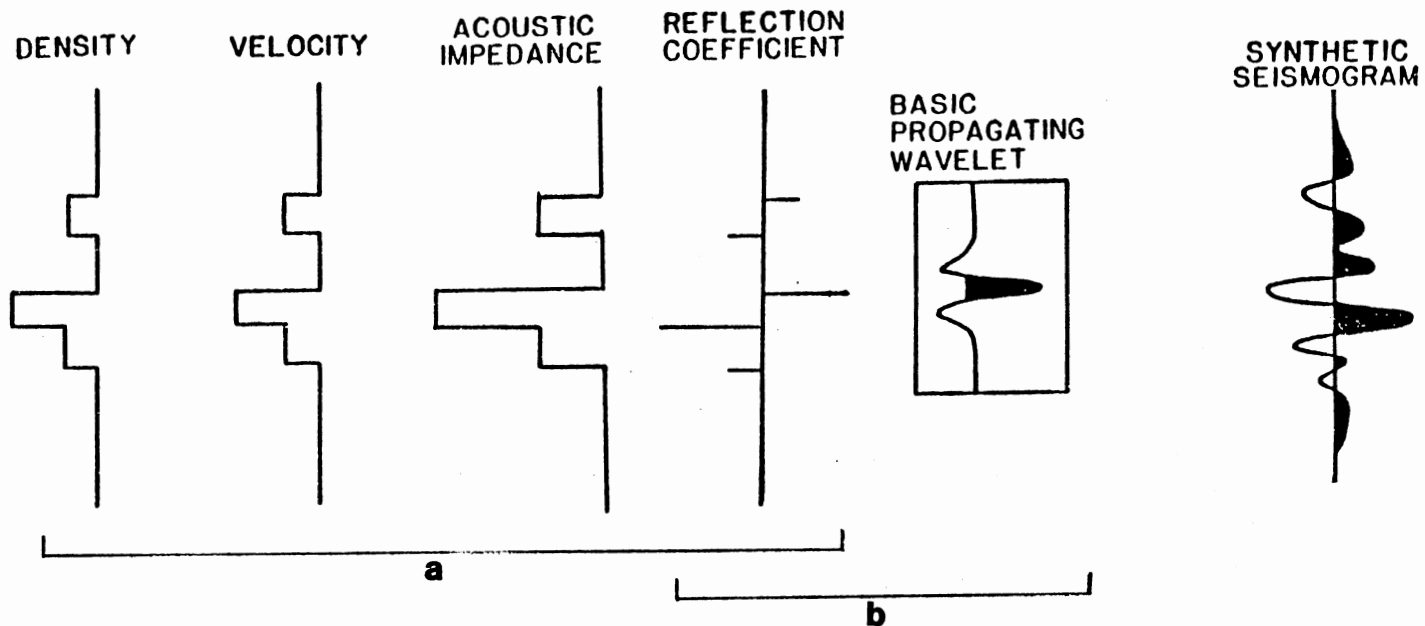
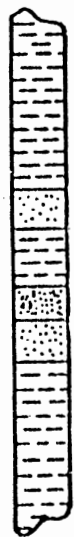


Figure 5. Construction of a Synthetic Seismogram:
 a) obtaining reflection coefficient by using the density and velocity values
 b) convolution of the reflection coefficient with the propagating wavelet and producing synthetic seismogram
 (After Dedman and others, 1975 and Hick, 1983)

construction of a geologic cross section in the plane of the seismic section with sufficient detail to reproduce the vertical and lateral distribution of seismic events (Galloway and others, 1977). Figure 6 shows the methodology for generating the two-dimensional model.

Seismic modeling is subdivided into two major types: 1) inverse and 2) forward (direct) modeling. Inverse modeling involves computing a possible model from the observation of the geophysical effects. It includes the whole interpretation process and always contains ambiguity and uncertainty. In forward modeling, the geophysical effects are calculated from the model and compared actual measured data. A single word, "modeling", often infers forward modeling (Sheriff and Geldard, 1985). Forward modeling can be accomplished by using physical and computer models and is a very useful tool for interpreting real seismograms and planning field data acquisition. In order to obtain a complete solution in complex geological structures, a combination of computer and physical modeling methods may be necessary. Physical modeling is well equipped to solve problems of wave propagation in complicated structures (Sheriff, 1985; Marhadi, 1983; and Liang, 1981). Physical modeling involves experiments in the laboratory with miniature physical models which must be geometrically, dynamically, and kinematically similar to the sections being modeled. Geometrical similarity is achieved by utilizing equal angles and proportional lengths

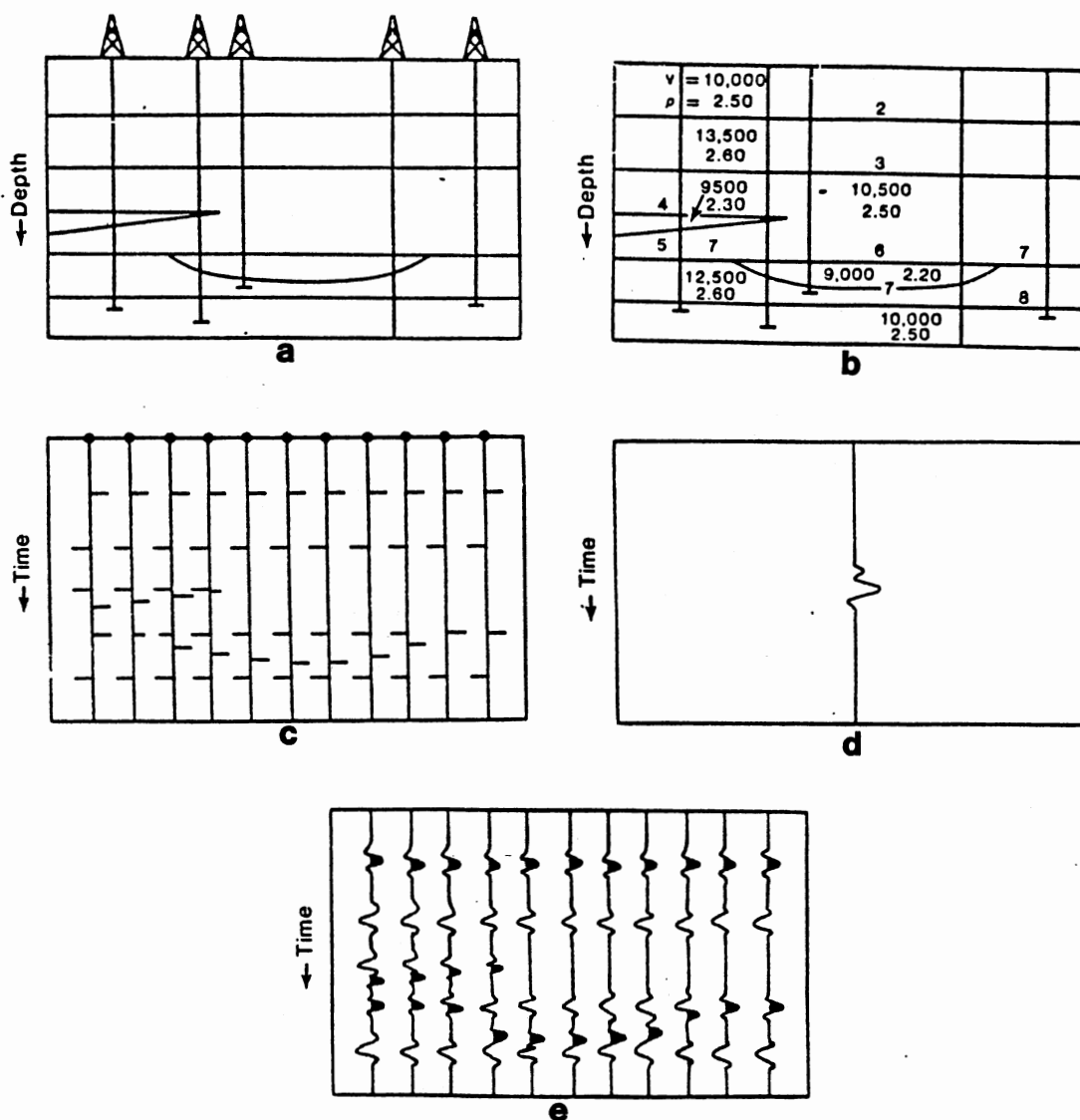


Figure 6. Methodology for Generating a Two-dimensional Seismic Model:

- Preparing geologic model
- Assigning velocity, density, and thickness values and layer numbers
- Impulse-response model, computing amplitude of seismic response, reflection coefficients, and transmission effects
- selecting a wavelet
- convolution of impulse-response model with wavelet, obtaining noise-free synthetic seismic section.

(After Ryder and others, 1981)

to those in the system. Dynamic similarity concerns the ratio of mass distribution whereas kinematic similarity concerns the ratio of times. The Poisson ratio, which is a dimensionless quantity, of the miniature physical model and the sections being modeled must have the same value (Sheriff, 1985). However, there are two major disadvantages of physical modeling: 1) it is almost impossible to construct a complete model, in large sections, without disturbing the geometric, dynamic, and kinematic analogies, and 2) building a complete model and performing the measurements is very time consuming (Meister and Dresen, 1987). Physical modeling has become less common, because of the disadvantages mentioned above, and has been replaced by Ray Trace modeling (Figure 7).

Rays are the paths and perpendiculars to the instantaneous wavefront (Figure 8). The ray trace theory assumes that a wavefront may be depicted by a few typical rays pointing in the direction of the propagation of energy. If this assumption fails, an inaccurate picture of the energy propagation results. Because one particular ray may not be a representative of the surrounding rays, it is necessary to use wave theory calculations (Lindsey and Dedman, 1975). Although the ray trace solution is an approximation, it is very helpful in determining which portions of complex two-dimensional structures can be expected to be seen on the seismic section, that is, to identify gross effects, and to help interpreters visualize

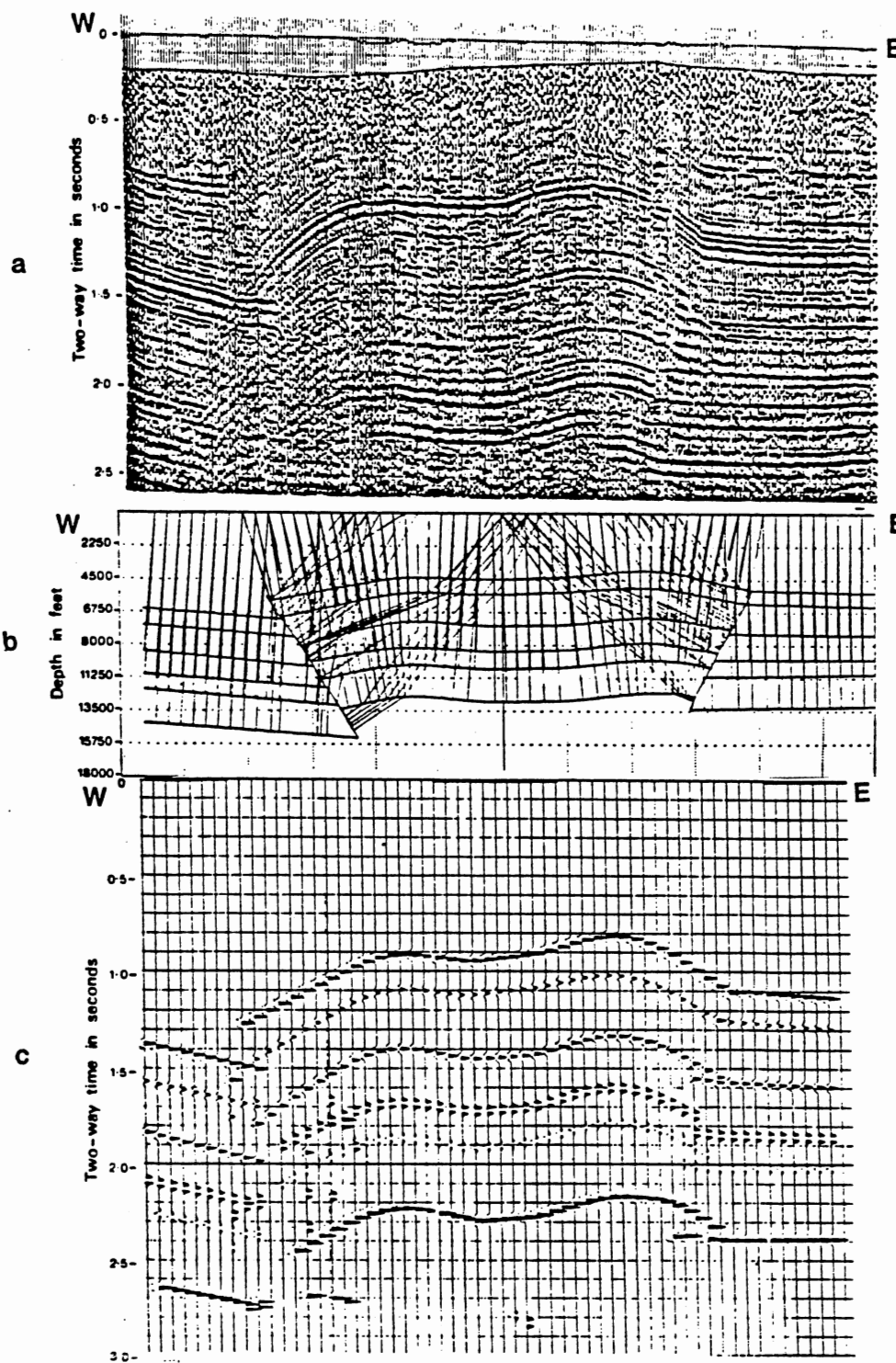


Figure 7. Ray Trace Modeling:
 a) Real seismic section
 b) Geologic model with computed ray paths
 c) Synthetic seismic section
 (From McQuillin and others, 1984)

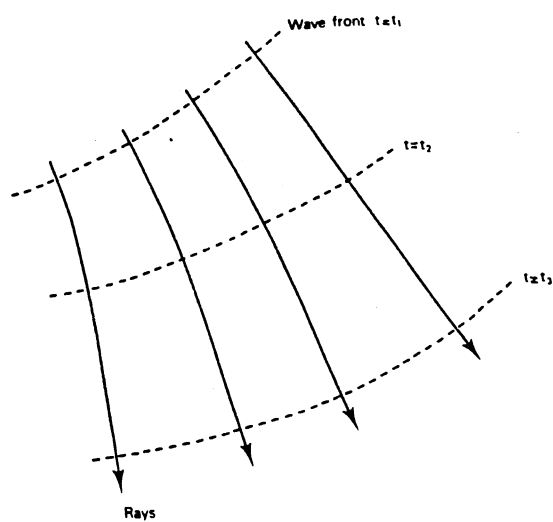


Figure 8. Schematic Relationship
Between Wavefronts
and Rays (From
McQuillin and others,
1984)

where recorded energy originates. A synthetic seismic section produced by ray tracing represents the main reflection alignments in very close places. However, the synthetic section also shows holes, blind zones, and breaks in continuity. On the real section, these are filled by diffractions and multiples (Anstey, 1977).

Wave theory is based upon the Huygens' Principle, which states that every point on a wavefront is the source of a new spherical wave (Figure 9-a). If the radii of the spherical waves are large enough, the waves can be treated as plane waves (Figure 9-b). The magnitude of reflection from each point on the boundary depends on both i , the inclination of the particle motion, and r , the distance from the source. If i equals zero degrees, the energy returned to the receiver is a maximum contribution. A 90 degree i angle, signifies that the propagation of the particle motion is parallel to the boundary, therefore, the energy contribution is minimum and is negligible. If the shape of the wavefront is similar to the geometry of the boundary, the reflected energy is focused on the same point by all points of the boundary, producing a strong reflection (Hicks, 1983).

At least partial answers to the following questions should be obtained from each model study:

- "1 - What is the probable geologic cause of the anomaly?
- 2 - What is the character of anomaly?

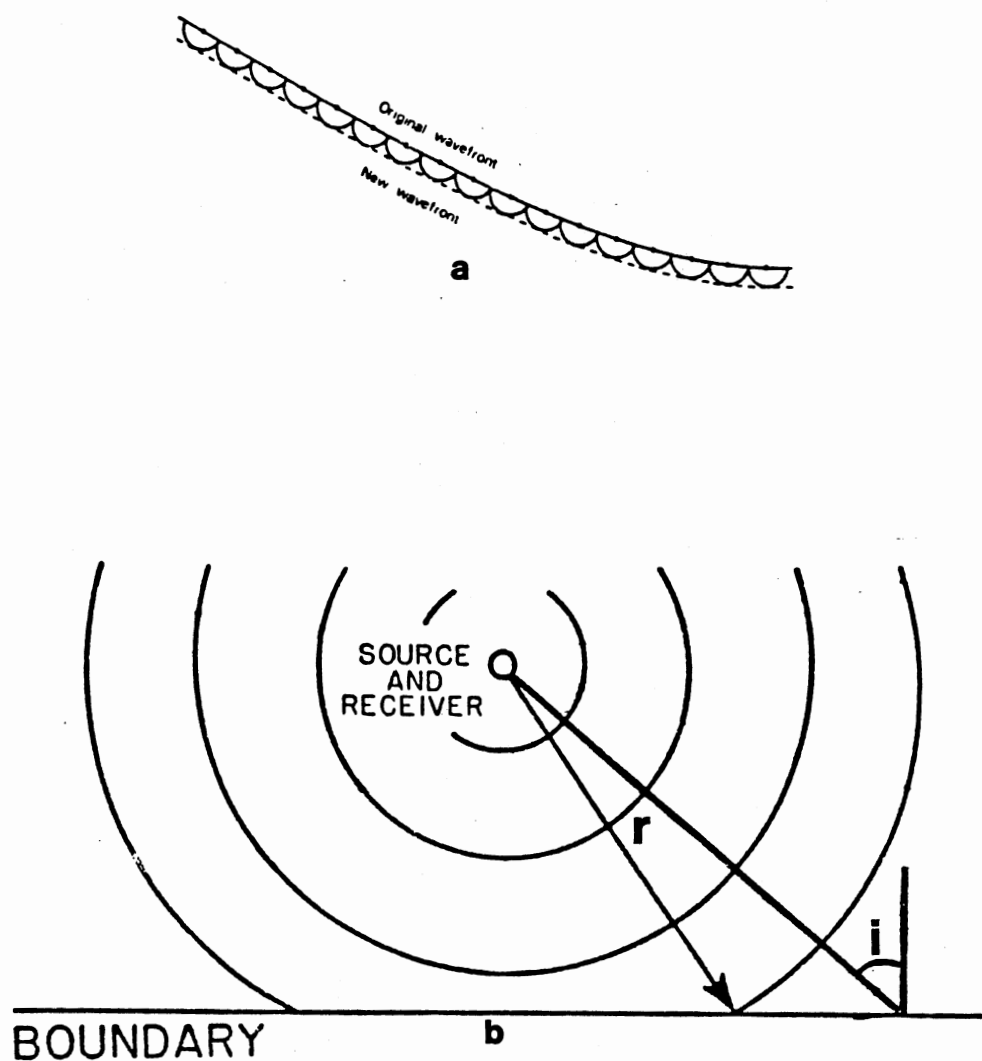


Figure 9. Wavefront Propagation and Huygens' Principle:
 a) Wavefront propagation according to Huygens' principle (McQuillin and others, 1984)
 b) A propagating wavefront illustrating Huygens' principle as applied to a reflection at an interface (After Hicks, 1983)

- 3 - Is a seismic anomaly associated with a given field?
- 4 - What is the probability that the given layers can be detected with field seismic data?" (Ryder and others, 1981).

CHAPTER III

GEOLOGIC OVERVIEW

Numerous papers dealing with the surface and subsurface geology of the Anadarko Basin have been published. South (1983) and Benthowski (1985) have reviewed the geology of Anadarko Basin in detail.

In the Anadarko basin, the early and middle Mississippian rocks are composed of fine grained cherty limestone and dolomite. The latest Chesterian (latest Mississippian) rocks are represented by carbonate in the north and black shale in the south (Benthowski, 1985). The Morrow Formation is classified as lower Pennsylvanian in age, and consists of a sequence of sandstone, shale, and thin limestone. These sediments unconformably overlay the Chesterian rocks. The upper boundary of the Morrow lies at the base of the Atokan Thirteen Finger Limestone which is composed of interbedded limestone and black shale (Benton, 1972).

The Morrow Formation is subdivided into two units: 1) the Upper Morrow and 2) the Lower Morrow. The Lower Morrow represents primarily marine deposition, whereas the Upper Morrow contains sediment deposited in a fluvial environment. The Lower Morrow is further divided into

eight depositional strikes of the sands which are labeled from the oldest, M1, to the youngest, M8 (Plates 2 to 7). M1 exists just outside of the area, to the southeast (Bentkowski, 1985).

At the time of the deposition of the Morrow, Anadarko Basin was basically flat. The eroded and faulted surface of the Chester had been filled by sediments. Today these sands are around 9000 feet deep below the surface (Halverson, 1987) and range in thickness from 50 to 1000 feet in the study areas.

The local structure is simple; the layers dip to the southwest and there are no major faults. The dip gradient to the southwest is between 17% and 2.9%. In the south-central section of the study area, the dip is steepest; whereas the dip is most gentle in the east-central region. An overview of the Morrow isopach (Figures 10 and 11) shows that the thickness of the isopach ranges from 53 feet in the northeast to 1023 feet in the southwest (Bentkowski, 1985).

Lane and Straka (1974) correlated the Springer beds with the Lower Morrow and proposed that the "usage of the term 'Springeran' as a visible subdivision of the lower Pennsylvanian be discontinued." Based on this statement, the term "Springer" has been eliminated within the study area and the entire interval between the bottom of Atoka and the top of Mississippian-Chesterian is now termed "Morrowan" (South, 1983, Bentkowski, 1985).

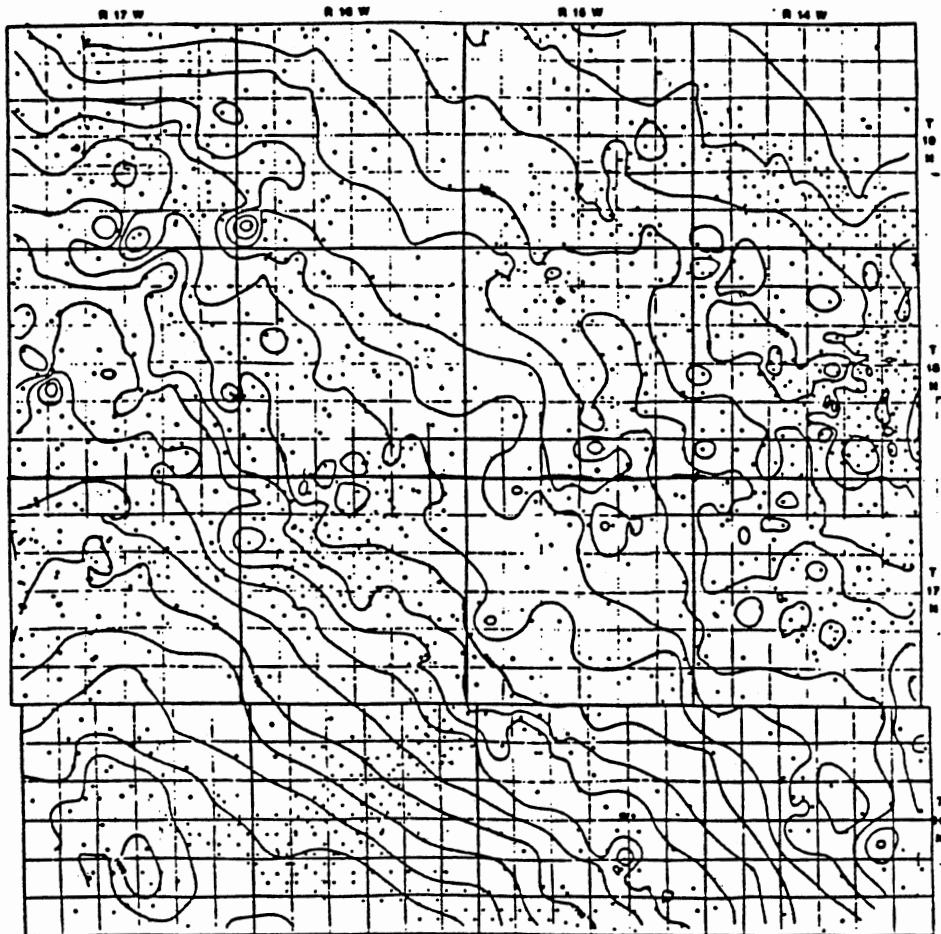


Figure 10. Total Morrow Isopach (From Bentkowski, 1985)

MORROW ISOPACH. EASTERN DEWEY COUNTY, OK

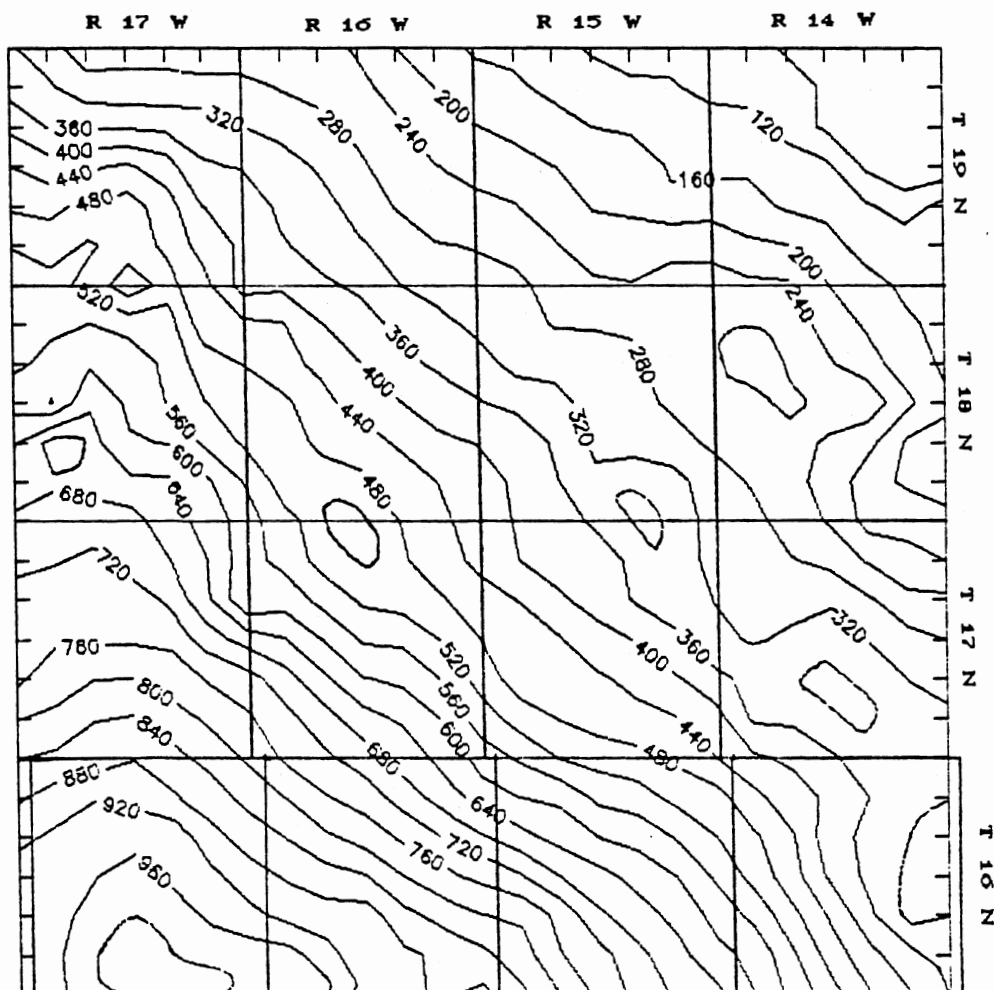


Figure 11. Computer-generated Isopach Map of the Morrow Formation Based on Bentkowski, 1985

The Morrow sands are encased within hundreds of feet of shale. The sonic and density logs indicate that the interval velocity of shale ranges from 9800 to 11500 ft/sec and the density varies from 2.4 to 2.55 gr/cm³; while the velocity of sand spans 13900 to 17000 ft/sec and has a density range of 2.4 to 2.65 gr/cm³. The velocity of Atoka and Parvin limestone varies from 18000 to 21500 ft/sec and its density has a range of 2.65 to 2.75 gr/cm³. These density and velocity contrasts result in good acoustic impedance contrasts. If the Morrow sands did not exist, the seismic energy would pass through the shale without reflection (Figure 12, ray paths A and B). However, the sand does exist and therefore reflects the seismic energy at the sand shale interfaces (Figure 12, ray path B) and thus will be shown as a reflector on the seismic section.

Deposition of Morrow sediments in the western Mid-Continent (Figure 13) was generally confined to the subsiding Anadarko and Ardmore Basins. Non-deposition controls the limits of the Morrow (Bentkowski, 1985).

Figure 14, a geologic column based on the gamma ray and resistivity logs, illustrates the Morrow and adjacent formations. A detailed stratigraphic correlation of the Morrow Formation was based on the interpolation of conventional wire-line logs.

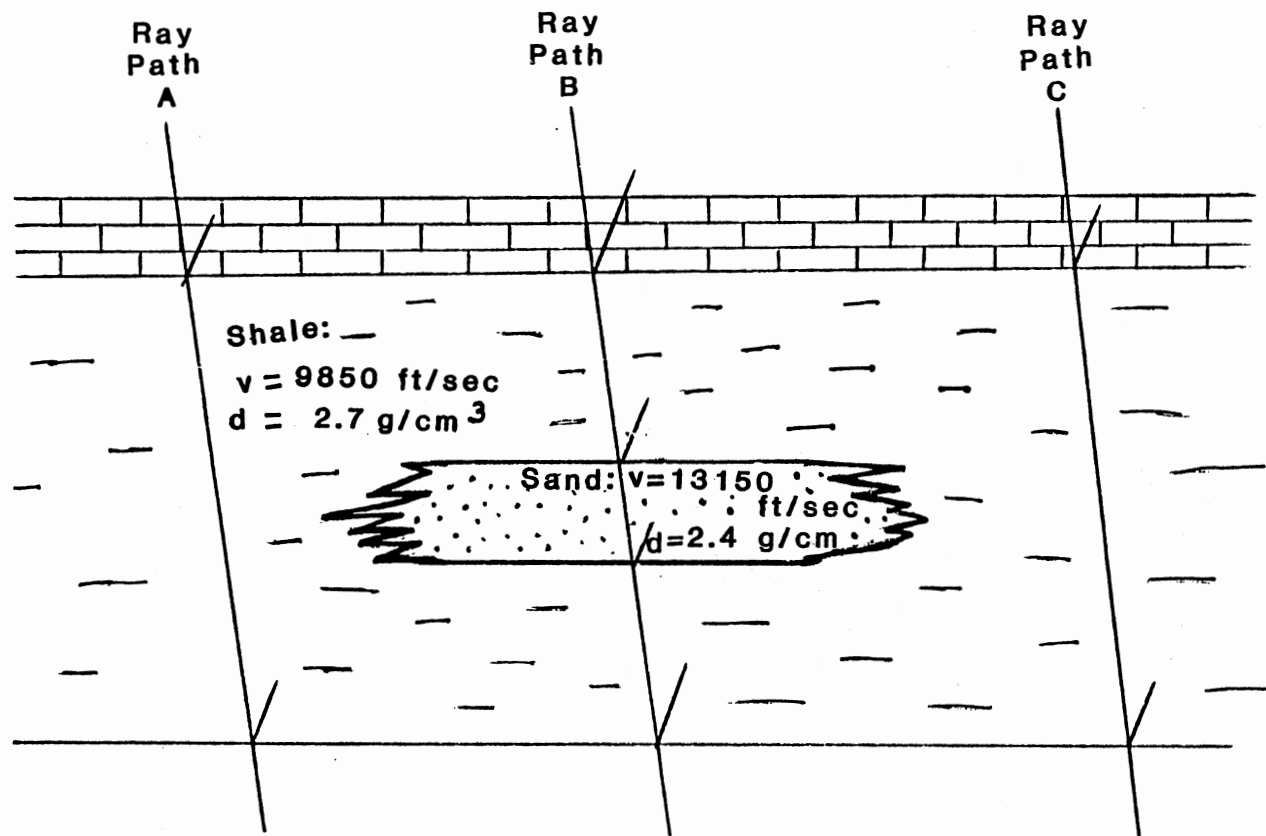


Figure 12. Impact of Changing Geology on Reflections

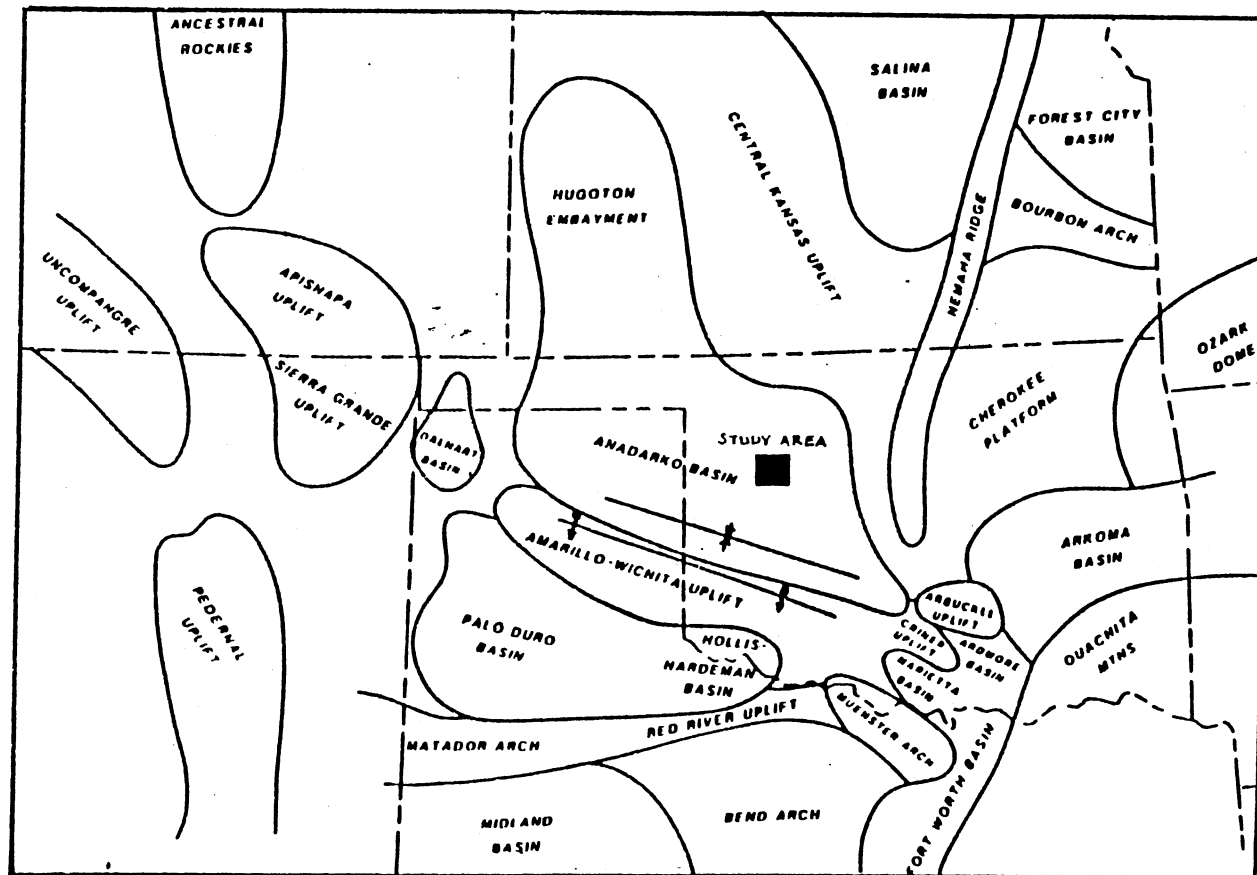


Figure 13. Principal Major Pennsylvanian Structural Features of the Southern Midcontinent (From Bentkowski, 1985)

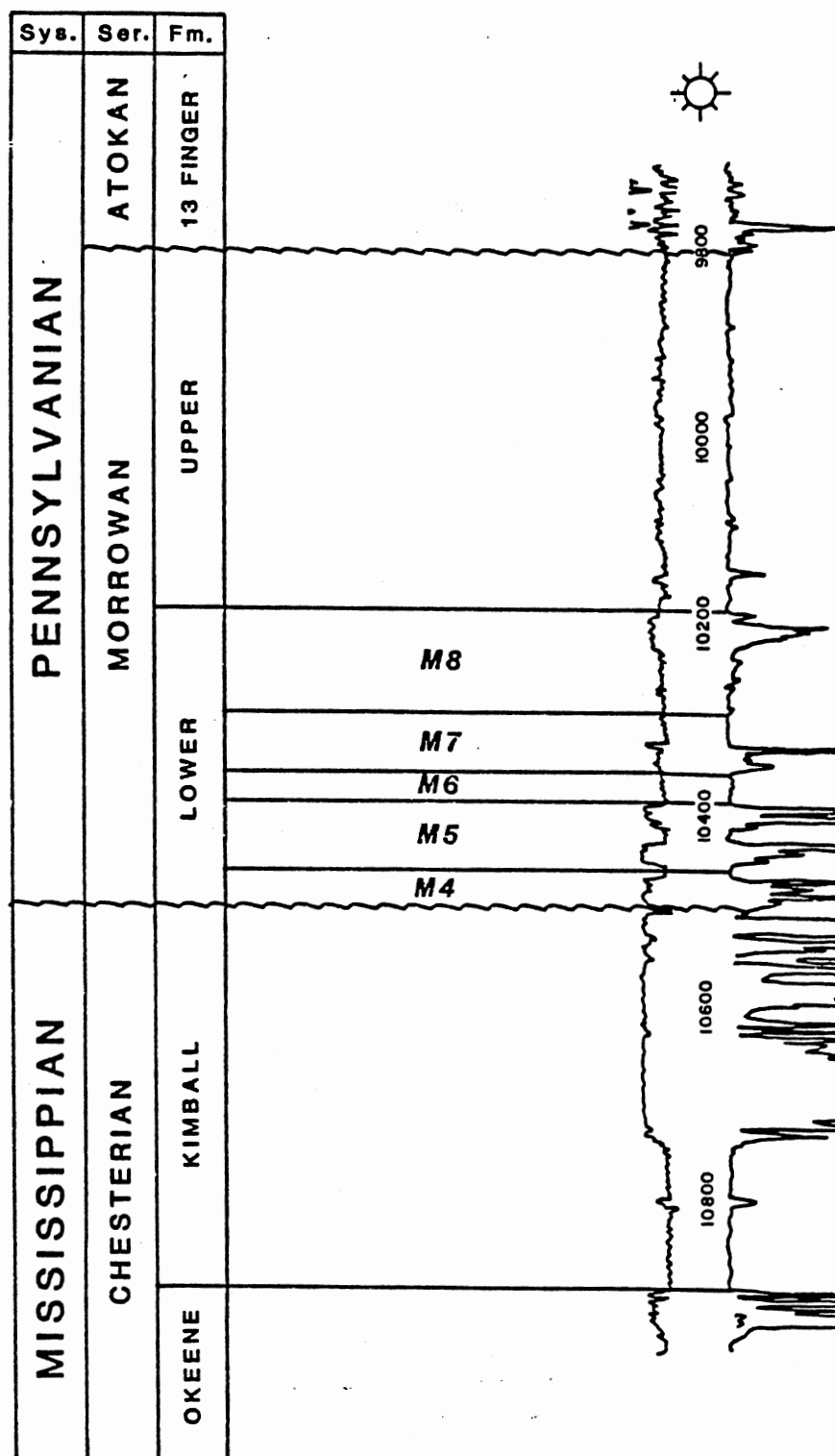


Figure 14. Type Log of the Morrow Formation in the Study Area (From Bentkowski, 1985)

CHAPTER IV

METHODOLOGY

The primary hardware required in this modeling study consists of a portable IBM-PC (or a system compatible with the IBM-PC) with an 8087 math co-processor, a color graphics card, a double disk drive system, a digitizer (MM1812 used), and Epson JX-80 and Okidata-Microline-193 printers.

The software utilized in this study is Geosim's seismic modeling software. This software includes four different programs: (1) Log Assist, (2) Synthetics Plus, (3) Step, and (4) Seismic Modeling System II with Ray Trace option.

Log Assist

Log Assist was designed to prepare log data for use in the other programs of the Geosim package. This program can be used to digitize, edit, convert, and print any log. It uses Faust's equation for converting data obtained from a resistivity log to a sonic log and Lindseth's and Gardner's equations for converting sonic logs to density or density logs to sonic. Faust's, Lindseth's, and Gardner's equations are generalized empirical relationships that may

or may not apply to the area selected to conduct seismic modeling. Many experiences indicate that these equations, which were derived from older rocks, are not applicable to younger rocks such as the ones found in the Gulf Coast. Before applying these equations to model the area, these empirical equations should be calibrated against the actual field data for formation velocity and density. Adjusting some of the constants in an equation will make it applicable to the area being worked (Geosim Manual, 1987).

Synthetics Plus

The primary function of Synthetics Plus is to generate one-dimensional synthetic seismograms from sonic, density, or both sonic and density logs. This program can be used to digitize wavelets as well as sonic and density logs and to generate and plot time-depth charts.

If only one of the two, density or sonic logs, is available, the program uses Gardner's or Lindseth's equation to create the second log. Then, it calculates the reflection coefficients and convolves them with a wavelet in order to obtain a synthetic seismogram (Geosim Manual, 1987).

Step

Step allows the utilization of density or sonic logs in building geologic models and in creating interpolated log sections as well as two-dimensional synthetic

seismograms from these interpolated log sections. Up to 30 layers and 50 logs can be used in one model (Geosim Manual, 1987).

Seismic Modeling System II

Seismic Modeling System II is used to build geologic models and to generate two-dimensional synthetic seismic sections using depth, velocity, and density data. This program employs ray-theory which is based on Snell's Law. The synthetic seismic section, created by Seismic Modeling System II, is noise free and utilizes vertical incidence ray paths. This section is directly comparable to migrated seismic data. The ray trace option creates normal incidence seismic sections which are comparable to unmigrated sections. The ray trace option (normal incidence) is very useful as an aid in solving complex structural problems (Geosim Manual, 1987). The procedure of the flow path utilized in this modeling study is shown in figure 15.

The effects of spherical spreading, short and long period multiples, diffracted events, inelastic attenuation, and random noise were not included in this study. Zero-phase wavelets were used because, as Schoenberger (1974) indicates, zero-phase wavelets have greater resolution capability than minimum-phase wavelets.

In the initial approach to seismic modeling of the Geary Field 40, 60, and 80 Hz symmetrical Ricker wavelets

GEARY FIELD

A) LOG
digitizing and
transforming logs

B) constructing
geologic model
(cross section)
determining
thickness values.

C) SYN PLUS
using sonic or density
logs. obtaining 1-D
synthetic seismic models

D) comparing with
actual seismic data,
if do not fit
calibrating models
by changing wavelet

E) STEP
using sonic or density
logs. obtaining 2-D
seismic sections
from log interpolations

F) SMS II
using B and velocity,
density, thickness values.
obtaining noise-free
2-D synthetic seismic
sections

G) comparing with E. if
do not fit calibrating
models by changing
velocity, density
values.

H) comparing E and F
with existing actual
seismic lines

EASTERN DEWEY COUNTY

I) LOG
digitizing and
transforming logs

J) constructing
geologic models
(cross sections)
determining
thickness values.

K) SYN PLUS
using sonic or density
logs. obtaining 1-D
synthetic seismic models
by using correct wavelet
from D

L) STEP
using sonic or density
logs. obtaining 2-D
synthetic seismic sections
from log interpolations

M) SMS II
using J . velocity
density values from F
thickness values from J

N) comparing L and M
if do not fit
calibrating M by
changing velocity,
density values.

COMPARING
N WITH G

Figure 15. Flow Chart Utilized in this Modeling Study

were used (Appendix A). Frequency of 80 Hz was chosen as the frequency value to be used for all further seismic modeling, as it provides the best results.

Normal incidence sections were also generated by using the ray trace option of the Seismic Modeling System II in the Geary Field study, however, these models did not differ from the vertical incidence models. Thus, the ray trace option was not used in the Eastern Dewey County model.

Model Site Selection

Previous investigations dealing with seismic modeling of the Geary Field, Canadian County, Oklahoma have been conducted by Clement (1977). Geosim Seismic Modeling software was applied to Geary Field for testing and calibrating the programs. Corrected model parameters (velocity, density, wavelet) were obtained and correlated with the available seismic data. The calibrated model parameters were then applied to the Eastern Dewey County test site where no real seismic data is available. Dewey county is approximately 8 miles northwest of Geary Field and has similar subsurface geology (Clement, 1977 and Bentskowski, 1985).

Acoustic Stratigraphy

Both Geary Field and Eastern Dewey County are abundant in well control. All wells in these areas have been logged with resistivity tools as well as with gamma ray,

spontaneous potential, and/or density and sonic tools (Clement, 1977 and Bentkowski, 1985).

Sandstone velocities, calculated from sonic logs, range from 14000 to 17000 ft/sec, depending on the type of cementation, shale content, and amount of porosity. Accompanying densities from logs span 2.4 to 2.6 gr/cm³. Shale velocities vary from 9800 to 11500 ft/sec, and their accompanying densities fall between 2.4 and 2.55 gr/cm³. The bracketing limestones have densities ranging from 2.65 to 2.75 gr/cm³, and velocities measuring 18000 to 21500 ft/sec (Clement, 1977).

The generalized acoustic stratigraphic model for the Morrow Formation in eastern Dewey County consists of an interval of 50 to 1000 feet and is bracketted, top and bottom, by one high velocity limestone, Atoka Limestone, and one quite low velocity shale, Mississippian-Chesterian Shale (Bentkowski, 1985). The Geary Field interval is 350 to 800 feet (Clement, 1977).

Modeling Procedures

The following modeling parameters were extracted from the geologic cross sections and their associated borehole logs: (1) density in gr/cm³, (2) velocity in ft/sec, (3) thickness in ft, and (4) geometry. These borehole logs, which consist of resistivity, gamma ray, density, and sonic logs, were digitized and input into the software. Generated synthetic sonic or density logs were also

obtained. Each geological model was constructed using a flat datum in order to remove structural dip.

All available resistivity, gamma ray, sonic, and density logs were digitized by using the Log Assist program and the Summagraphics MM1812 digitizer. Faust's equation was used by Log Assist to transform resistivity logs to sonic.

Faust's empirical relation between resistivity and sonic velocity, which was used as a default value in the program, can be stated as follows:

$$\text{Sonic Value} = 900 \times (\text{resistivity} \times \text{depth})^{\text{Exp } 0.16667}.$$

After several tests and comparisons between field sonic and computer-generated sonic logs, the constant value in Faust's equation was changed from 900 to 1400. In the process of converting sonic logs to density logs, the constant values in Gardner's equation remained unaltered.

Synthetic seismograms and digitized sonic, digitized density, or computer-generated sonic logs were used in the Synthetics Plus program to obtain one dimensional synthetic seismic sections. Then, the synthetic seismograms, which were obtained from Synthetics Plus, were compared with actual seismic lines. If the results of the comparison were negative, then the wavelet type or the frequency of propagating wavelet was changed. Thus, the correct wavelet type, which will be used in Step and Seismic Modeling System II, was selected.

As defined in the previous section, both Step and

Seismic Modeling System II create two-dimensional synthetic seismic sections. Step uses only sonic and density logs. The input of computer-generated or actual sonic and density logs into the Step program produced two-dimensional log interpolations. These interpolated logs were then convolved with the wavelet and two-dimensional synthetic seismic sections were obtained.

The depth, geometry, density, and velocity values, which were taken from the geologic cross sections and borehole logs, for each layer were loaded into the Seismic Modeling System II program. Two-dimensional vertical incidence and, using the ray trace option, two-dimensional normal incidence synthetic seismic sections were obtained. The ray trace option was used only in the Geary Field modeling study. These synthetic sections were then compared with actual seismic lines.

CHAPTER V

MODEL APPLICATIONS

Sensitivity Analysis

One concept that has direct relevance to the seismic expression of the Morrow Formation is tuning thickness. The dominant frequency and its corresponding wavelength placed the seismic response of the Morrow sands within the thin bed regime and below the tuning point where there is a direct relationship between the amplitude of reflection and the thickness of the sands (Halverson, 1987). The model in Figure 16-a illustrates the geologic model of a sand wedge, higher velocity, which is encased within a shale of lower velocity. The tuning thickness model was applied to the sand wedge present in the geologic model using gas, oil, and water saturation conditions. Figures 16-b, c, and d show the seismic responses to the geologic model under the various fluid saturation conditions. As the wedge becomes thinner, the reflections from the top and the base of the sand wedge merge together, resulting in a constructive interface between the two reflections. At the point where it becomes impossible to distinguish two different reflectors, the constructive interface is at its maximum; in other words, the amplitude is maximum at

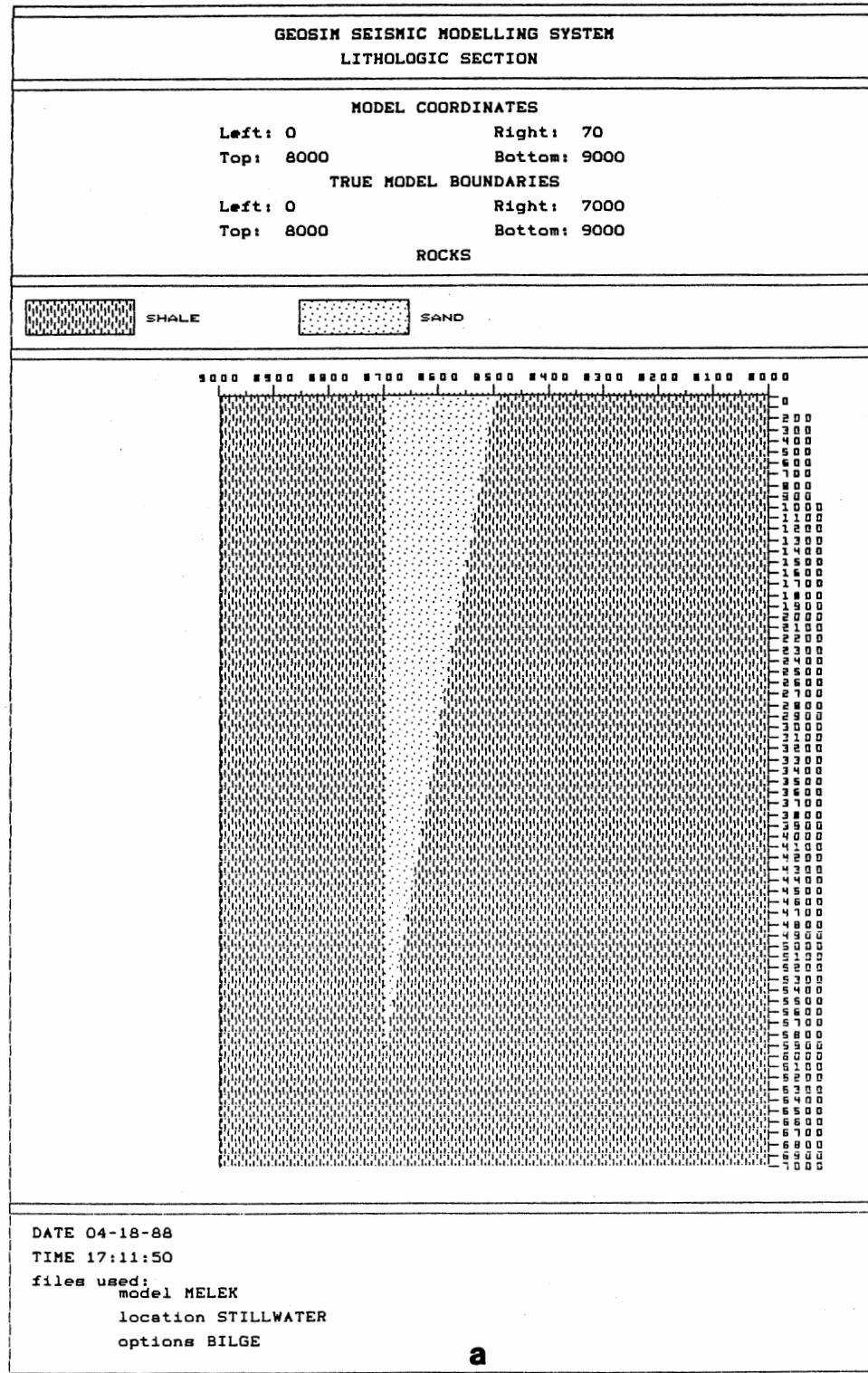


Figure 16-a. Geologic Model for Tuning Thickness

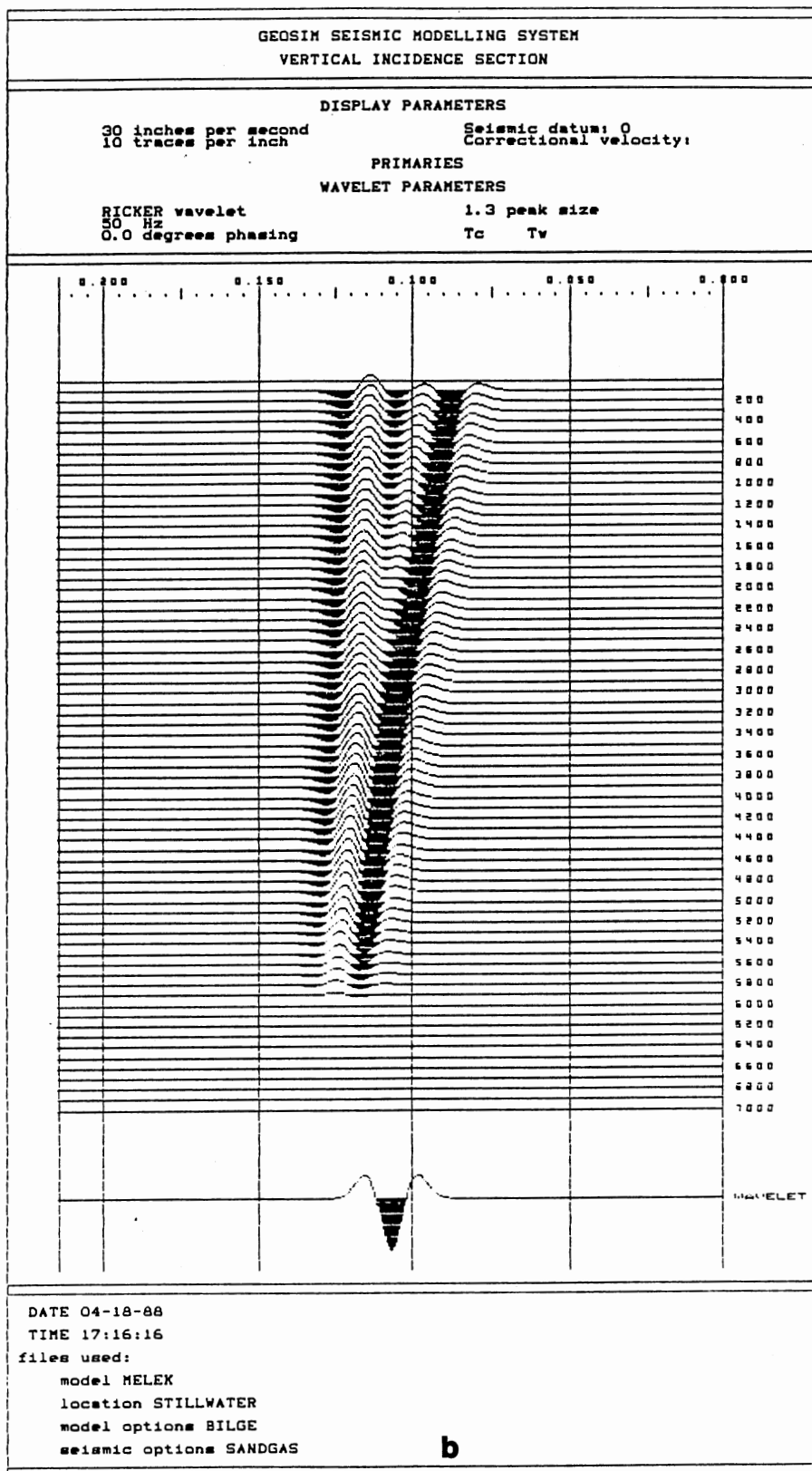


Figure 16-b. Seismic Response of the Geologic Model
for Gas Saturated Sand Wedge

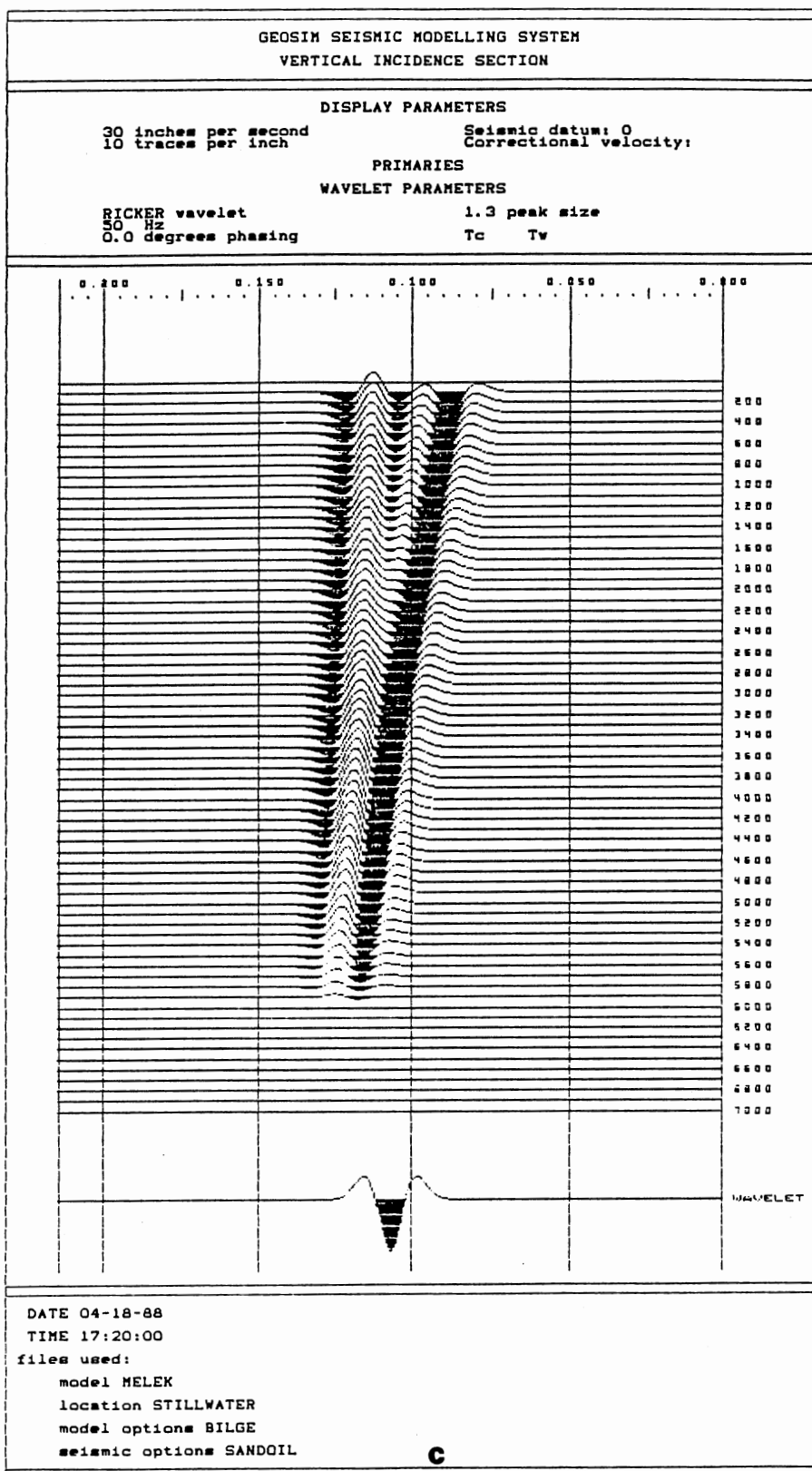


Figure 16-c. Seismic Response of the Geologic Model
for Oil Saturated Sand Wedge

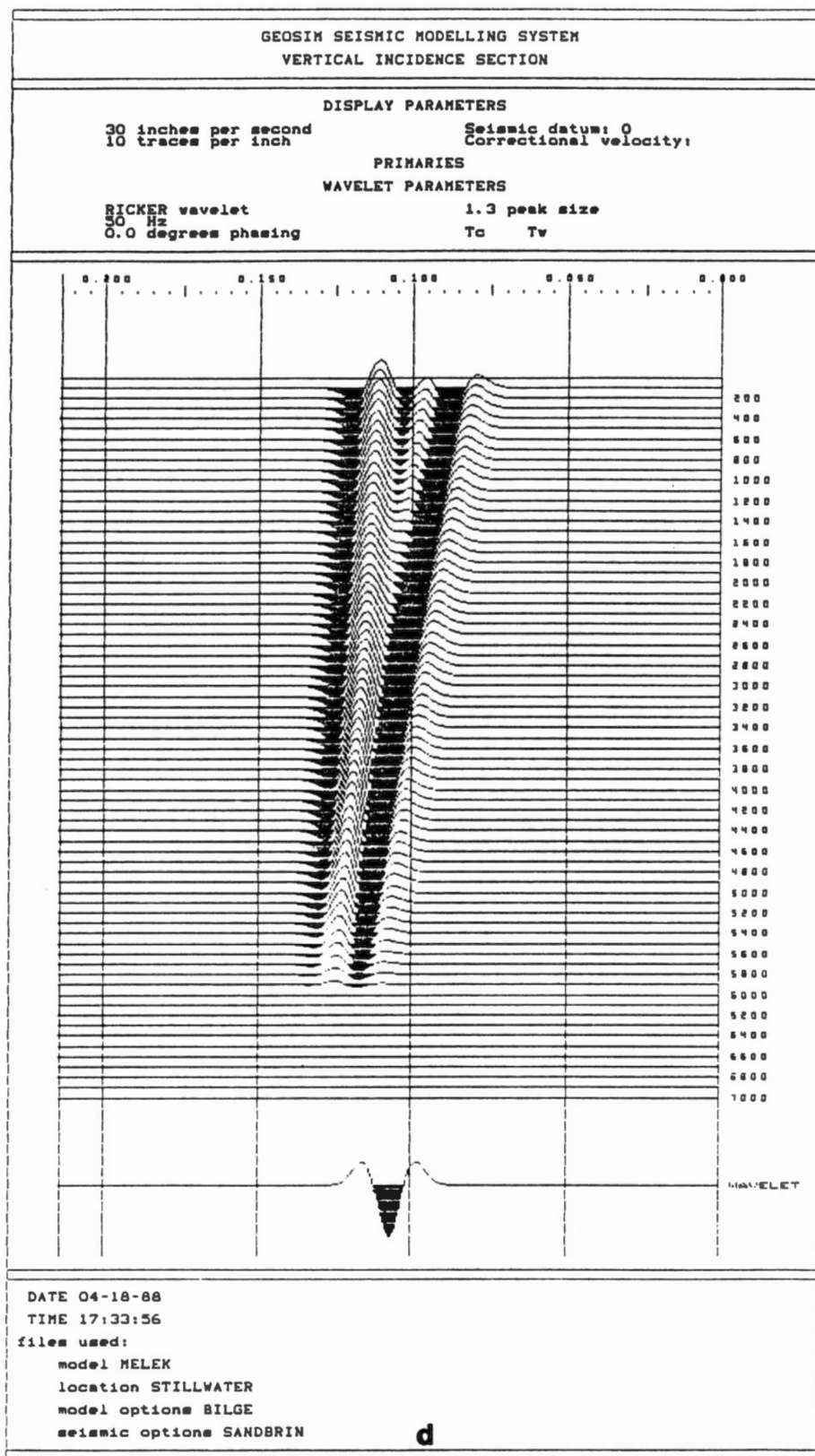


Figure 16-d. Seismic Response fo the Geologic Model
for Brine Saturated Sand Wedge

this point. This point is referred to as the tuning point. Beyond this point, the amplitude of the reflection decreases linearly as the wedge thickness decreases.

Different tuning thicknesses were obtained for each fluid saturation condition. The assumptions, which were derived from sonic and density logs, of the velocity and density values as well as the resulting tuning thicknesses of the sand wedge and surrounding shale are as follows:

	V (ft/sec)	d (gr/cm ³)	Tun. Thick.
Shale :	11500	2.55	-----
Sand w/ gas :	15000	2.50	50'
Sand w/ oil :	15500	2.57	60'
Sand w/ brine:	17000	2.65	70'

These velocity and density values represent deeply buried low porosity sediments. The density contrast attributed to the fluid content does not create a significant contrast between the shale and sandstone. On the other hand, sediments found in the Gulf Coast and in California characteristically have lower velocity and density values which are generally associated with higher porosities. The density contrast of the fluids associated with higher porosities leads to higher contrast between shale and gas-filled sandstone; therefore, it is difficult to distinguish between the shale and gas-filled sandstone.

The results of the sensitivity analysis show that the vertical resolution varies from 50 to 70 feet for different fluid saturation conditions. This can be

attributed to the proximity of the velocity and density values of the sandstone and shale. It is apparent that sandstone must range in thickness between 50 and 70 feet in order to be differentiated on the synthetic seismic sections (Figures 27 through 32). This range in thickness corresponds to core data collected in the Eastern Dewey County study (Bentkowski, 1985). Unfortunately, detailed core data was not available from Geary Field.

Geary Field Model

The reference map (Figure 17) shows the position of the seismic lines and the six wells in Geary Field, Canadian County, Oklahoma, which were used to construct the geological cross section (Plate 1) and to obtain the velocity and density values for each layer. Wells Robinson #1, Thunder #1-18, Cruse #1, Huff #1, Leck #1, and DeLana were used to construct the geologic cross section and wells Cruse #1 and Leck #1 were used to construct the synthetic seismograms (one-dimensional models). Cross section A1-A2 cuts across seismic lines 181 and 383, which cross each other approximately 3/4 miles south of well Cruse #1.

Synthetic Seismograms

The synthetic seismograms (one-dimensional models) from wells Cruse #1 and Leck #1 are illustrated in Figures 18 and 19. The density logs were loaded into the program

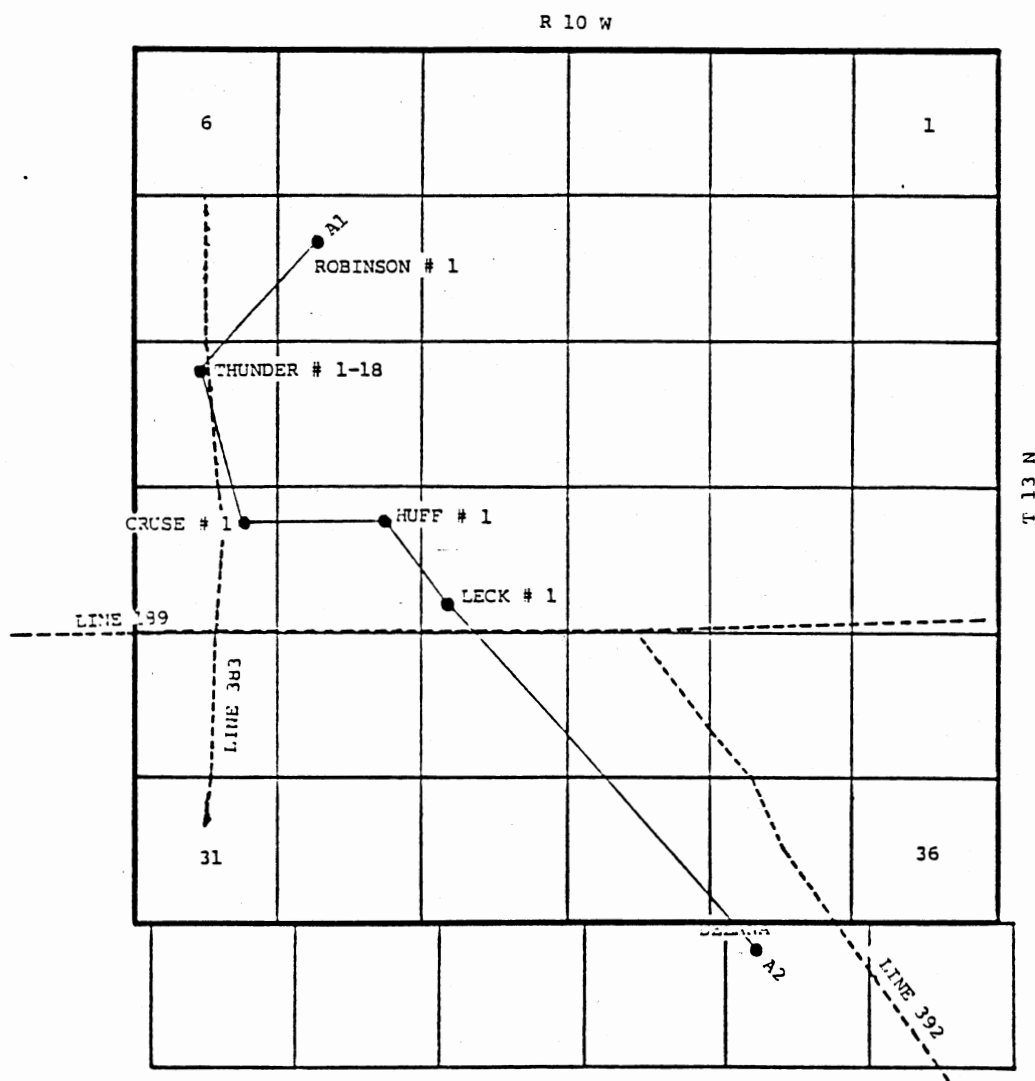


Figure 17. Reference Map Showing Cross Section A1-A2, Seismic Lines, and Wells Used to Construct the Cross Section in Geary Field

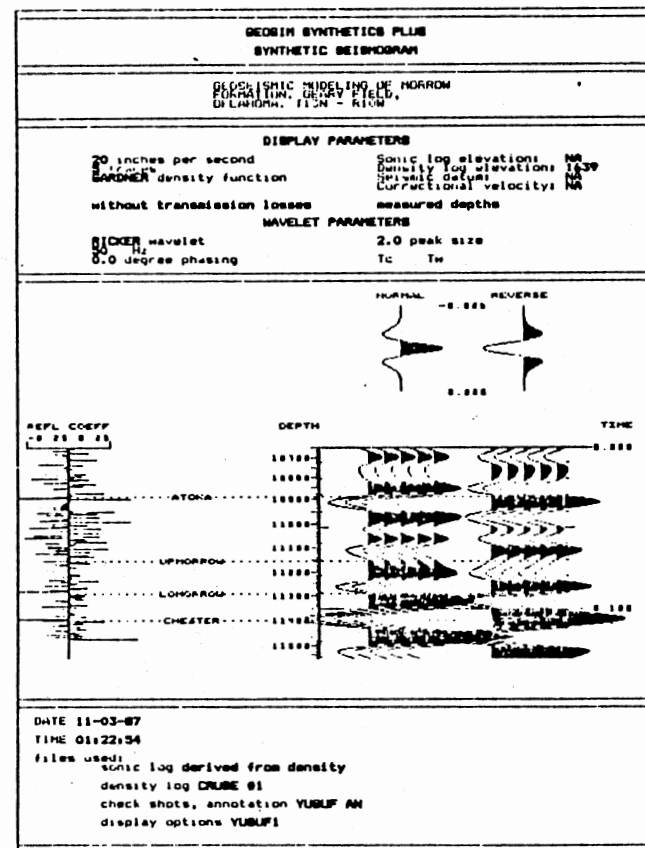
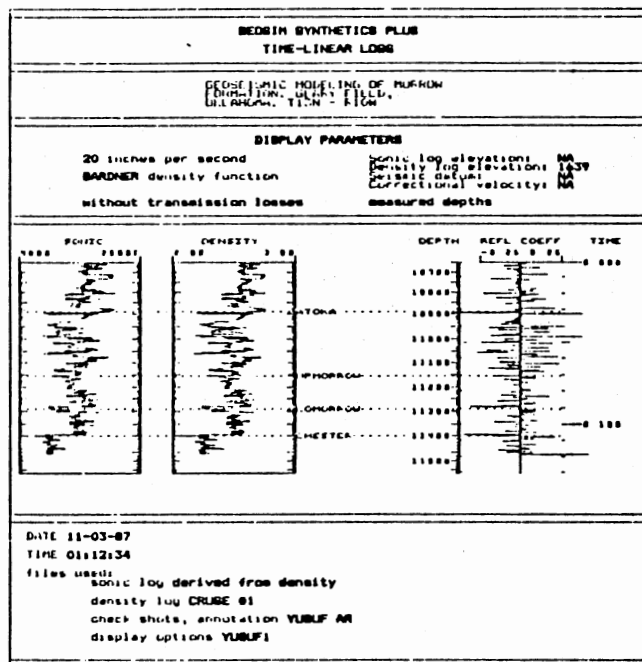


Figure 18. Synthetic Seismogram for Well Cruse #1, Geary Field

and the synthetic sonic logs were derived through the program using Gardner's equation. Then, the program generated the reflection coefficients which were convolved with the 50 Hz zero phase Ricker wavelet, producing the synthetic seismograms. Figures 20 and 21 show the comparison of the synthetic seismograms from wells Cruse #1 and Leck #1 and seismic lines 383 and 189, respectively. Inspection of the synthetic seismograms in relation to the seismic data allows one to notice a satisfactory correlation. The synthetic seismogram for Cruse #1 shows one amplitude anomaly, whereas the seismogram for Leck #1 shows two amplitude anomalies; therefore, Cruse #1 and Leck #1 can not be correlated with seismic lines. These unexpected anomalies can be caused by the domination of shale content or vertical changes in density and velocity, conversion from density logs to sonic or sonic logs to density, or recording errors.

After several tests changing velocity, density, and wavelet frequency, the following values were found to supply the best fit to the synthetic seismograms and the actual seismic sections:

Atoka Limestone :	19000 ft/sec, 2.70 gr/cm ³
Parvin Limestone:	20000 ft/sec, 2.70 gr/cm ³
Mch Shale :	10000 ft/sec, 2.40 gr/cm ³
Upper Morrow :	14000 ft/sec, 2.50 gr/cm ³
Lower Morrow :	17000 ft/sec, 2.65 gr/cm ³
Ricker wavelet :	50 Hz

AREA ANADARKO BASIN
QUAD. GEARY
LINE 383

Continental Oil Company
Exploration Geophysics

GM-278

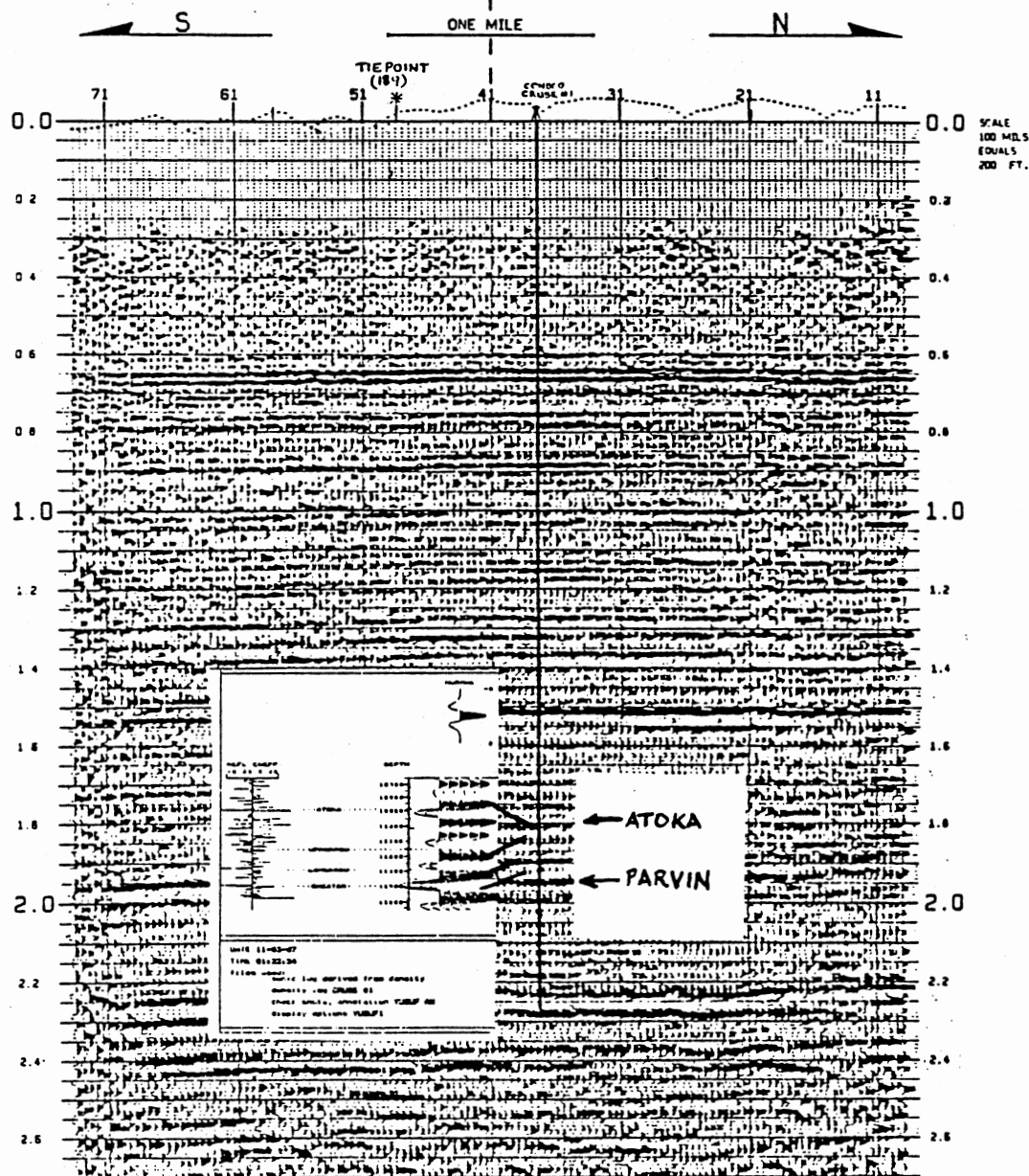


Figure 20. Comparison of Synthetic Seismogram for Well
Cruse #1 with Seismic Line 383, Going Through
the Well

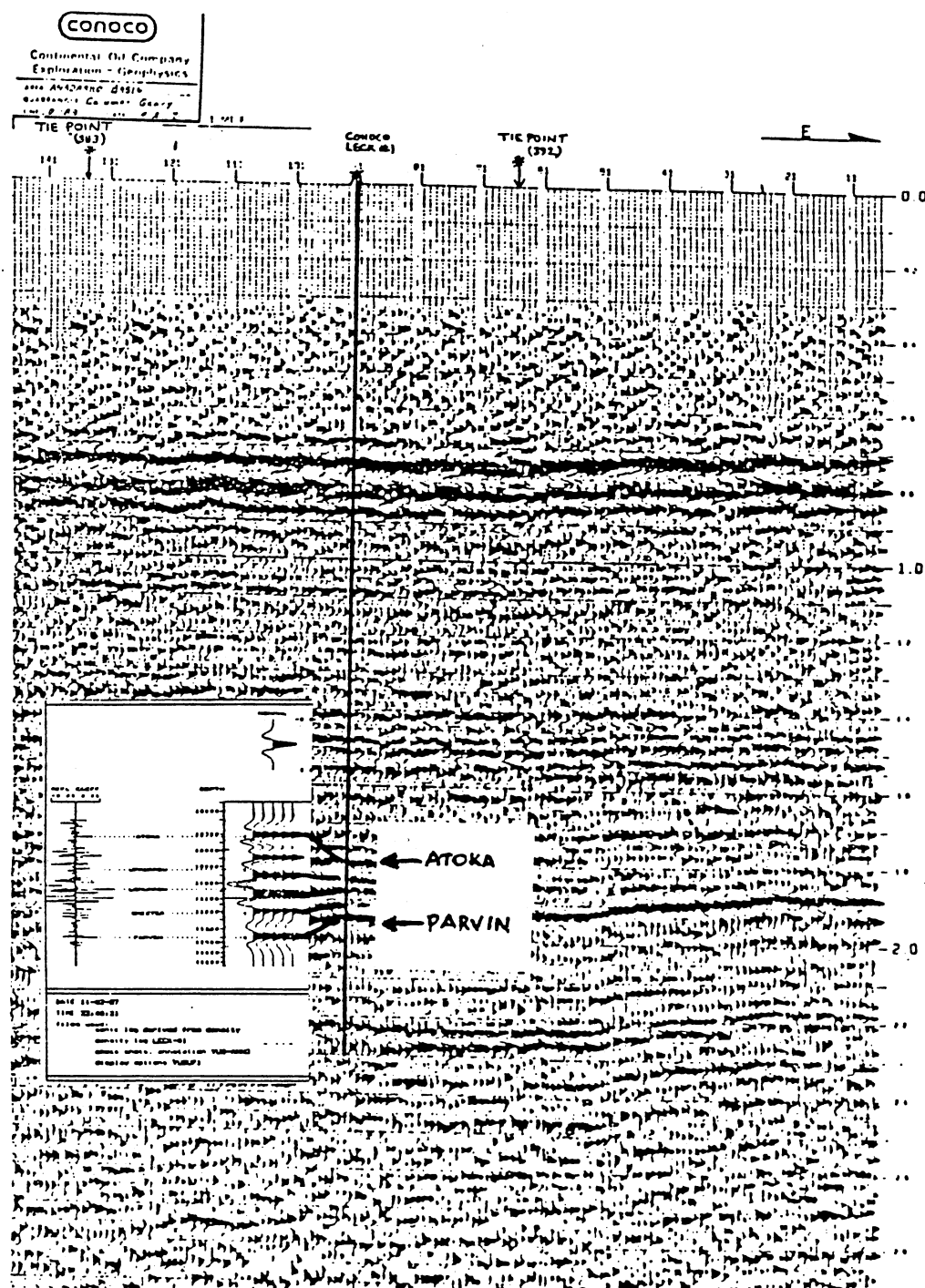


Figure 21. Comparison of Synthetic Seismogram for Well Leck #1 with Seismic Line 383, Going Through the Well

Two-Dimensional Models

Two-dimensional synthetic seismic sections for the geologic model have been obtained by using Step and Seismic Modeling System II.

The sonic logs from wells Thunder #1-18, Cruse #1, Huff #1, and Leck #1 were loaded into the Step program and an interpolated log section (Figure 22-a) was generated. Then, the program generated a two-dimensional seismic section (Figure 22-b). The Atoka Limestone-Upper Morrow, Lower Morrow-Mississippian Chesterian Shale (Mch Shale), and Mch Shale-Parvin Limestone boundaries are easily seen; however, the Upper Morrow-Lower Morrow boundary is not easily detectable. Several frequencies for the wavelet were tested, and the best result was achieved using the 50 Hz frequency in Step.

The geologic model (Plate 1, cross section A1-A2) was developed from the resistivity logs of the six wells. The velocity and density values for each layer were obtained by inspecting the velocity and density logs. In order to create a noise-free two-dimensional seismic model, the geologic model, velocity values, and density values for each layer were placed into the Seismic Modeling System II program. Figures 32, 33, 34, and 35 (Appendix A) show the seismic responses of the geologic model for the 40, 60 and 80 Hz frequencies. The results of these frequency applications show that the higher the frequency, the

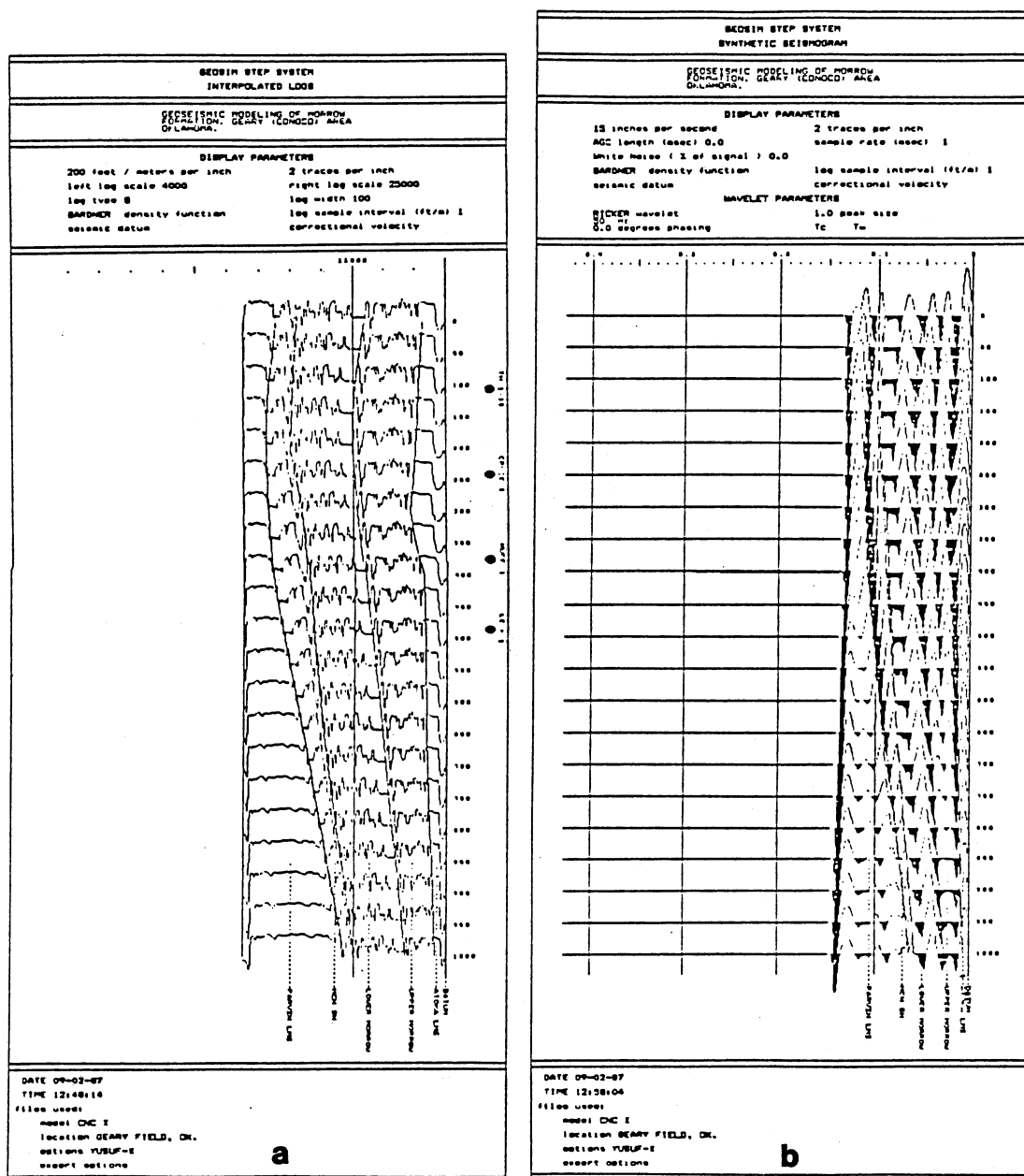


Figure 22. For Geary Field:

- a) Two-dimensional synthetic seismogram
- b) Interpolated log section

higher the resolution. The 80 Hz frequency provided the best result. In figures 33 through 35, the diagrams on the upper portion of each page show vertical incidence and are labeled as "a", whereas the diagrams on the lower portion of each page show normal incidence, which is the product of the ray trace option of Seismic Modeling System II, and are labeled as "b". It is evident that the vertical incidence models and the normal incidence models are almost identical due to the simple structure of the layers. As was previously mentioned, normal incidence sections are very useful when complex structural problems exist. Figure 23 shows the comparison between the two-dimensional synthetic seismic section and the actual seismic section, line 383. The northern portion of the synthetic and actual seismic sections, between wells Robinson and Cruse #1, have been compared. This comparison provided an excellent fit.

Eastern Dewey County Model

The reference map in Figure 24 shows the cross sections from A1-A2 through F1-F2 and the well locations. Table I (Appendix B) contains the list of file, company, and well names used to construct the cross sections of eastern Dewey County.

Synthetic seismograms for wells Blaine Simon #1 (Figure 25), Addis #1 (Figure 36, Appendix B), and Prophet #1 (Figure 37, Appendix B) were constructed by using the

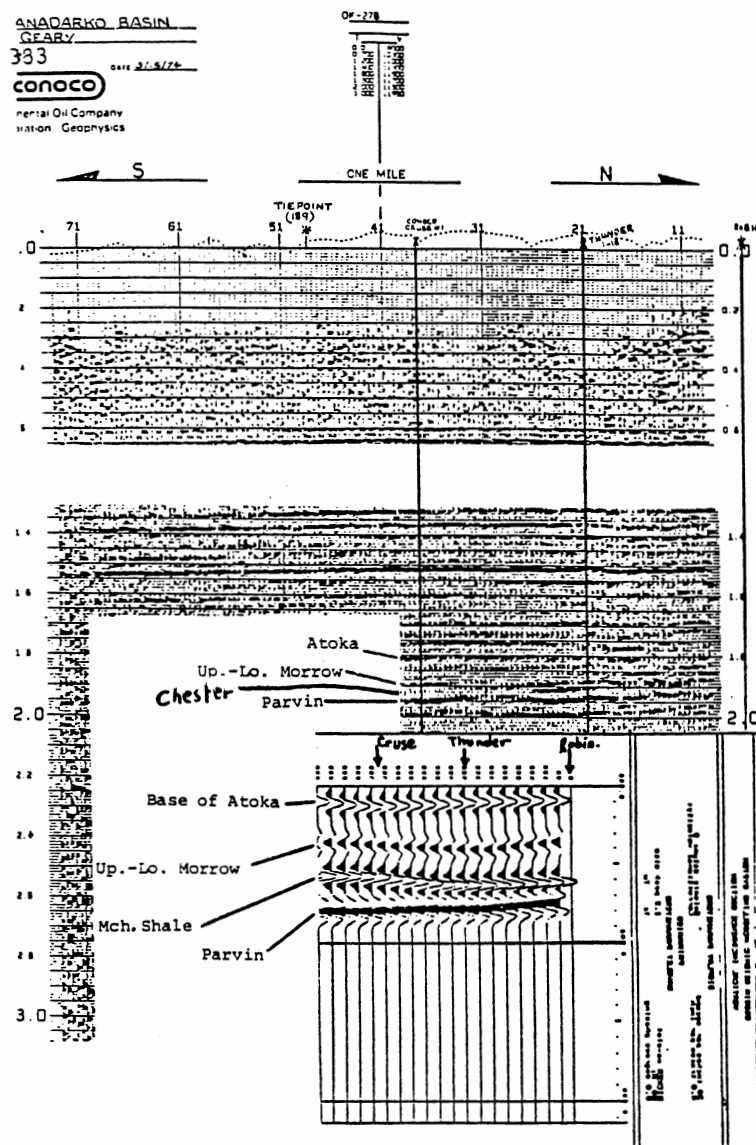


Figure 23. Comparison of Two-dimensional Synthetic Seismic Section and Line 383 Between Wells Cruse #1 and Robinson

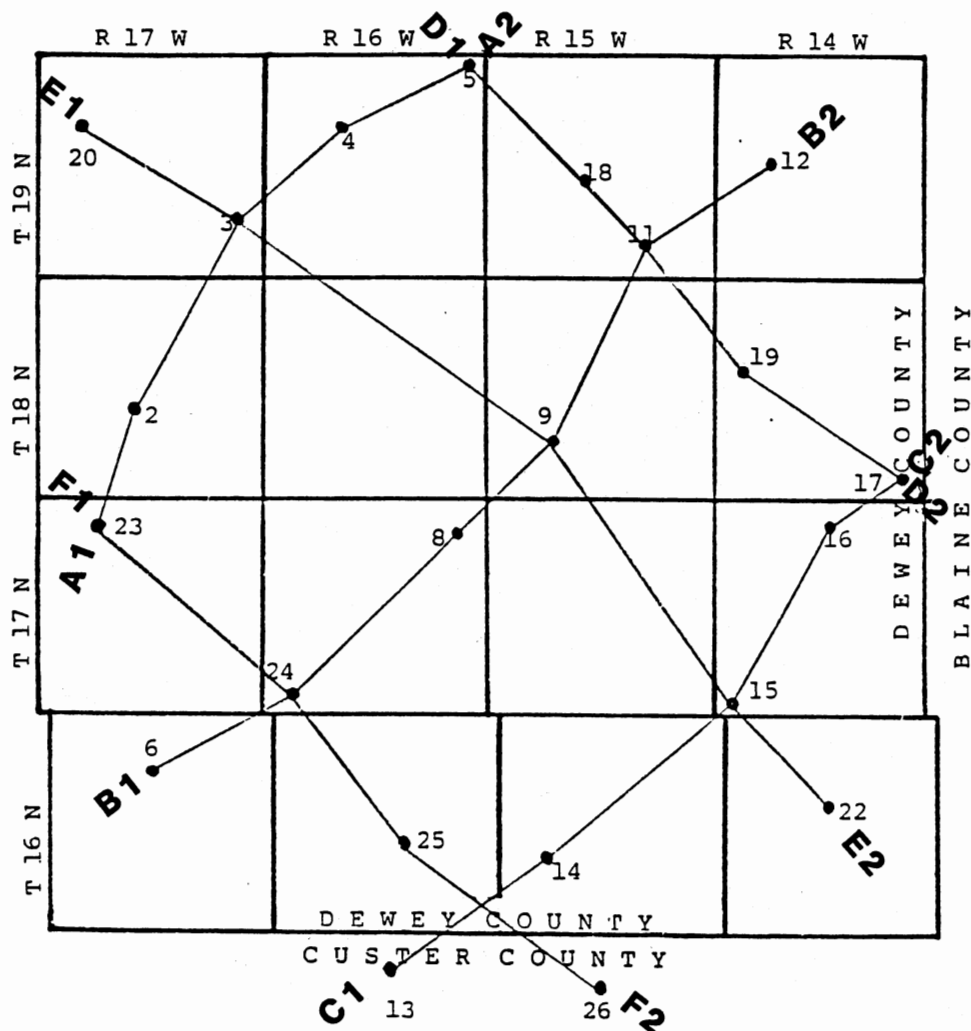


Figure 24. Reference Map Showing Cross Sections from A1-A2 to F1-F2, and Wells Used to Construct the Cross Sections in Eastern Dewey County

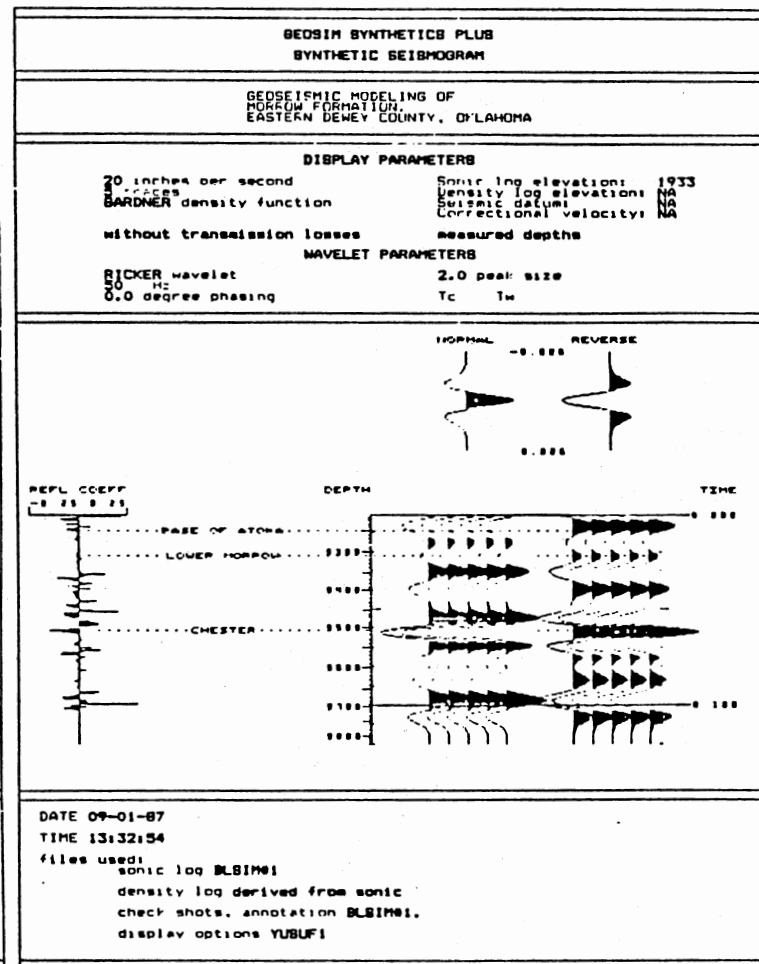
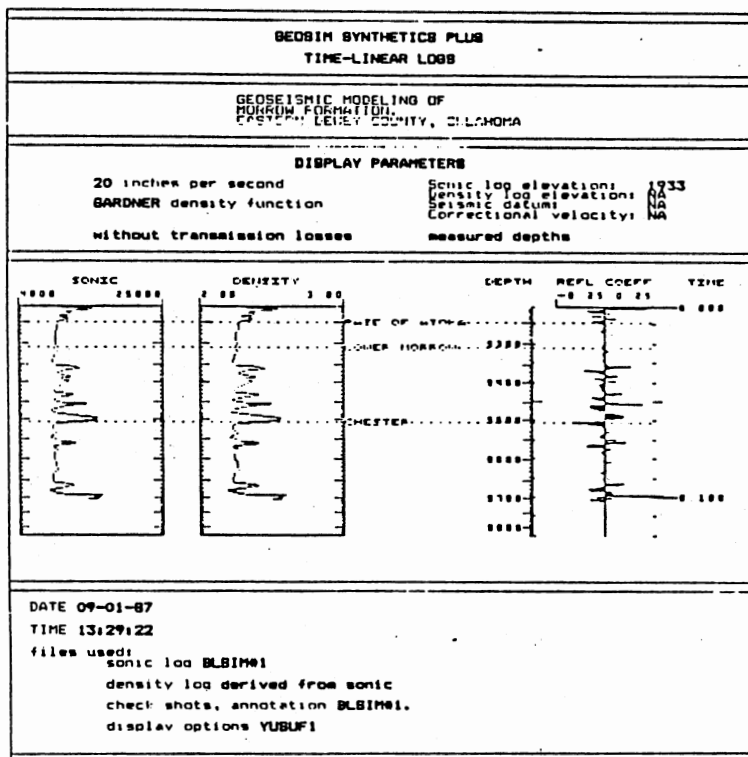


Figure 25. Synthetic Seismogram for Well Blain Simon #1

sonic logs, generated from the resistivity logs, and the density logs, derived from computer-generated sonic logs. The Synthetics Plus program calculated the reflection coefficients and, by convolving these reflection coefficients with the 50 Hz Ricker wavelet, produced the synthetic seismograms. These synthetic seismograms satisfactorily fit each other as well as the synthetic seismograms from wells Cruse #1 and Leck #1, which were used in the Geary Field model.

The interpolated log sections and the corresponding two-dimensional synthetic seismic sections for each cross section are shown in Figures 38 through 43 (Appendix C). The results of the log interpolations are reasonable and the layer boundaries are detectable. However, this is not true for the two-dimensional synthetic seismic sections, especially cross section D1-D2. In the other cross sections, the Atoka-Morrow boundary can be seen but the Morrow-Mississippian Chesterian Shale (Mch Shale) boundary is not detectable. It is obvious that during the interpolation process logs interfere with each other, and, as a result, an unknown percentage of noise can be added to interpolated logs. This noise, along with vertical changes of velocity and density and unavoidable errors which occur during the conversion of resistivity logs to sonic logs and/or sonic logs to density logs is responsible for the inaccuracies in the synthetic seismic section.

For the geometry, which was developed using resistivity and gamma-ray logs (Plates 2 to 7, cross sections A1-A1 through F1-F2 in pocket), the following velocity and density values have been loaded into the Seismic Modeling System II program:

Atoka Limestone	: 19000 ft/sec, 2.70 gr/cm ³
Mch Shale	: 9800 ft/sec, 2.65 gr/cm ³
Upper Morrow	: 14000 ft/sec, 2.50 gr/cm ³
M8	: 16000 ft/sec, 2.60 gr/cm ³
M7	: 15000 ft/sec, 2.45 gr/cm ³
M6	: 14200 ft/sec, 2.65 gr/cm ³
M5	: 15500 ft/sec, 2.54 gr/cm ³
M4	: 14000 ft/sec, 2.42 gr/cm ³
M3	: 16000 ft/sec, 2.60 gr/cm ³
M2	: 15000 ft/sec, 2.50 gr/cm ³
M1	: 14000 ft/sec, 2.65 gr/cm ³

The noise-free vertical incidence, two-dimensional synthetic seismic sections, and the corresponding geologic models are shown in color (in pocket) and in black and white (Figures 26 through 31). The results are quite impressive. The Atoka-Upper Morrow, Upper Morrow-Lower Morrow, and Lower Morrow-Mch Shale boundaries can easily be detected, although the sand layers in the Lower Morrow are not detectable due to the thickness of the layers and the close acoustic impedance contrasts between these layers.

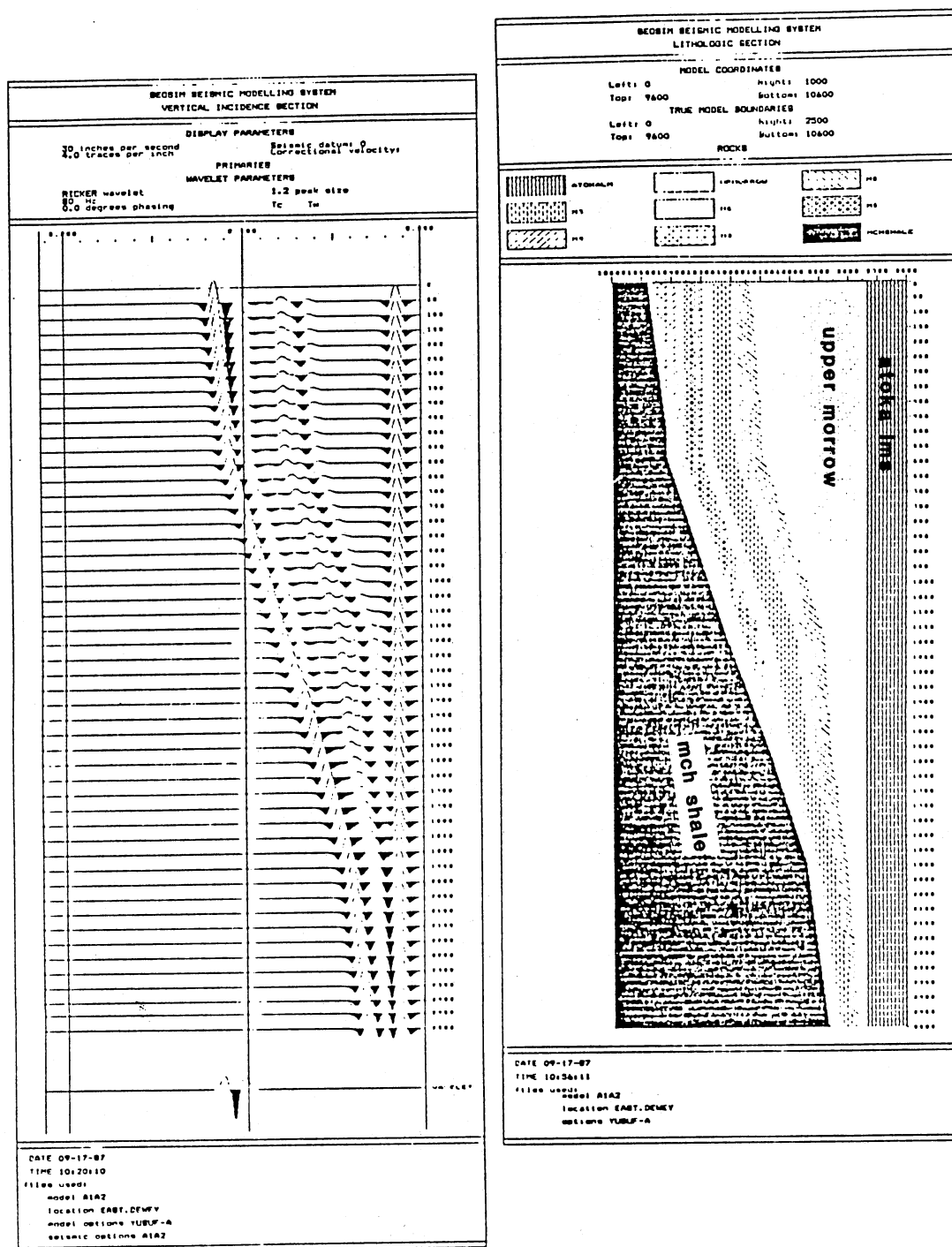


Figure 26. Geologic Model for Cross Section A1-A2, and its Seismic Response, Eastern Dewey County

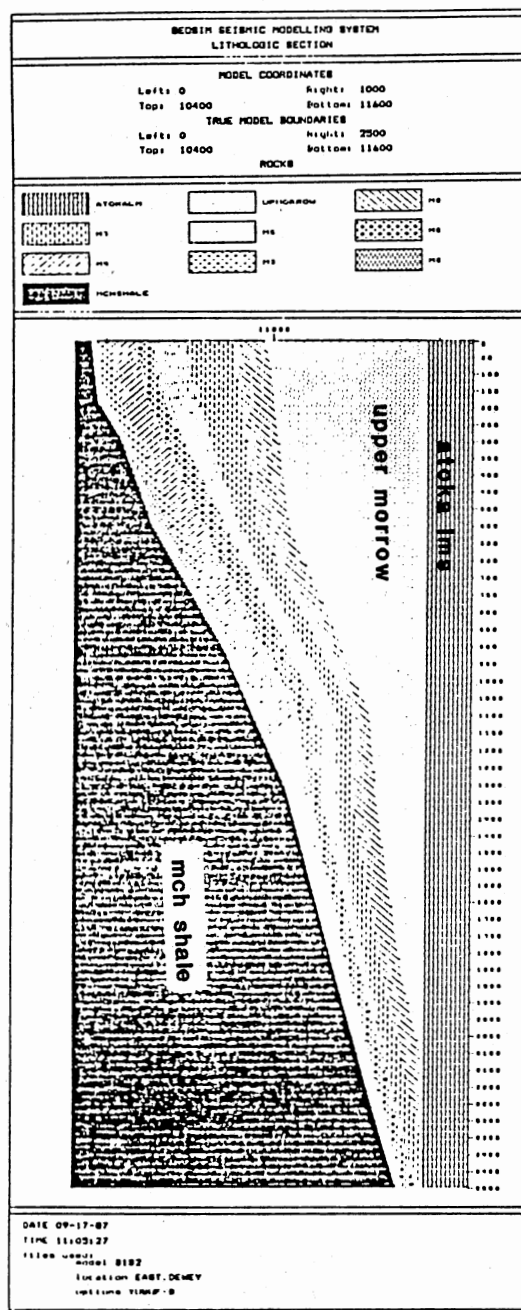
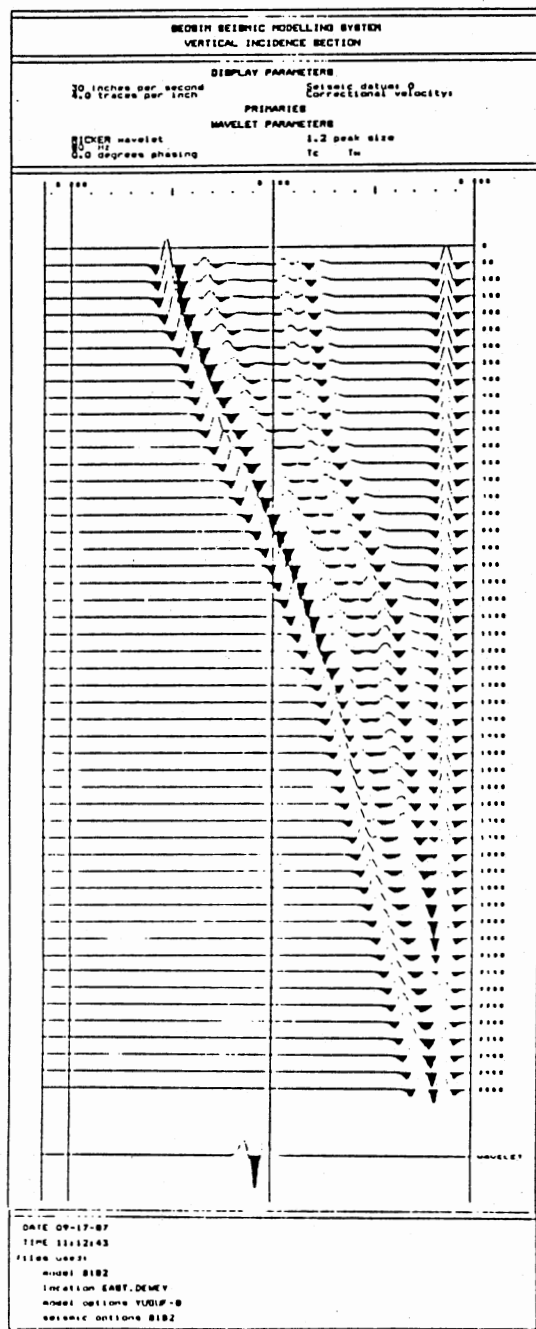


Figure 27. Geologic Model for Cross Section B1-B2, and its Seismic Response, Eastern Dewey County

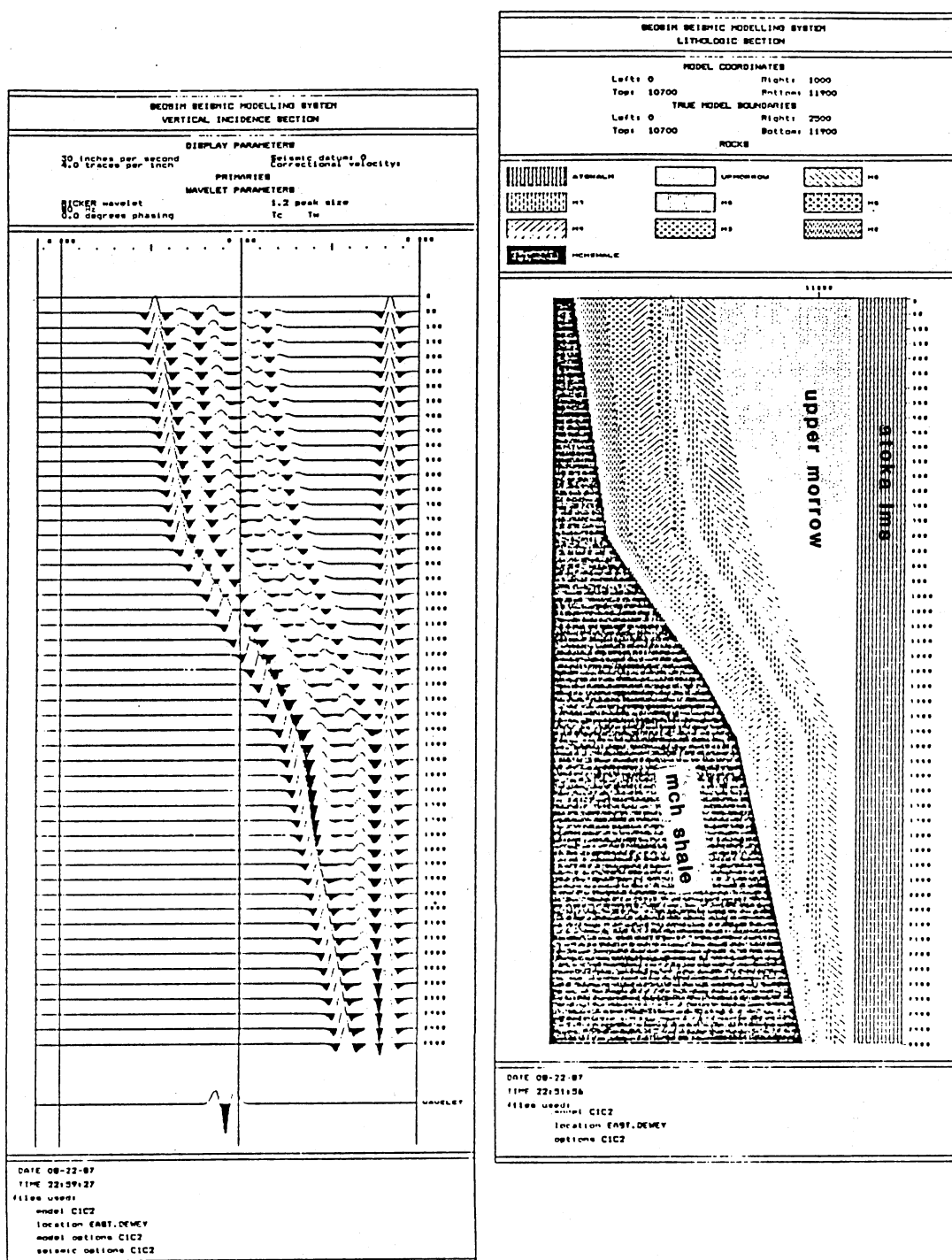


Figure 28. Geologic Model for Cross Section C1-C2, and its Seismic Response, Eastern Dewey County

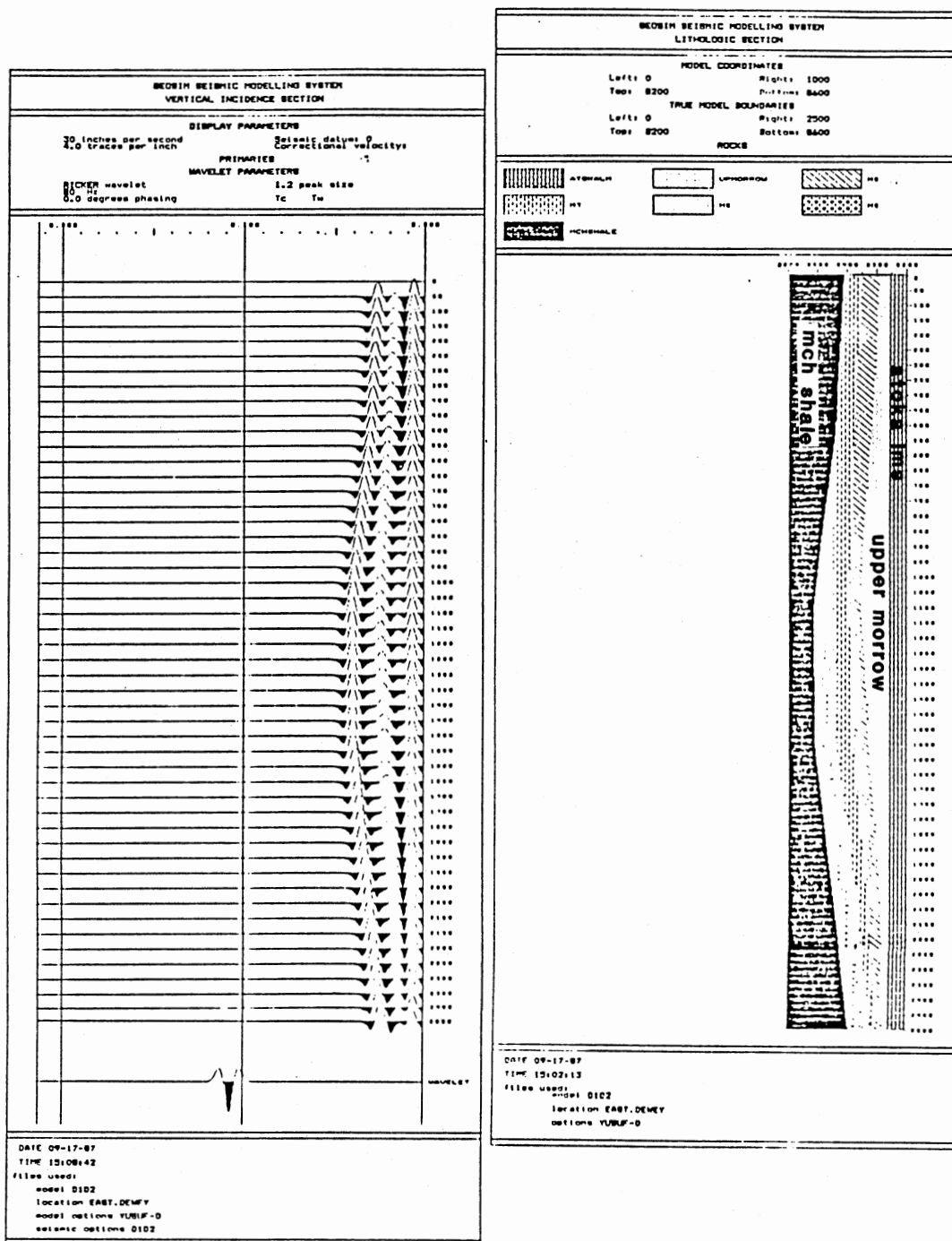


Figure 29. Geologic Model for Cross Section D1-D2, and its Seismic Response, Eastern Dewey County

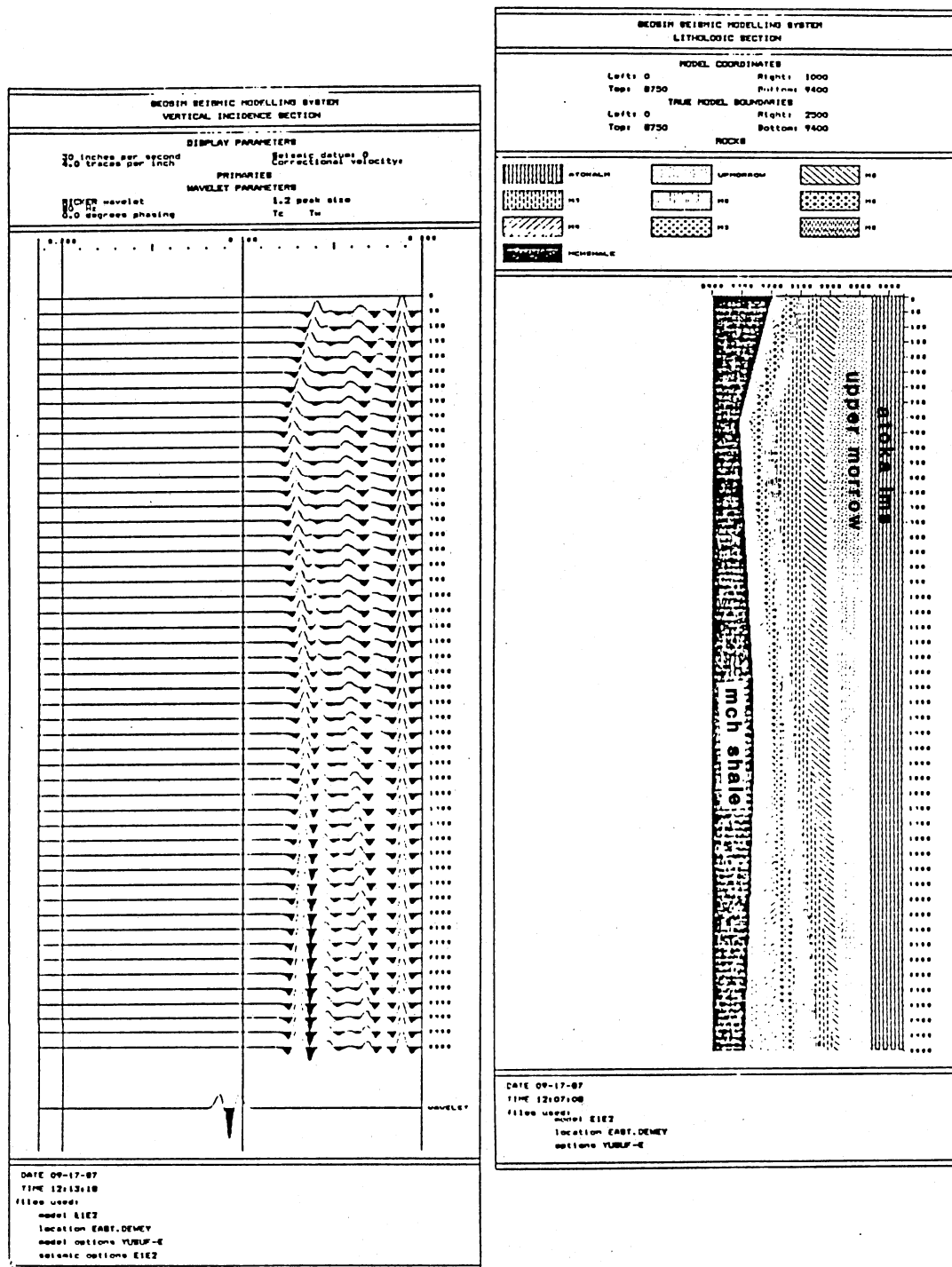


Figure 30. Geologic Model for Cross Section E1-E2, and its Seismic Response, Eastern Dewey County

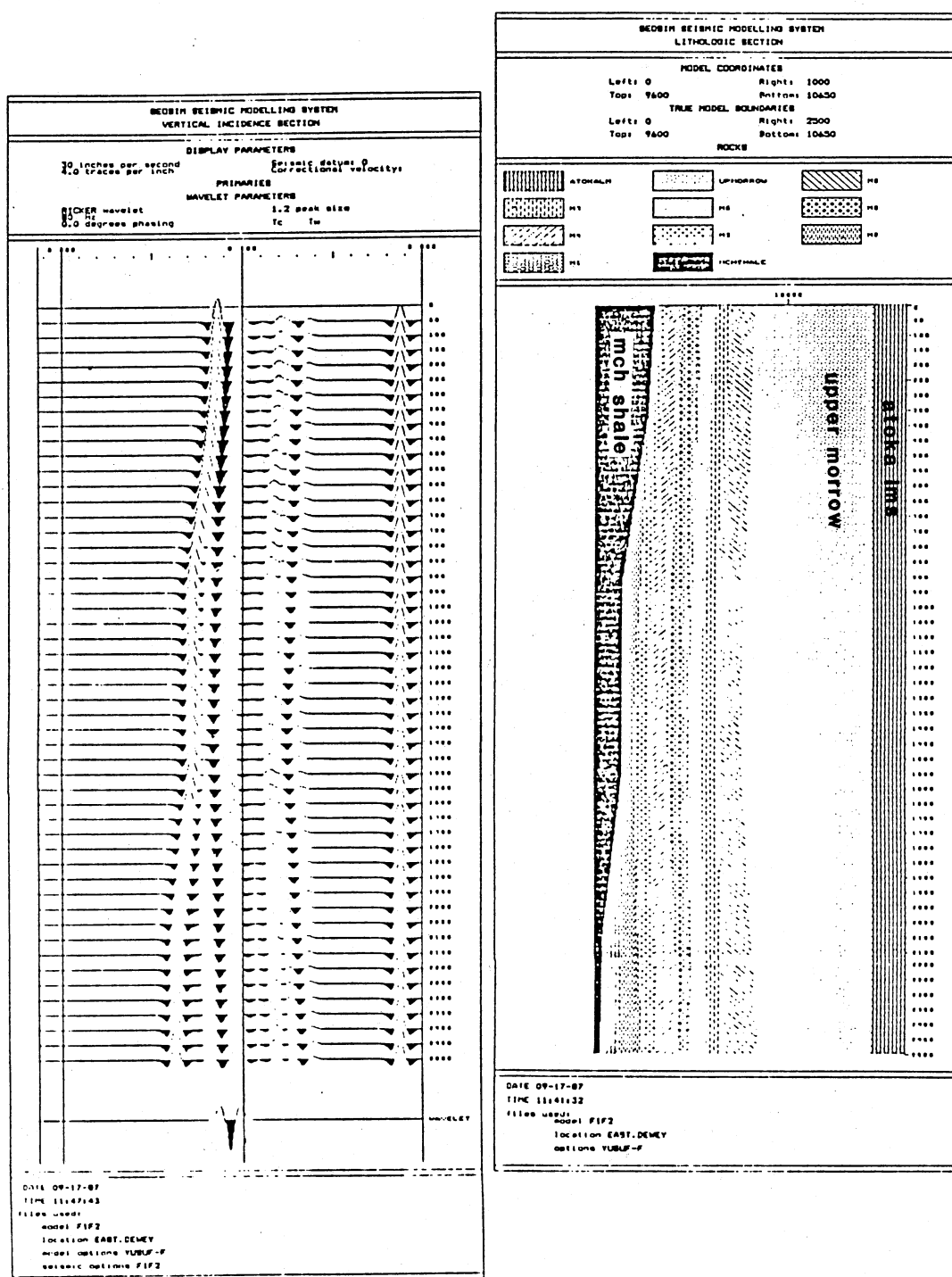


Figure 31. Geologic Model for Cross Section F1-F2, and its Seismic Response, Eastern Dewey County

CHAPTER VI

SUMMARY AND CONCLUSIONS

The seismic expression of the Morrow Formation in two fields has been demonstrated. Extensive modeling has been performed successfully by utilizing the Geosim Seismic Modeling package and has been tied to the seismic data in Geary field.

Faust's, Gardner's, and Lindseth's equations, which were used for converting the logs from resistivity to sonic, sonic to density, or density to sonic, are empirical relationships. For example, Faust's equation, which is given as a default value in the Log Assist program,

$$\text{Sonic} = 900 \times (\text{Depth} \times \text{Resistivity})^{\text{Exp } 0.16667}$$
considers depth only. Conversely, not only depth but also fluid content, environmental pressure, mineral composition, granular nature of the rock matrix, and age affect rock resistivity, density, and velocity. It is obvious that neglecting each of these factors will cause additional errors in the converted sonic logs. As a result, when transforming these converted sonic logs to density logs by using one of the equations mentioned above, the margin for error will be doubled. Therefore,

the two-dimensional log interpolations and synthetic seismic sections created by the Step program were positive but not very impressive. In the Geary Field study, the real density logs from wells Cruse #1 and Leck #1 were used in the Synthetics Plus program to derive sonic logs and the results were positive. Computer-generated sonic and density logs were used in the eastern Dewey County study for wells in which both sonic and density logs were not available.

Fresnel zone effects and lateral and vertical changes of velocity and density have not been considered during this study. However, two-dimensional synthetic seismic sections, generated by the Seismic Modeling System II program, appear to provide an excellent match with the field seismic data for Geary Field. Nevertheless, it cannot be guaranteed that the results of the modeling study of the eastern Dewey County section will give an excellent match.

The following is a list of important summaries and conclusions:

1. Due to the possibility of producing similar seismic responses from different geologic conditions, seismic modeling is one of the most important parts of seismic interpretation (Figure 2).
2. The results of the sensitivity analysis (Figures 16-a, b, c, and d) show that the vertical

resolution varies from 50 to 70 feet for gas, oil, and water saturation conditions. It was concluded that this variance can be attributed to the proximity of the velocity and density values of the sandstone and shale.

3. This modeling study showed that if the thickness of a layer is less than 50 feet, the layer will not be detectable (Figures 16-a, b, c, and d).
4. The velocity and density contrasts between sand, shale, and limestone create acoustic impedance and reflection coefficients, which make the boundaries detectable and responsible for reflections.
5. The density, velocity, geometry and thickness of each layer can be obtained by analyzing wire line logs.
6. The Seismic Modeling System II program does not permit any noise that may exist in nature to be considered. If the program did allow the addition of a percentage of these noise levels, such as 10%, 20%, 30% or more, the limitations of this noise could have been demonstrated.
7. Using computer-generated sonic and density logs should be avoided in the Synthetics Plus and Step programs because of the empirical relationships (explained in Chapter IV, METHODOLOGY, Modeling Procedures) used in deriving them.

8. The Seismic Modeling System II Program gives quicker and more realistic results than the Step program (Figures 26 through 32 vs. Figures 38 through 43, respectively).

REFERENCES

- Angona, F. A., 1960, Two-Dimensional Modeling and its application to seismic problems: *Geophysics*, v. 25, p. 468-482.
- Anstey, N. A., 1977, *Seismic interpretation: The Physical aspects*: International Human Resources Development Corporation, Boston. 625 p.
- , 1980, *Seismic Exploration for Sandstone Reservoirs*: International Human Resources Development Corporation, Boston. 136 p.
- Badley, M. E., 1985, *Practical Seismic Interpretation*: International Human Resources Development Corporation, Boston, 266 p.
- Benton, J. W., 1972, *Subsurface Stratigraphic Analysis, Morrow (Pennsylvanian), North Central Texas County, Oklahoma*: Oklahoma City Geological Society, *Shale Shaker Digest*, vols. XXI-XXIII, 1970-1973, p.1-29.
- Bone, M. R., Giles, B. F., and Tegland, E. R., 1983, Analysis of seismic data using horizontal cross-sections: *Geophysics*, v. 48, p.1172-1178.
- Davis, H. G., 1971, *The Morrow-Springer Trend, Anadarko Basin, Target for the 70's*: Oklahoma City Geological Society, *Shale Shaker Digest*, vols. XXI-XXIII, 1970-1973, p. 83-93.
- , 1974, *High Pressure Morrow-Springer Gas Trend Blaine and Canadian Counties, Oklahoma*: *Shale Shaker*, v.24, Feb. 1974, no. 6, p. 104-118.
- Delaplanche, J., Hagemann, R. F., and Bollard, P. G. C., 1963, An example of the use of synthetic seismograms: *Geophysics*, v. 28, p. 842-854.
- Dedman, E. V. , Lindsey, J. P., and Schramm, M. W., 1975 a, *Stratigraphic modeling: in New Trends in Seismic Interpretation*, A seminar sponsored by the Denver Geophysical Society, Golden, Colorado, April 1975, 37 p.

- , 1975 b, Stratigraphic modeling: A step beyond bright spot: World Oil, v. 180, no. 6, p. 61-65.
- Dobrin, M. B., 1976, Introduction to Geophysical Prospecting: McGraw-Hill, Inc., New York, 630 p.
- Durwood, J. P., 1959, Stratigraphic Traps Along North Shelf of Anadarko Basin, Oklahoma: AAPG Bulletin, v. 43, no. 1, p. 39-59.
- Faust, L. Y., 1951, Seismic velocity as a function of depth and geologic time: Geophysics, v. 16, p.192-206.
- Galloway, W. E., Yancey, M. S., and Whipple, A. P., 1977, Seismic stratigraphic model of depositional platform margin, Eastern Anadarko Basin, Oklahoma : in C. E. Payton, ed., Seismic Stratigraphy-applications to hydrocarbon exploration. AAPG Memoir 26, p. 439-449.
- Gardner, G. H. F., Gardner, L. W., and Gregory, A. R., 1974, Formation velocity and density. The diagnostic basis for stratigraphic traps: Geophysics, v. 39, p. 770-780.
- Halverson, J. R., 1987, Seismic Expression of the Upper Morrow Channel Sands, Western Anadarko Basin: Presented at the 40 th Annual Midwest Regional SEG Meeting in Dallas, Texas.
- Hilterman, F. J., 1975, Amplitudes of seismic waves-A quick look: Geophysics, v.40, no. 5, p. 745-762.
- Khaiwka, M. H., 1973, Geometry and depositional environment of Morrow Reservoir Sandstones, Northwestern Oklahoma: Oklahoma City Geological Society, Shale Shaker Digest, vols. XXI-XXIII, 1970-1973, p. 170-192.
- Lane, R. H., and Straka, J. J., 1974, Late Mississippian and Early Pennsylvanian Conodonts of Arkansas and Oklahoma: The Geological Society of America, Special Paper, no. 152, 144 pp.
- Lindseeth, R. O., 1979, Synthetic sonic logs - a process for stratigraphic interpretation: Geophysics, v. 44, p. 3-26.
- Lindsey, J. P., and Dedman, E. V., 1975, Structural Modeling: in New Trends in Seismic Interpretation, A seminar sponsored by the Denver Geophysical Society, Golden, Colorado, April 1975, 41 pp.

- Lindsey, J. P., Schramm, M. W. Jr., and Nemeth, L. K., 1976, New Seismic technology can guide field development: World Oil, v. 182, no.7, p. 59-63.
- Martinez, R. D., and Stanford, B. J., 1981, A seismic stratigraphy case history in Northeast Mexico: Presented at the 50 th Annual SEG Meeting, Los Angeles, California.
- McQuillan, R., Bacon, M., and Barclay, W., 1984, An introduction to seismic interpretation: Houston, Gulf Publishing Company, 287 p.
- Meckel, L. D., and Nath, A. K., 1977, Geologic considerations for stratigraphic modeling and interpretation: in C. E. Payton, ed., Seismic Stratigraphy-applications to hydrocarbon exploration. AAPG Memoir 26, p. 417-438.
- Meister, J., and Dresen, L., 1987, Hybrid Seismic Modelling: A Technique to Combine Physical and Computer Methods for Vertical Wave Incidence: Geophysical Prospecting, v. 35, p. 815-831.
- Mitchum, R. M., Vail, P. R., and Sangree, J. B., 1977, Seismic stratigraphy and global changes of sea level, Part 6: in C. E. Payton, ed., Seismic stratigraphy-applications to hydrocarbon exploration. AAPG Memoir 26, p. 117-133.
- Meissner, R., and Meixner, E., 1969, Deformation of seismic wavelets by thin layers and layered boundaries: Geophysical Prospecting, v.17, p. 1-27.
- Nath, A. K., 1975, Reflection amplitude, modeling can help locate Michigan Reefs: Oil and Gas Journal, v.73, no. 11, p. 180-182.
- Neidell, N. S., 1975, What are the limits in specifying seismic models?: Oil and Gas Journal, v.73, no. 7, p. 144-147.
- , and Poggiagliolmi, E., 1977, Stratigraphic modeling and interpretation - geophysical principles and techniques: in C. E. Payton, ed., Seismic-stratigraphy applications to hydrocarbon exploration. AAPG Memoir 26, p. 389-416.
- Ryder, R. T., Lee, M. V., and Smith, G. N., 1981, Seismic models of sandstone stratigraphic traps in Rocky Mountain Basins: AAPG, Tulsa, Oklahoma, 77 pp.

- Schoenberger, M., 1974, Resolution comparison of minimum-phase and zero-phase signals: *Geophysics*, v. 39, p. 826-833.
- Schramm, M. W., Dedman, E. V., and Lindsey, J. P., 1977, Practical stratigraphic modeling and interpretation: in C. E. Payton, ed., *Seismic stratigraphy-applications to hydrocarbon exploration*. AAPG Memoir 26, p. 477-502.
- Sheriff, R. E., 1975, Factors affecting seismic amplitudes: *Geophysical Prospecting*, v. 23, p. 125-138.
- , 1977, Limitations of resolution of seismic reflections and geologic detail derivable from them: in *Seismic Stratigraphy-applications to hydrocarbon exploration*. AAPG Memoir 26, p. 3-14.
- , 1976, Inferring stratigraphy from seismic data: *AAPG Bulletin*, v. 60, no. 4, p. 528-542.
- , 1984, *Encyclopedic Dictionary of Exploration Geophysics*: Society of Exploration Geophysicists, Tulsa, 323 p.
- , 1985, Aspects of Seismic Resolution: in *Seismic Stratigraphy II*, AAPG Memoir, 39, p. 1-10.
- , and Geldart, L. P., 1985, *Exploration Seismology*, v. 2, Data-Processing and interpretation: Cambridge University Press, London. 221 p.
- Simson, S. F., Nelson, H. R. Jr., 1984, Seismic stratigraphy moves towards interactive analysis. Part I: *World Oil*, v. 199, no. 7, p. 55-58.
- , 1985, Seismic stratigraphy moves towards interactive analysis. Part II: *World Oil*, v. 200, no. 4, p. 95-98.
- , 1985, Seismic stratigraphy moves towards interactive analysis. Part III: *World Oil*, v. 200, no. 5, p. 93-96.
- Takken, S., 1967, Subsurface geology of the North Gotebo Area, Oklahoma: *Oklahoma City Geological Society, Shale Shaker Digest*, vols. XV-XVII, 1964-1967, p. 330-338.
- Widess, M. B., 1973, How thin is a thin bed?: *Geophysics*, v. 38, p. 1176-1180.

APPENDIXES

APPENDIX A

GEOLOGIC MODEL FOR GEARY FIELD
AND ITS SEISMIC RESPONSE FOR
DIFFERENT FREQUENCIES

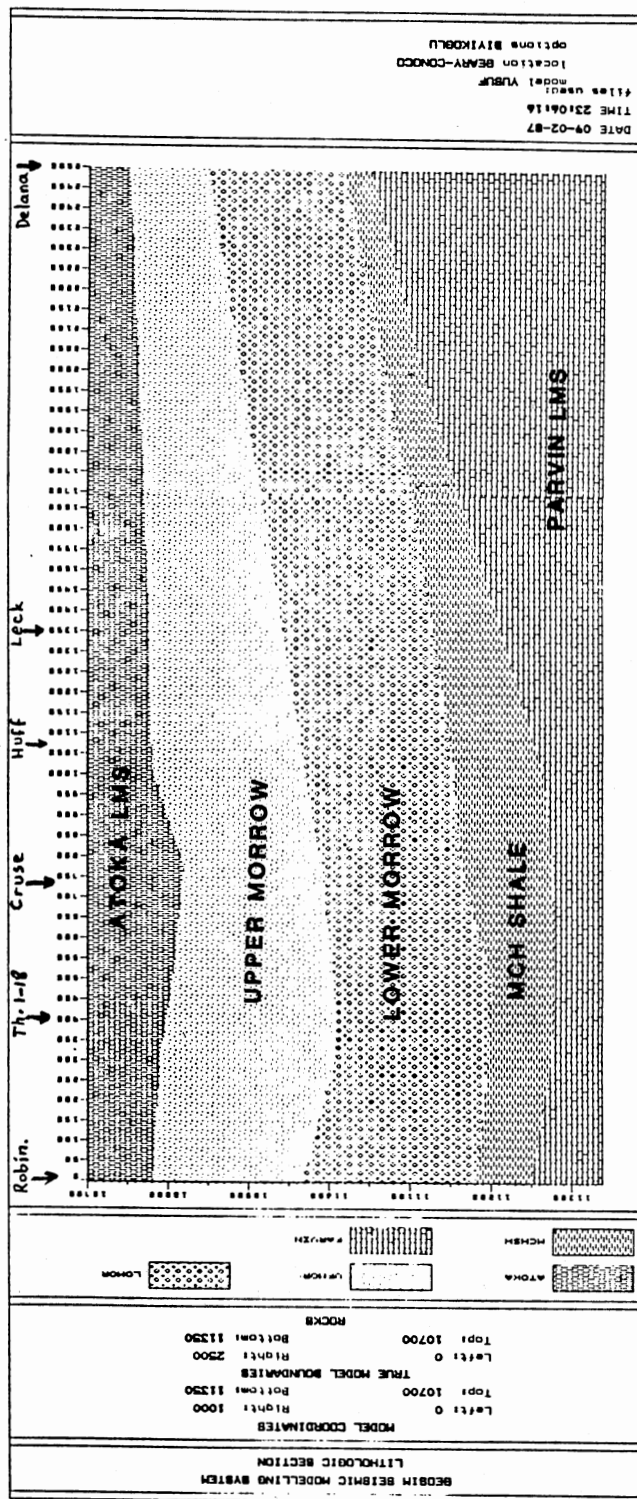


Figure 32. The Geologic Model in Geary Field

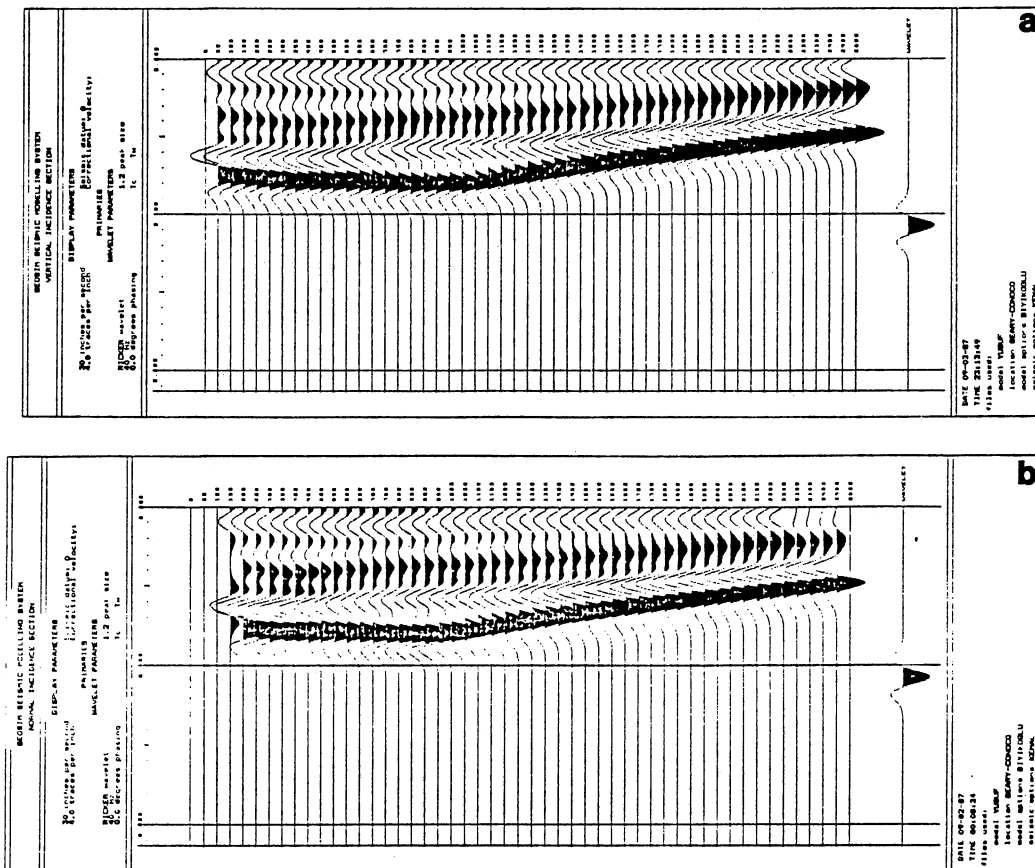


Figure 33. Seismic Response of the Geologic Model for Frequency 40 Hz: a) Vertical incidence b) Normal Incidence

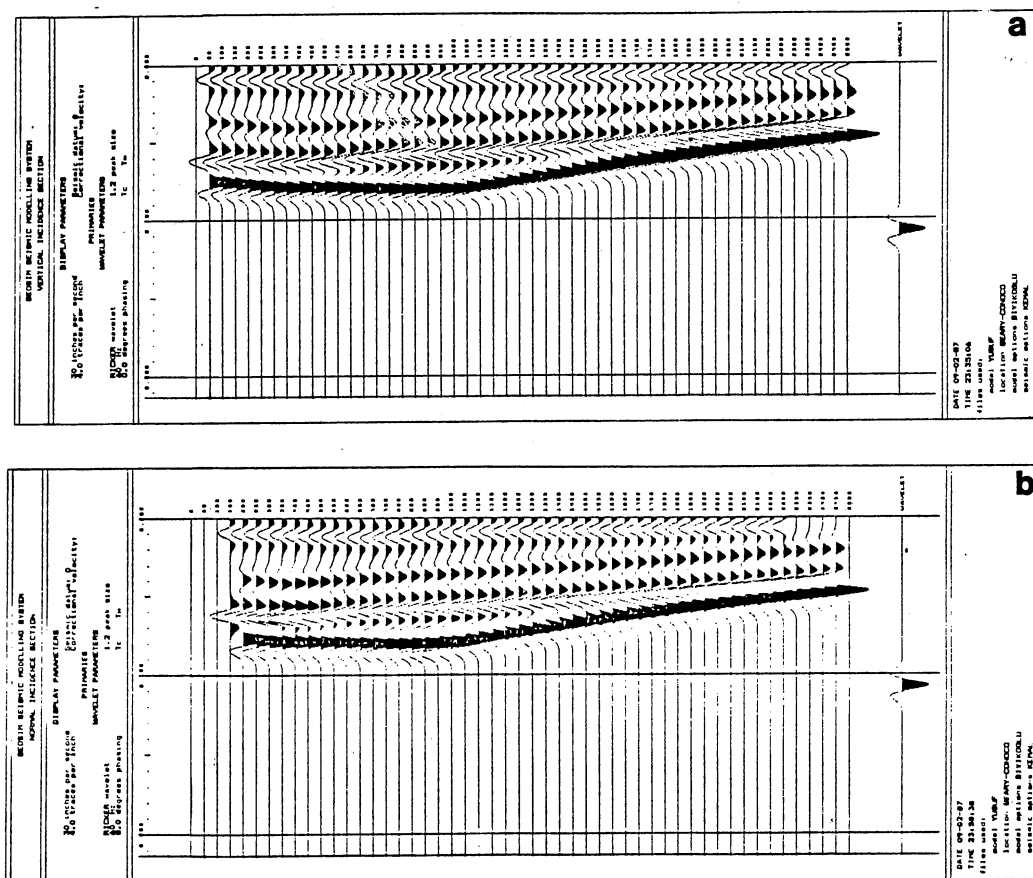


Figure 34. Seismic Response of the Geologic Model for Frequency 60 Hz: a) Vertical incidence b) Normal Incidence

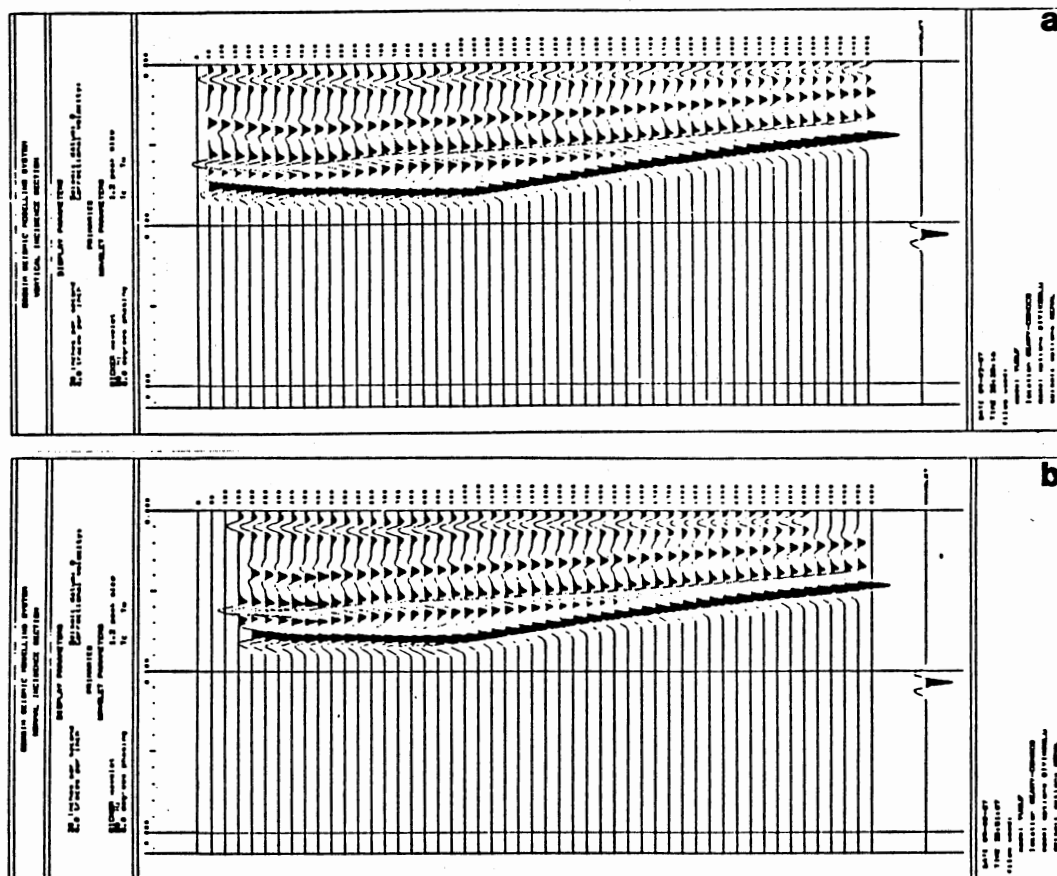


Figure 35. Seismic Response of the Geologic Model for Frequency 80 Hz: a) Vertical incidence b) Normal incidence

APPENDIX B

**LIST OF LOGS AND SYNTHETIC SEISMOGRAMS
FOR EASTERN DEWEY COUNTY**

TABLE I
FILE, COMPANY, AND WELL NAMES USED TO
CONSTRUCT GEOLOGIC CROSS SECTIONS
OF EASTERN DEWEY COUNTY

<u>FILE NAME</u>		<u>COMPANY</u>	<u>WELL NAME</u>
<u>A1-A2</u>			
YUSUF-23	(F1-F2)	Champlin Expl.	Thompson B #1
YUSUF-2		Unit Drilling	Squire #1
YUSUF-3	(E1-E2)	Woods Petro.	Moldrup #25-2
YUSUF-4		Michigan-Wisconsin	Duke #1
YUSUF-5	(D1-D2)	Southland Royalty	Ward #1-1
<u>B1-B2</u>			
YUSUF-6		Hickerson Oil	Robertson #1
YUSUF-24	(F1-F2)	Enserch Expl.	Prophet #1
YUSUF-9	(E1-E2)	Calvert Drilling	Addis #1
YUSUF-11	(D1-D2)	McCulloch Oil	L.L.Light #1-34
YUSUF-12		Brock Hydrocarb.	Blackwomen #1-17
<u>C1-C2</u>			
YUSUF-13		Sunray DX Oil	Frans #1
YUSUF-14		Amoco Prod.Co.	Frans A Unit #1
YUSUF-15		Fossil Oil & Gas	Rice #1-31
YUSUF-16		Apache Corp.	Blane Simon Unit #1
YUSUF-17	(D1-D2)	Lvo Corp.	P. Wills #1
<u>D1-D2</u>			
YUSUF-5	(A1-A2)	Southland Royalty	Ward #1-1
YUSUF-18		Calvert Drilling	Clark #1
YUSUF-11	(B1-B2)	McCulloch Oil	L.L.Light #1-34
YUSUF-19		Ladd Petroleum	B.F.Evans #2
YUSUF-17	(C1-C2)	Lvo Corp.	P.Wills #1
<u>E1-E2</u>			
YUSUF-20		TXO	Spies #1
YUSUF-3	(A1-A2)	Woods Petro.	Moldrup #25-2
YUSUF-9	(B1-B2)	Calvert Drilling	Addis #1
YUSUF-22		Hall-Jones	Pansy Beck #1
<u>F1-F2</u>			
YUSUF-23	(A1-A2)	Champlin Expl.	Thomson B #1
YUSUF-24	(B1-B2)	Enserch Expl.	Prophet #1
YUSUF-25		Mobil Oil	M.V.Herring #1
YUSUF-26		Mobil Oil	C.S.Dobbins #1

APPENDIX C

INTERPOLATED LOG SECTIONS AND TWO-DIMENSIONAL
SYNTHETIC SEISMIC MODELS FOR CROSS
SECTIONS A1-A2 THROUGH F1-F2

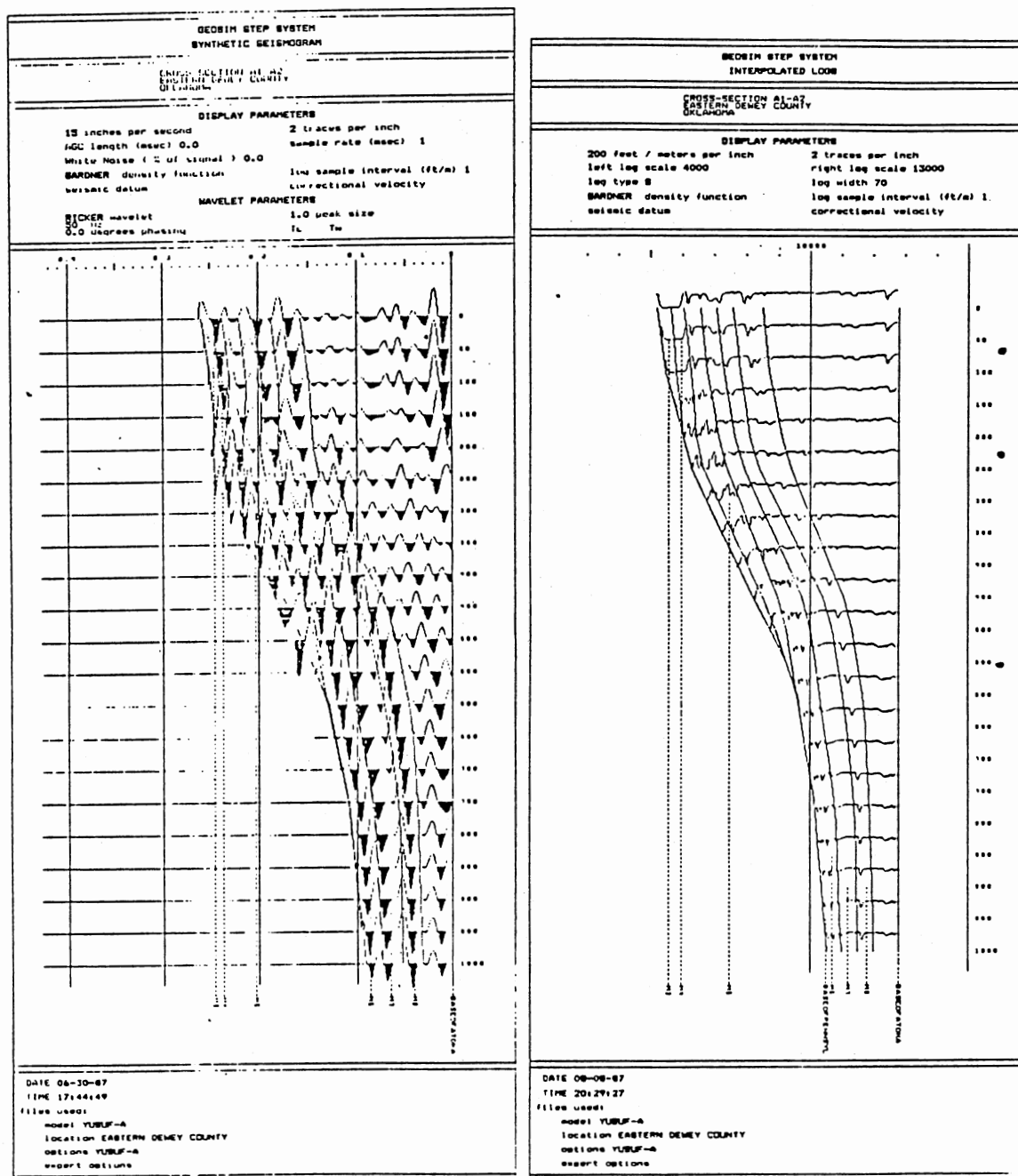


Figure 38. Interpolated Log Section and Two-dimensional Synthetic Seismic Model for Cross Section A1-A2 of Eastern Dewey County

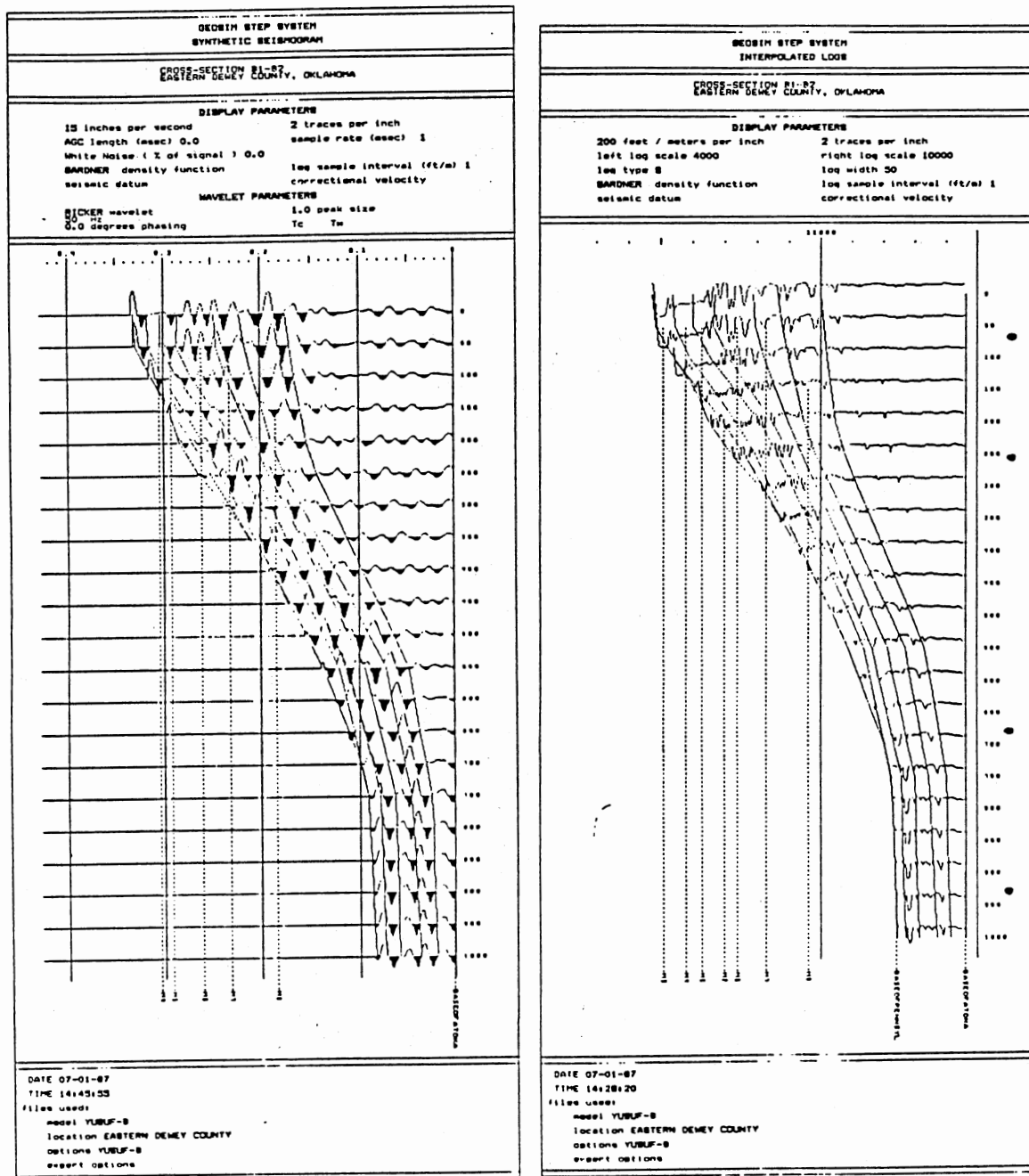


Figure 39. Interpolated Log Section and Two-dimensional Synthetic Seismic Model for Cross Section B1-B2 of Eastern Dewey County

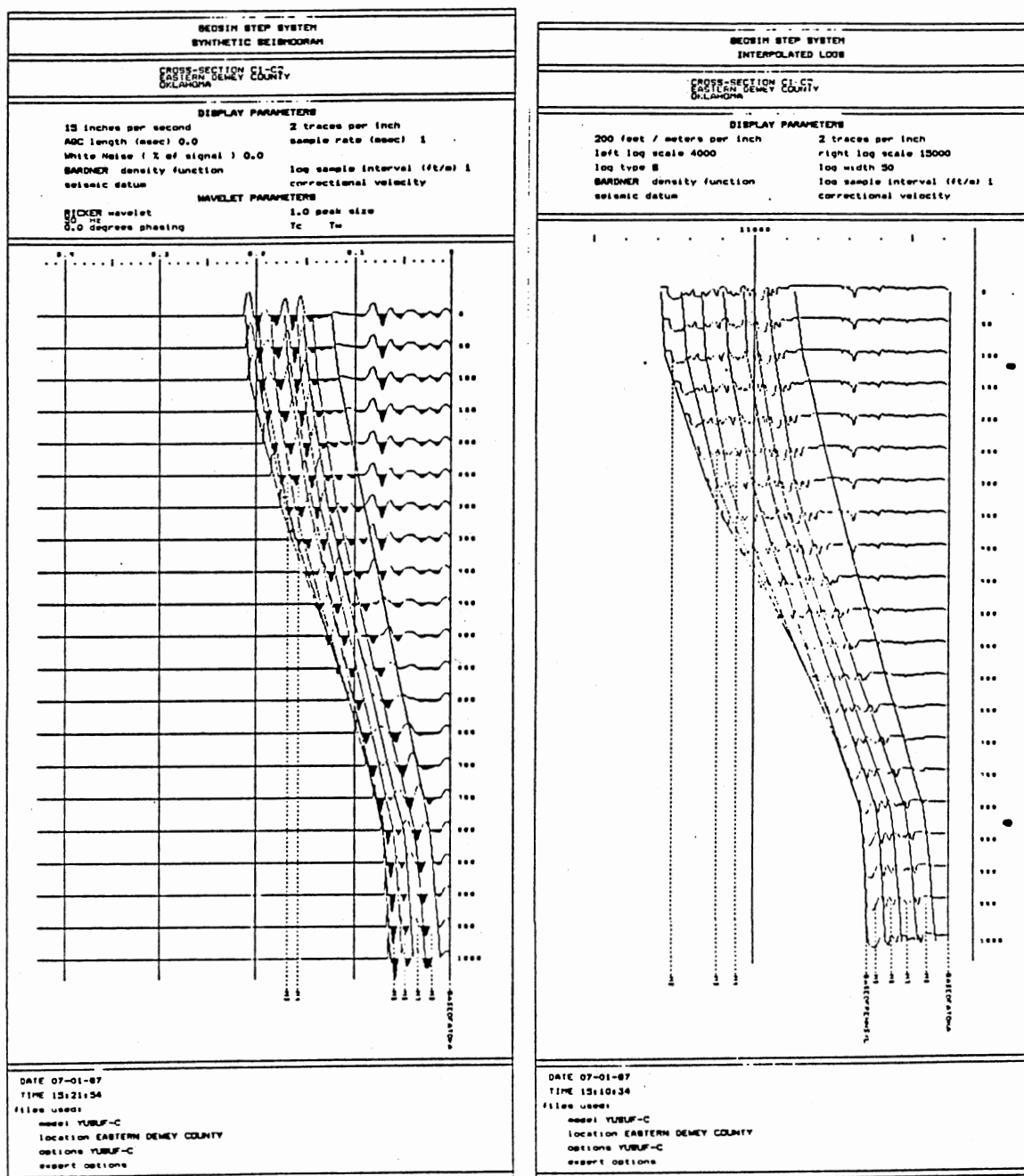


Figure 40. Interpolated Log Section and Two-dimensional Synthetic Seismic Model for Cross Section C1-C2 of Eastern Dewey County

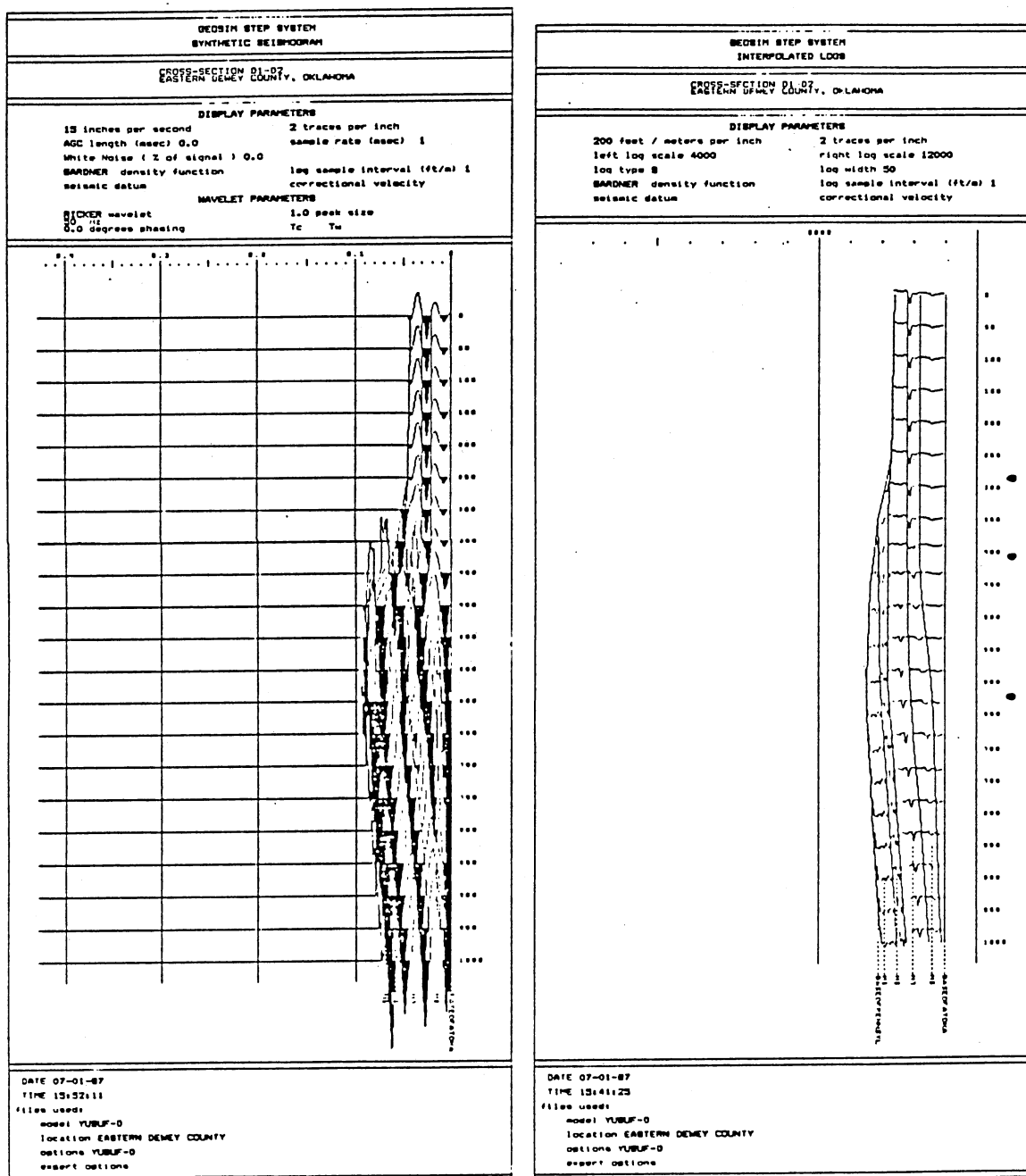


Figure 41. Interpolated Log Section and Two-dimensional Synthetic Seismic Model for Cross Section D1-D2 of Eastern Dewey County

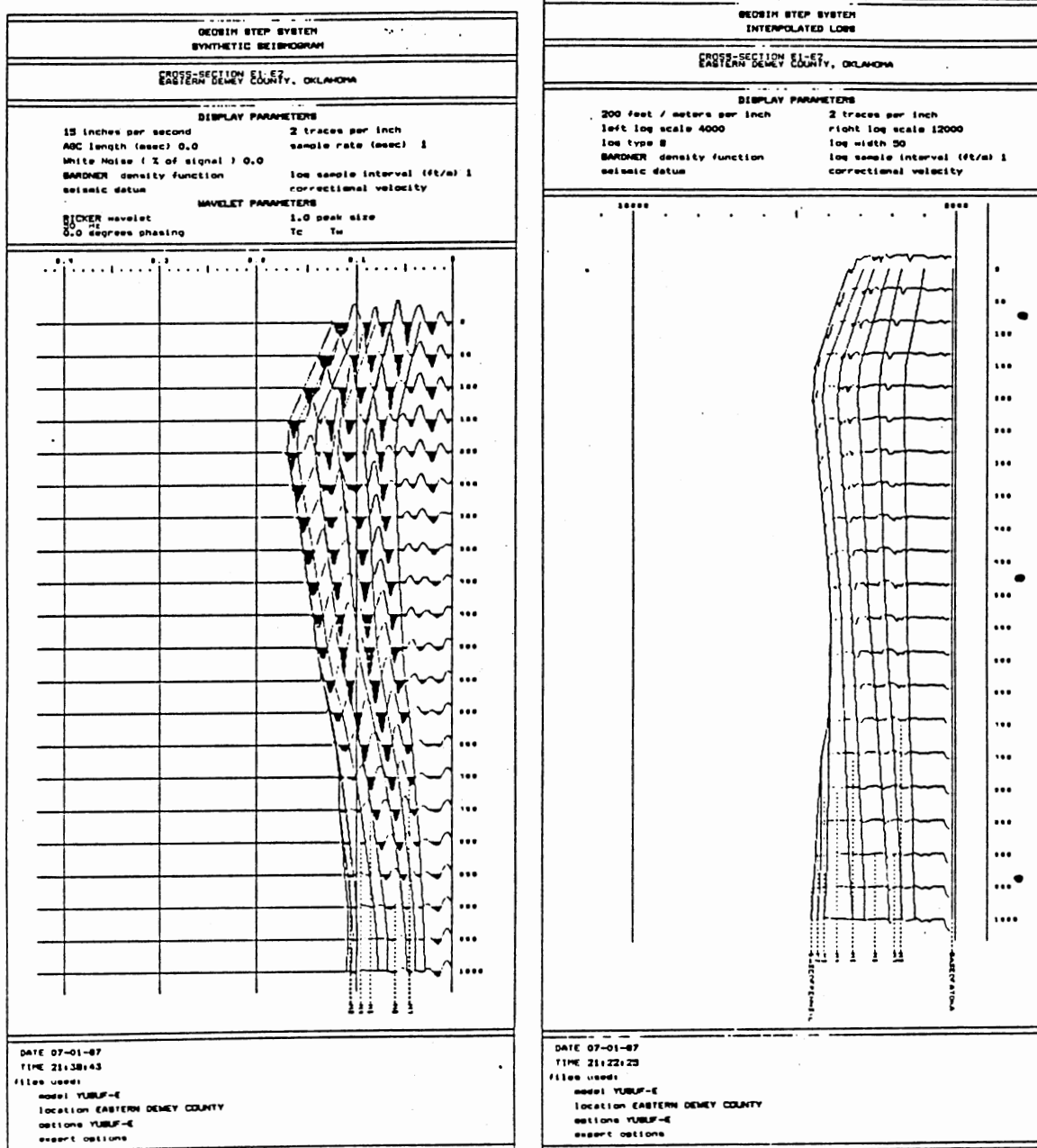


Figure 42. Interpolated Log Section and Two-dimensional Synthetic Seismic Model for Cross Section E1-E2 of Eastern Dewey County

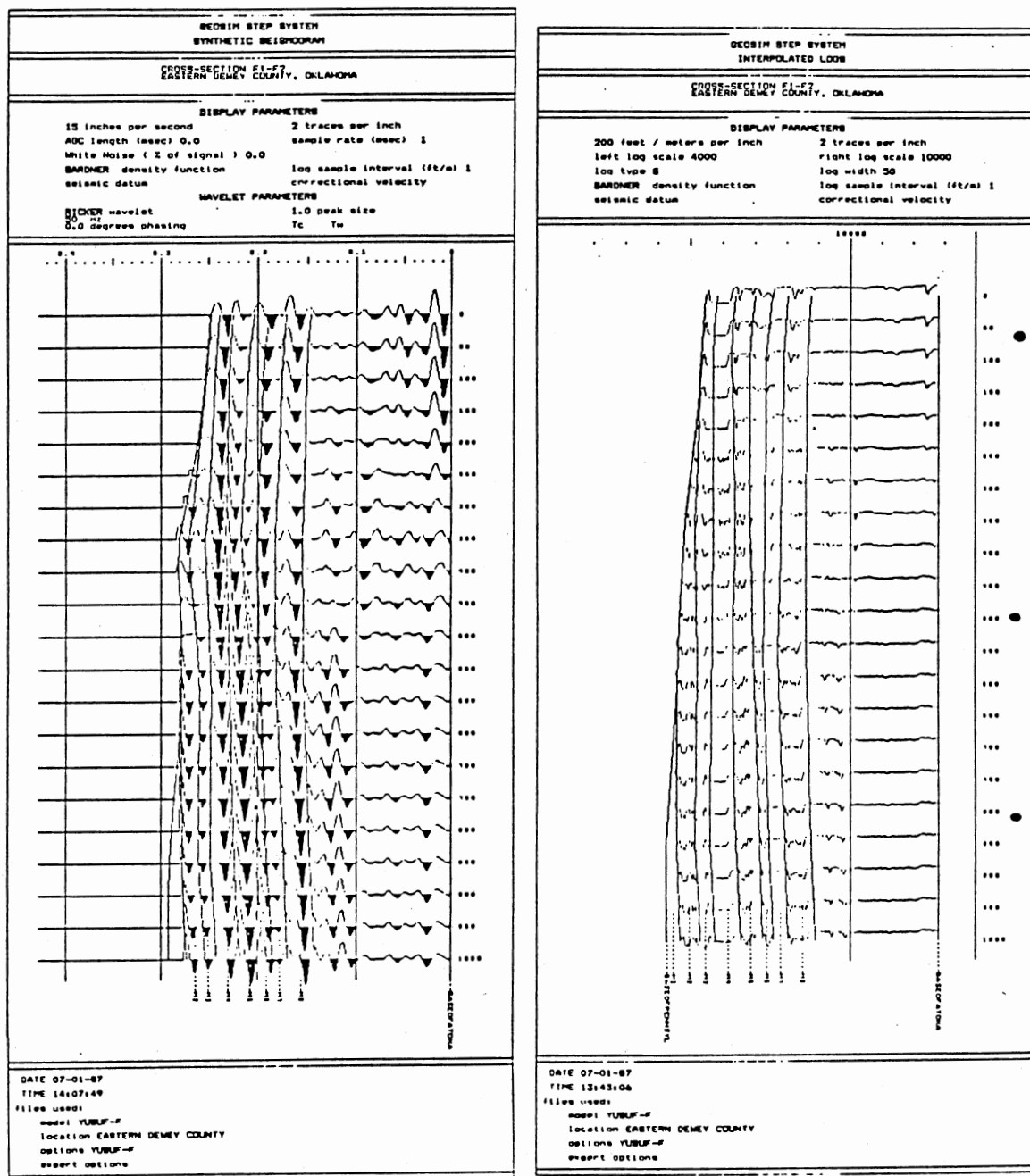


Figure 43. Interpolated Log Section and Two-dimensional Synthetic Seismic Model for Cross Section F1-F2 of Eastern Dewey County

APPENDIX D

OVERVIEW OF BASIC SEISMIC
PRINCIPLES

OVERVIEW OF BASIC SEISMIC PRINCIPLES

Basic Seismic Principles

A simplified view of the seismic method can be demonstrated by setting up an energy source, transmitting this source into the subsurface formations, and then recording the echoes as the energy is reflected from interfaces between formations.

The seismic waves that are transmitted through the earth consist of alternating compressions and dilatations. When these waves travel through an elastic and homogeneous medium, the particles of the medium are first compressed and then become farther apart during dilatation. Figure 44-a shows the particle motion for a compressional wave (P wave) passing through an elastic, homogeneous medium. Waves also cause particle motion at right angles to the direction of propagation; these are caused by shear or transversal waves (S waves). Figure 44-b shows the particle motion for a shear or transversal wave. In addition, there are other types of waves that travel along the earth's surface: Rayleigh waves, which travel along the free surface with elliptical particle motion (Figure 44-c), and Love waves, which have transversal particle motion, and occur in a low-speed surface layer overlying a high speed layer.

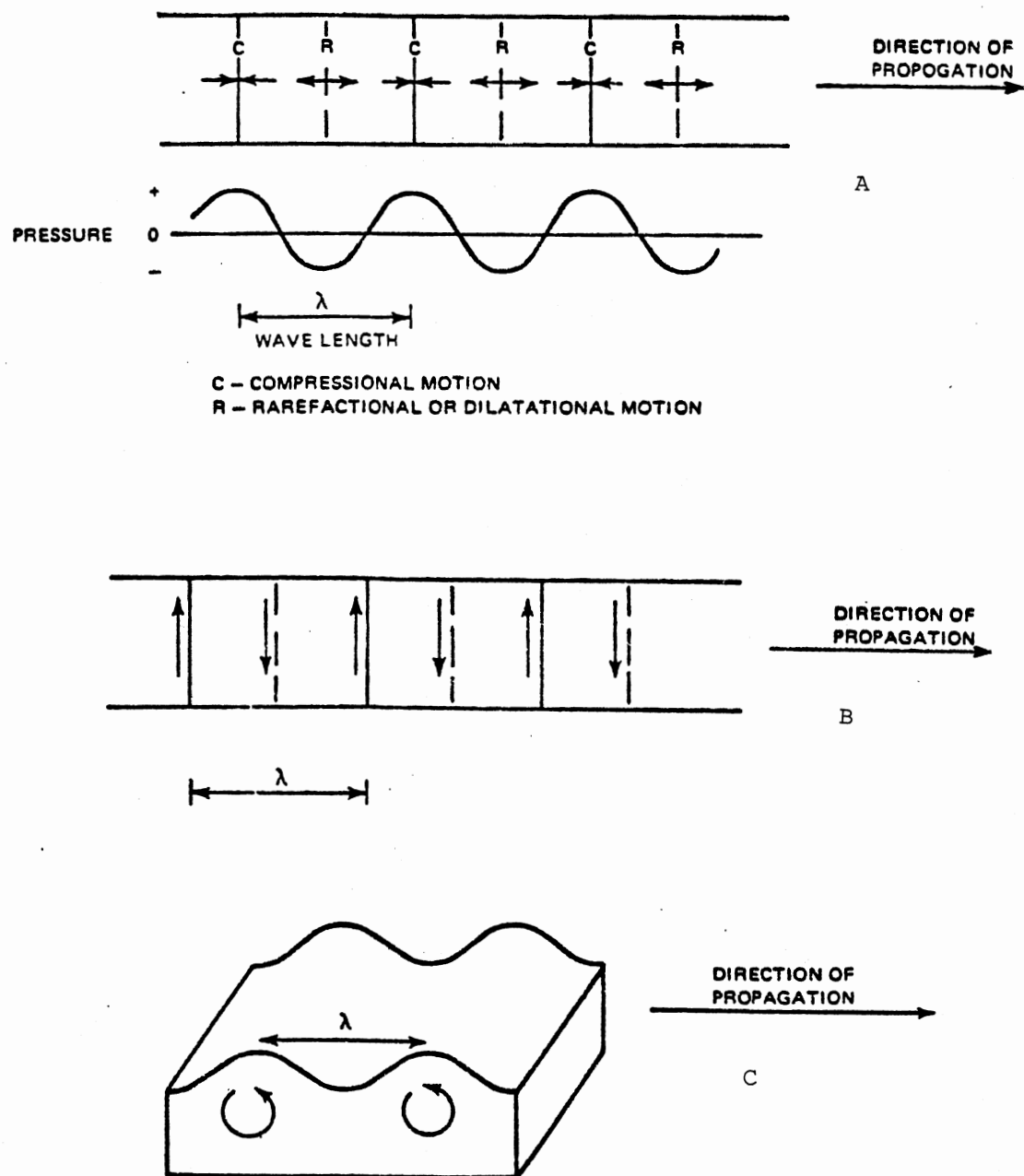


Figure 44. Particle Motion of Waves

- A) Particle motion of P waves
 - B) Particle motion of S waves
 - C) Particle motion of Rayleigh waves
- (From McBeath, 1981)

P waves travel in a solid at a higher speed than S waves, therefore, their reflection times are much shorter than S waves' reflection times. On land, the geophones used in seismic prospection are designed specifically for the P waves and do not respond to S waves. P waves are the dominant type of waves associated with seismic reflection energy.

The seismic reflections that return to the surface depend on the angle of incidence at which a ray strikes each layer, and the acoustic impedance, which is given by the product of density and velocity, contrast across each reflecting boundary. As it has been formulated by Snell (1621) and referred to in numerous books and articles, Snell's law states that seismic energy travels the fastest path, not the shortest path, between two points. This law also states that when a ray propagates (Figure.45) from one medium with velocity V_1 , to another medium with velocity V_2 , its direction of propagation is:

$$\frac{\sin i}{\sin r} = \frac{V_1}{V_2}$$

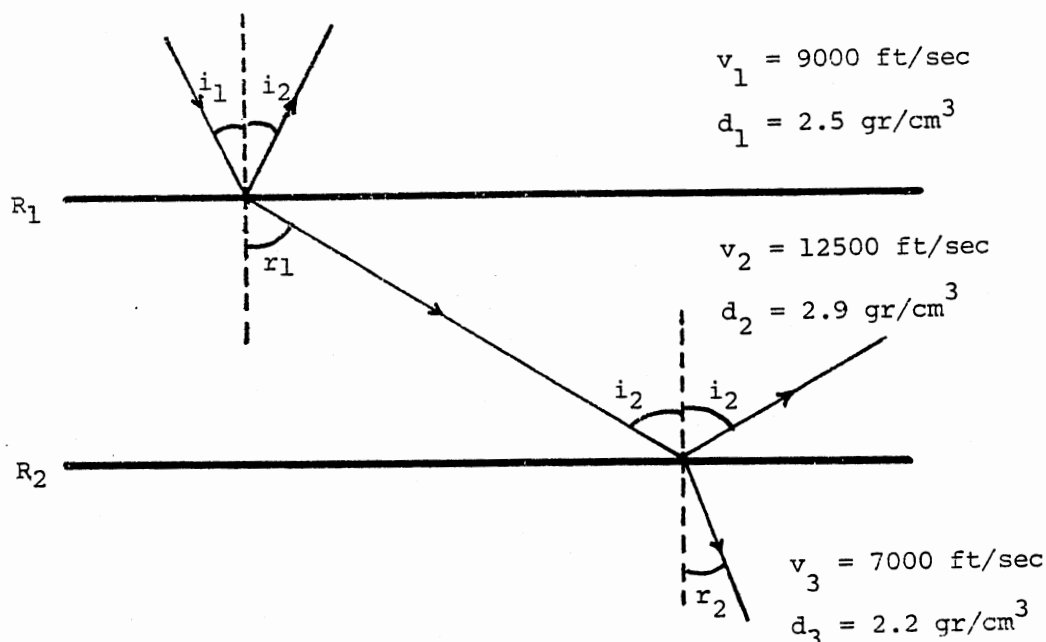
Where:

i : incidence angle

r : refracted angle

V_1 : velocity of first medium

V_2 : velocity of underlying medium



Snell's Law:

$$\frac{\sin i_1}{9000} = \frac{\sin r_1}{12500} = \frac{\sin i_2}{12500} = \frac{\sin r_2}{7000} = p$$

Acoustic impedance: $A = v \cdot d$

$$A_1 = 9000 \cdot 2.5 = 22500$$

$$A_2 = 12500 \cdot 2.9 = 36250$$

$$A_3 = 7000 \cdot 2.2 = 15400$$

Reflection Coefficient: $R = \frac{A_n - A_{n-1}}{A_n + A_{n-1}}$

$$R_1 = \frac{36250 - 22500}{36250 + 22500} = +0.234$$

$$R_2 = \frac{15400 - 36250}{15400 + 36250} = -0.404$$

Figure 45. Snell's Law and Numerical Examples of Acoustic Impedance and the Reflection Coefficient

If a series of horizontal layers, this equation can be written as:

$$\frac{\sin i}{v} = p$$

Where:

V : velocity

p : raypath constant.

If the incidence angle is greater than critical angle, total reflection occurs.

The incident energy is divided between the reflected and transmitted waves. The amount that is reflected is associated with the observed amplitude for each reflection on the recordings. The reflected amplitude is controlled by the reflection coefficient, which is defined by Dobrin (1966, p. 41) as the square root of the ratio of reflected energy in a P wave to the incident energy at a boundary. The amount of reflected energy in this boundary is dependent upon the acoustic impedance, which is the product of density and velocity, contrast of each layer, and has a value between +1 and -1 for incident angles which are less than critical.

Reflection coefficient is computed from:

$$R = \frac{d_2 v_2 - d_1 v_1}{d_2 v_2 + d_1 v_1} = \frac{A_2 - A_1}{A_2 + A_1} = \left(\frac{E_r}{E_i} \right)^{1/2}$$

Where:

R : reflection coefficient

E_r : reflected energy

E_1 : incident energy

d_1 : density of the first layer

V_1 : velocity of the first layer

d_2 : density of underlying layer

V_2 : velocity of underlying layer

$A = (d) \cdot (V)$: acoustic impedance

Peterson and others (1955) showed that this formula can be approximated as:

$$R = \frac{1}{2} \ln \frac{d_1 V_1}{d_2 V_2}$$

Gardner and others (1974) gave the empirical relationship between density and velocity as:

$$d = 0.23 v^{0.25}$$

Combining Peterson's and Gardner's equations we obtain:

$$R = 0.625 \ln \frac{V_1}{V_2}$$

Rock density and velocity depend upon the intergranular elastic behavior of the mineral composition of the rock matrix, fluid content, cementation, porosity, and environmental pressure (Gardner et. al. 1974). Faust (1953) confirmed that density and velocity increase with an increase in age of formulations and depth of burial. Figure 46 shows density-velocity relationships in rocks of different lithology.

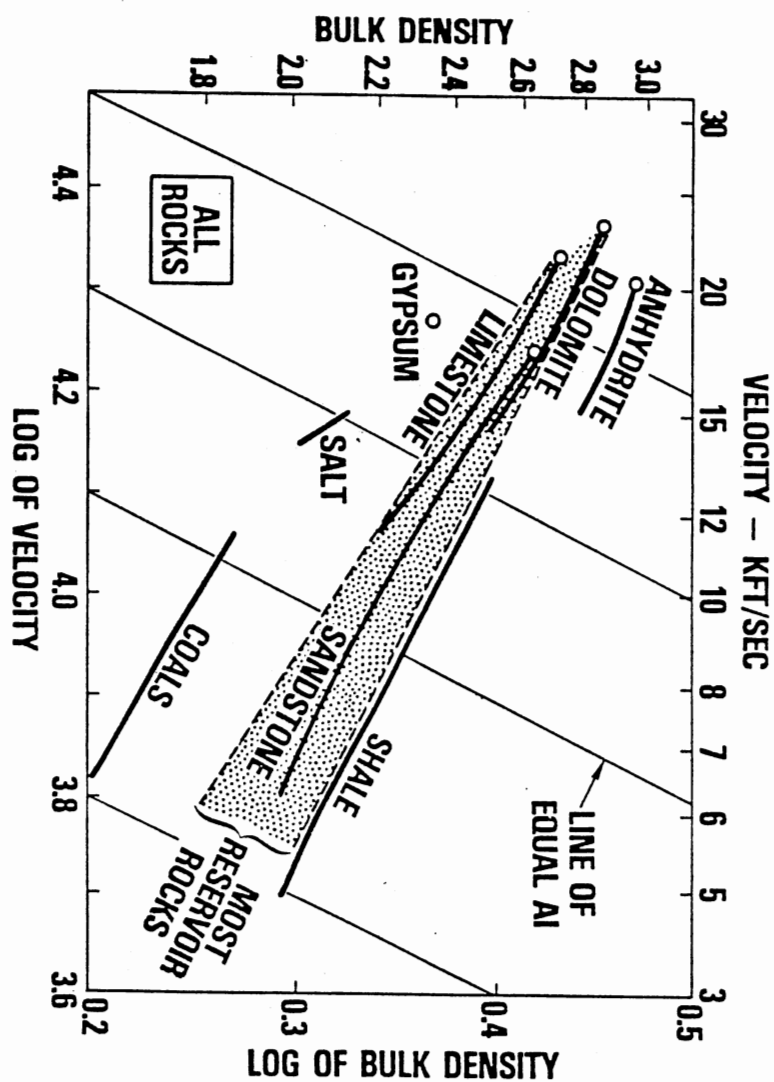


Figure 46. Density-Velocity Relationship in Rocks of Different Lithology and Acoustic Impedance Graph (From Gardner et. al. 1974)

The magnitude of the acoustic impedance contrast controls the magnitude of the reflection. In other words, the magnitude of reflections is a function of the acoustic impedance contrast; large reflections are produced by large impedance contrasts between layers. If the thicknesses of the units are large enough and/or the units have large impedance contrast, then the units can be easily identified on a seismic section. However, if the units are thin and/or the acoustic impedance contrast is lower, the units might not be seismically visible. Therefore, the acoustic impedance contrasts between the layer and the adjacent layers and the thickness of the layers are the two critical factors which determine whether or not the layers are visible on a seismic section.

Figure 47 is a schematic diagram showing the seismic visibility of a unit. The zone, separating visible and invisible zones, depends on the wavelet shape, frequency, the quality of amplitude preservation and the signal-to-noise ratio. In short the zone is dependent on the quality of the seismic data. Reflection coefficients are convolved with a propagating seismic wavelet to obtain a seismic trace.

A seismic wavelet propagates as an incident wave through different layers while each boundary of layers yields a reflected wave similar to the incident wave. The propagating wavelet, which is a symmetrical and relatively broad band, is a two-sided, zero-phase signal (Figure 48), which is ideal. Schoenberger (1974) indicated that these

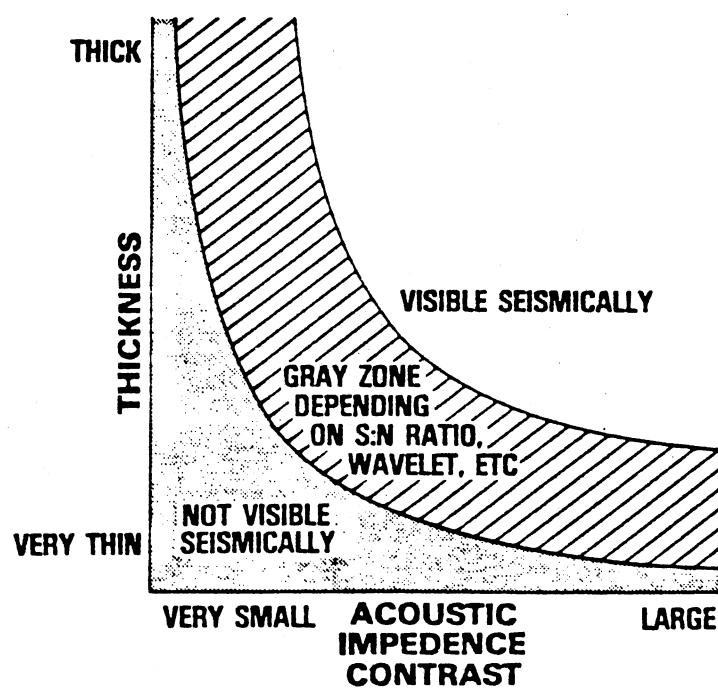


Figure 47. Schematic Graph Showing Seismic Visibility of a Unit (From Meckel and Nath, 1977)

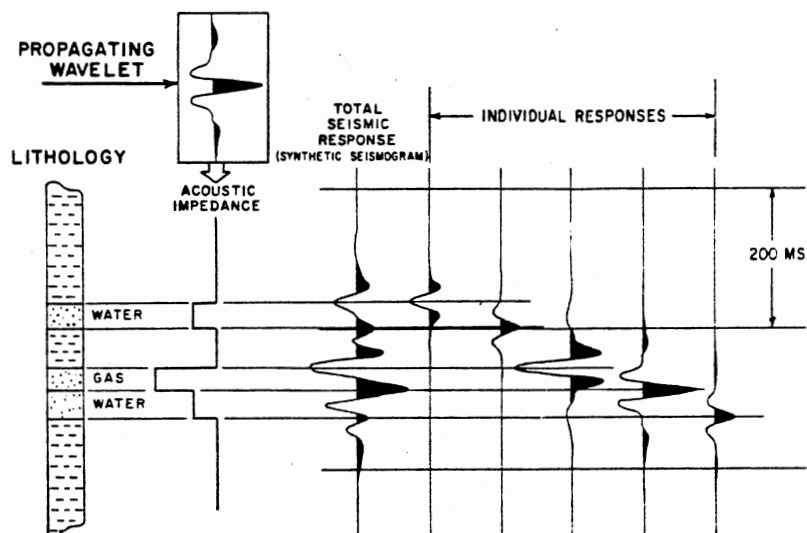


Figure 48. Relationship Between Lithology, Propagating Wavelet, and Seismic Response (From Dedman et. al. 1975 a-b)

two-sided zero-phase signals possess a superior degree of seismic response resolution. In addition, these signals provide a precise indication of reflector depth, reflection time, and reflector spacing. Unfortunately, in real conditions the wavelets are not symmetrical and total seismic response of the layers is seriously deteriorated. In figure 47, individual reflections associated with shale-water sand interfaces occur within a rapid time sequence so that the responding wavelets overlap. This produces the total seismic response which is the summation of the individual responses, and each waveform has some meaning that is related to acoustic impedance (Dedman and others, 1975 a,b).

Frequency, continuity of reflections, and amplitude are important parameters which are used to interpret a seismic section. For example, frequency, which is the reciprocal of period, is related to lateral changes in interval velocity. The continuity of a reflection gives information about depositional environment and process, and bed continuity. As it is explained by Sheriff (1975), the third parameter, amplitude, provides information about fluid content, lateral variation in lithology, layer thickness and spacing, and acoustic impedance of layer boundaries. Figure 49 and Table 2 show factors affecting seismic amplitudes. The type of pore fluid can significantly change the reflection amplitude depending on the acoustic impedance contrast with the surrounding lithologies. Principally, because of the changes in pore fluid, three modifications in reflection amplitude

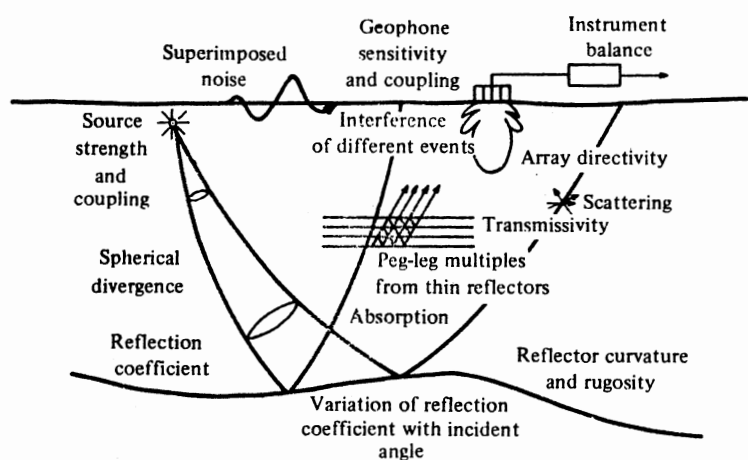


Figure 49. Factors Which Affect Amplitude
(From Sheriff, 1975)

TABLE II
FACTORS AFFECTING SEISMIC AMPLITUDES
(From Sheriff, 1975)

Amplitude Factor	The effect					Comments
	is constant for entire record	increases with time	depends on offset	depends on frequency	contains subsurface information	
Source strength and coupling	yes yes			possibly		
Spherical divergence and raypath curvature		yes yes	slightly slightly		in a sense	
Absorption		yes		yes	probably	
Scattering						Background noise
Intervening interfaces		yes	slightly			
Peg-leg multiples		yes	slightly	yes	in a sense	
Superimposed noise		somewhat		in a sense		
Interference of events			usually	in a sense		
Attenuation in near surface	yes			possibly		
Geophone sensitivity and coupling	yes yes			possibly		
Array directivity	yes		yes	yes		
Instrumentation	possibly	possibly	possibly			
Reflection					yes	
Reflector curvature and velocity focusing		in a sense in a sense			structural in a sense	
Reflector sharpness and rugosity						Minor effect Minor effect
Incident angle			yes		yes	

response are; (1) increase in trough amplitude resulting in an amplitude anomaly bright spot, (2) decrease in peak amplitude resulting in a dim spot, and (3) a peak-to-trough change within a small distance resulting in polarity reversal (Figure 50) (Mackel and Nath 1977).

Internal friction, inelasticity, piezoelectricity, hysteresis, and thermoelectricity are physical factors in connection with absorption. Low frequencies are attenuated slower than high frequencies (Figure 51-a), therefore, absorption acts as a low-pass filter. Absorption decreases the amplitude of the propagating signal; the resulting frequency loss deforms the wavelet shape (Sheriff 1975). According to Huygen's Principle, if a P wave is not normal to the boundaries between adjacent regions, it will produce a series of P waves and S waves at each acoustic impedance changes. Energy which is converted into S waves also helps the loss of amplitude. Spherical divergence causes the greatest decrease in amplitude with propagating distance (Figure 51-b). The energy decreases as the inverse square of the propagating distance and this energy loss causes the loss of amplitude (Sheriff 1975).

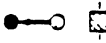

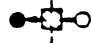
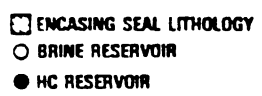
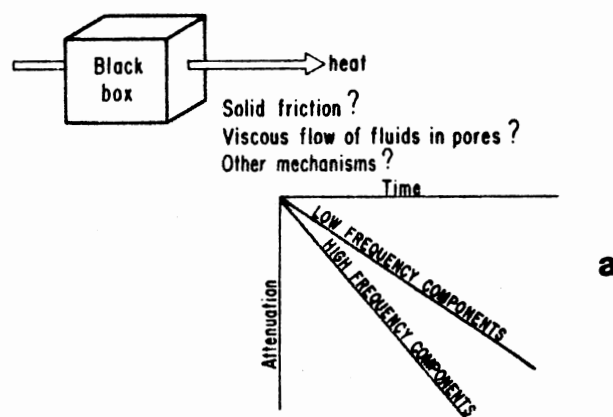
AI OF BRINE RESERVOIR IS:	ρV	AMPLITUDE CHANGE
① SMALLER THAN ENCASING LITHOLOGY		INCREASE IN TROUGH AMPLITUDE BRIGHT SPOT
① LARGER THAN ENCASING LITHOLOGY		DECREASE IN PEAK AMPLITUDE DIM SPOT
① SLIGHTLY LARGER THAN ENCASING LITHOLOGY		PEAK TO TROUGH POLARITY REVERSAL
ACOUSTIC IMPEDANCE OF:		
		

Figure 50. Variations in Amplitude Response
Due to Changes in Pore Fluid
(From Meckel and Nath, 1977)

ABSORPTION



SPHERICAL DIVERGENCE and RAY-PATH CURVATURE

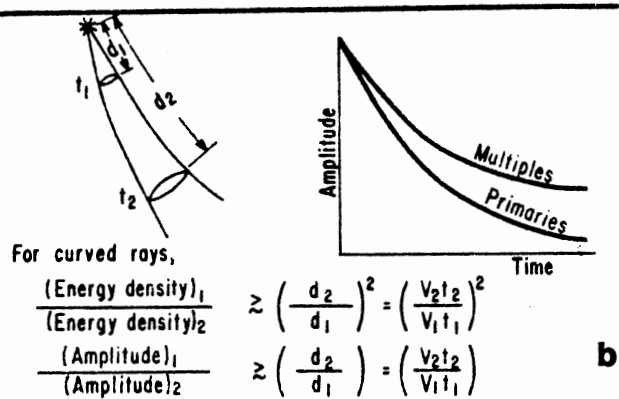


Figure 51. a) Absorption b) Spherical Divergence
(From Sheriff, 1975)

Horizontal Resolution

A Fresnel zone (Figure 52), which is a concept that controls horizontal resolution, is an area of a reflector between contact points with the wavefront. This area, which is principally responsible for the reflection event, is called the First Fresnel Zone (Figure 52). This zone returns energy to a receiving point on the surface so that constructive interference takes place at the receiving point. In the vertical incidence case (Figure 52-b), the data obtained is not information about the reflector at point P, but is an average over the whole Fresnel zone.

Figure 53-a and b show nomograms for determining Fresnel zone radii. In Figure 53-a, a straight line connecting the frequency and two-way travel time intersects the central line at the same point as a straight line connecting the velocity and the radius of the Fresnel zone. For example, a reflection at 2.0 seconds with a 30 Hz component corresponds to a Fresnel zone radius of 1290 ft. for an average velocity of 10 kilofeet per second (kft/s).

The size of the Fresnel zone depends on wavelength frequency (Figure 52 c) and the depth of the reflector. The radius of the Fresnel zone can be calculated using the following mathematical relations:

$$R = \frac{1}{2} (\lambda h)^{1/2} = \frac{1}{2} v \left[\frac{t}{f} \right]^{1/2}$$

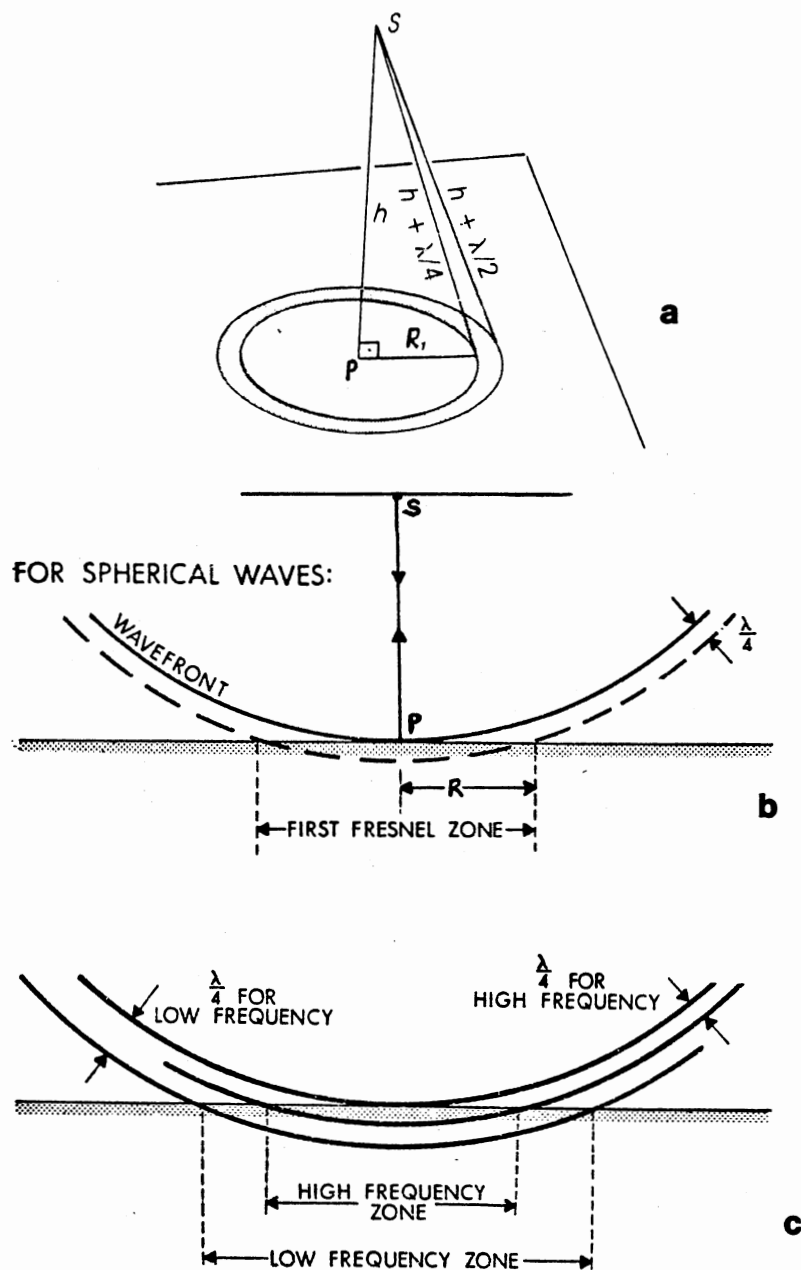


Figure 52. Fresnel Zone

- a) Source and receiver at S . The first Fresnel zone radius is R . The second Fresnel zone is the shaded annular ring. The wave-length is λ .
- b) First Fresnel zone for spherical waves reflected from interface
- c) Fresnel zone decreases with increasing frequency

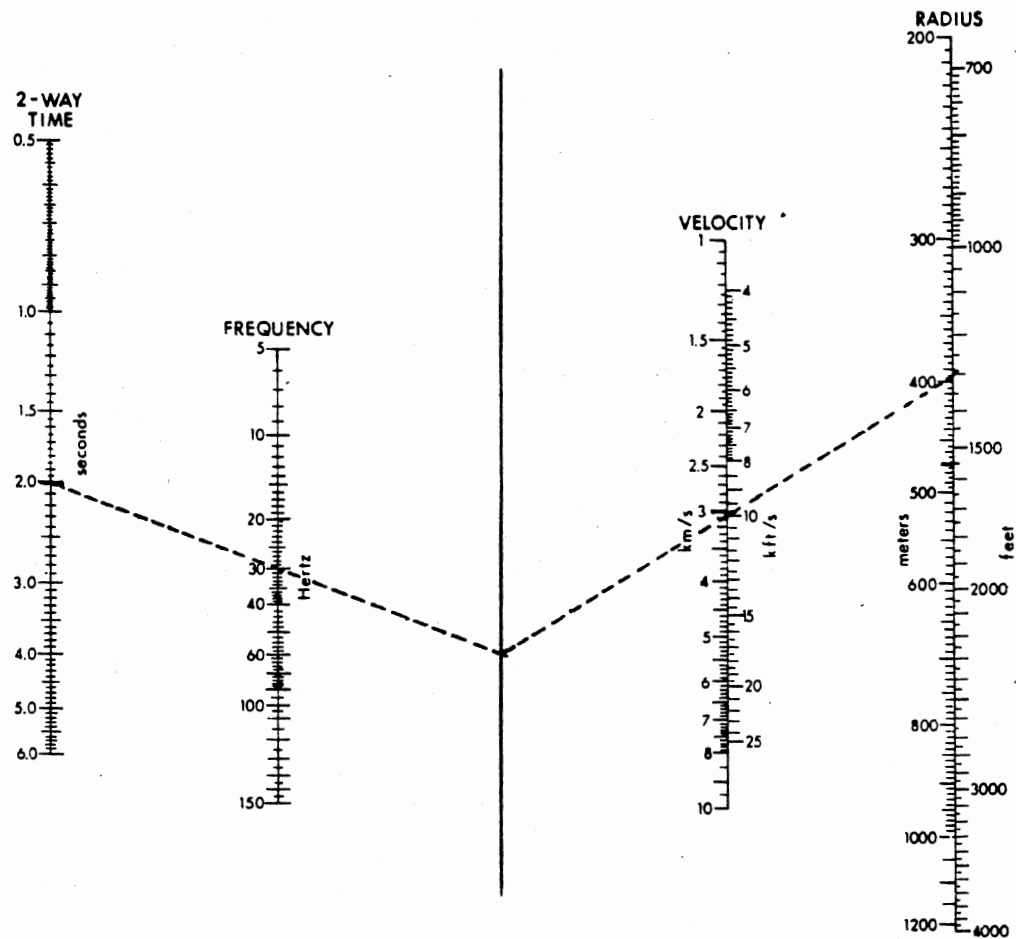


Figure 53-a. Nomogram for Fresnel Zone Radii
(From Sheriff, 1984)

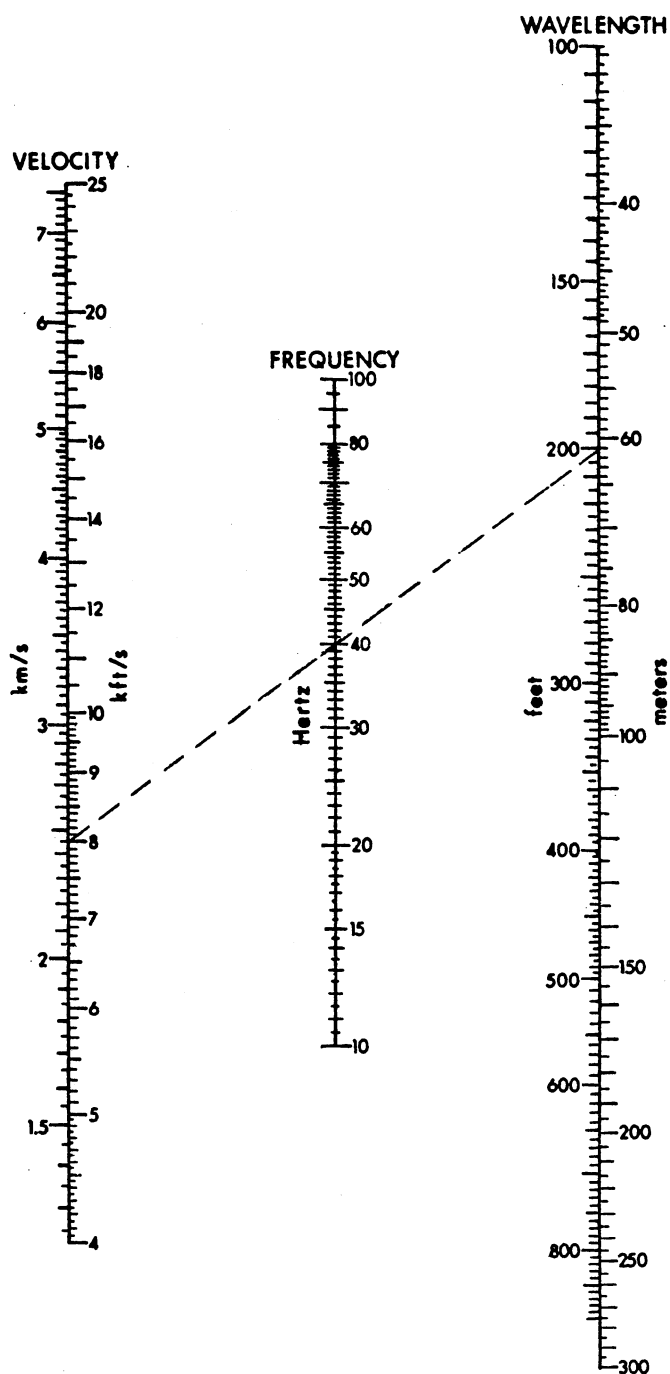


Figure 53-b. Nomogram; Relationship Between Velocity, Frequency, and Wavelet
 Example: $v=8\text{kf/sec}$,
 $f=40\text{ Hz}$, $\lambda=200\text{ ft}$
 (From Sheriff, 1980)

Where:

R : radius of Fresnel zone

λ : wavelength = V/f

h : depth

V : velocity

t : the arrival time

f : frequency

For a high frequency wave, the wavelength and Fresnel zone are small, and more seismic detail can be detected. Figure 54 shows the seismic signature of some sandstone bodies. When the widths of the sandstone bodies are narrower than the Fresnel zone, the seismic signature loses all reflection character and appears as a point diffraction.

Vertical Resolution

Vertical resolution is the ability to distinguish the reflections from the top and bottom of a layer. Vertical resolution depends on the sharpness of the wavelet; the sharper the pulse, the thinner the layer. The sharpness of the wavelet depends on its bandwidth. Better bandwidth is obtained by using a good source, spread geometry, and recording filters. The sharpness also depends on the phase, the most accurate is the zero-phase. A zero-phase wavelet is symmetrical about a peak (black) for a normal (positive) wavelet, and about a trough (white) for a reverse (negative) wavelet (Anstey, 1980) (Figure.55). Vertical resolution also depends upon the distance between the layers compared to

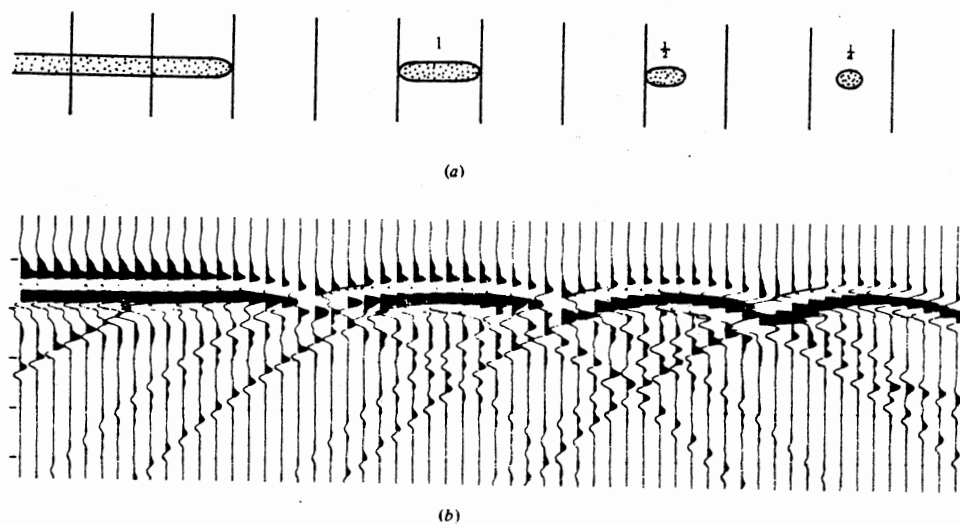


Figure 54. Reflections from Sandstone Bodies of Varying Widths Expressed in Terms of the Width of the Fresnel zone
(From Neidel and Poggiagliolmi, 1977)

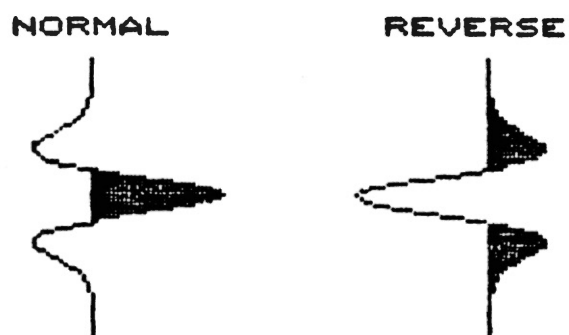


Figure 55. **Zero-phase** (Symmetrical) Normal (Positive), and Reverse (Negative) Wavelets

the wavelength. Widess (1973) stated that the limit of vertical resolving power is $1/8$ of the wavelength of the dominant frequency, which can be estimated by measuring the peak-to-peak or trough-to-trough length of individual high-amplitude reflections, of a source (Figure 56). When layer thickness b is large enough between each of the two interfaces, individual reflected wavelets are fully separated. When the thickness of the layer is equal to $1/8$ of the wavelength, the two wavelets superpose to form a single wavelet that has anomalously high amplitude. This thickness has been termed the critical resolution thickness or tuning thickness (Figure.57). If the layer thickness becomes thinner than tuning thickness, all resolution information become weaker and disappears.

Figure 58 shows the limit of vertical resolution for a single low-velocity thin bed using a 20 Hz Ricker and an 8 to 32 Hz Butterworth band-pass wavelet to compute the seismic models. A maximum amplitude takes place at the tuning thickness where the peak-to-trough separation becomes invariant (Neidell and Poggiagliolmi, 1977). Figure 59 illustrates the seismic responses of the thin and thick transitional bed contacts. The amplitude of a reflected wave decreases as the thickness of the transitional zone of an acoustically thin bed increases. Also the amplitude decreases as the thickness of the transitional zone of an acoustically thick bed becomes thicker (Meckel and Nath, 1977).

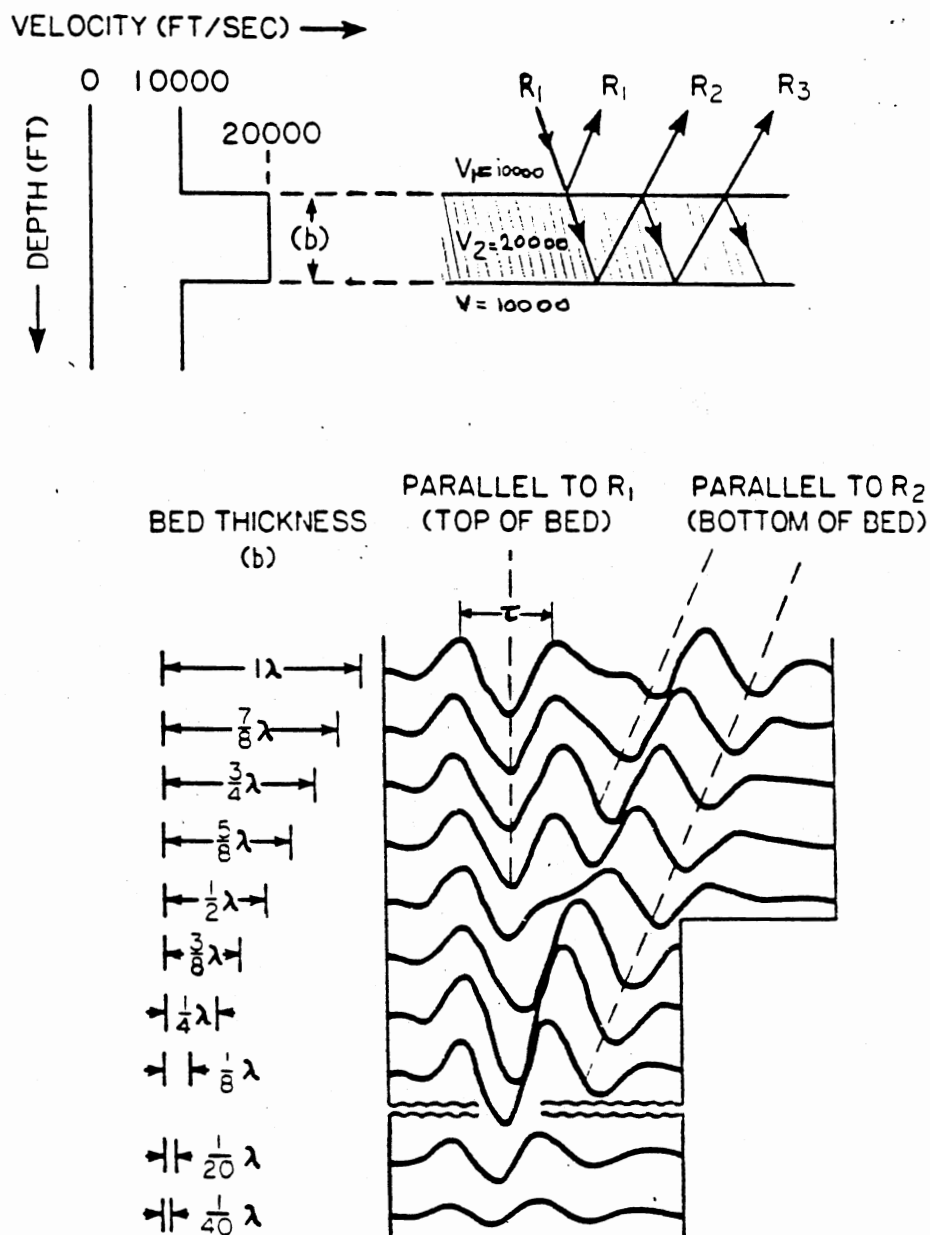


Figure 56. Widess Diagram Illustrating Limit of Vertical Resolution for a High Velocity Layer

b: thickness of bed

τ : predominant period of incident wavelet

λ : wavelength of the propagating wavelet

(From Widess, 1973)

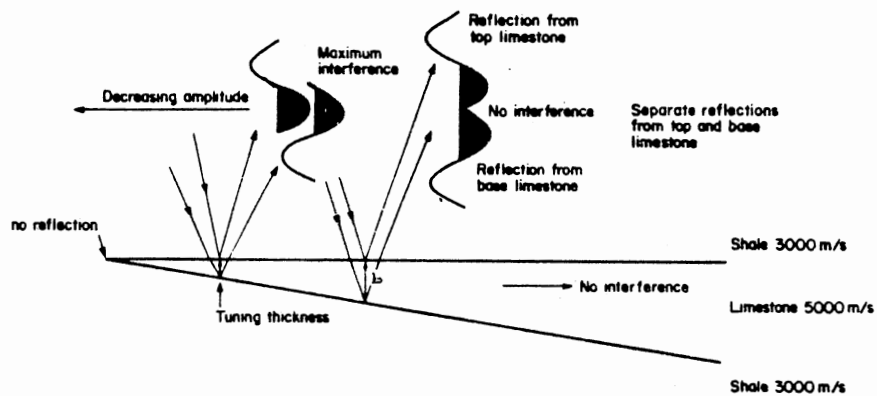


Figure 57. Limit of Vertical Resolution
(From Badley, 1985)

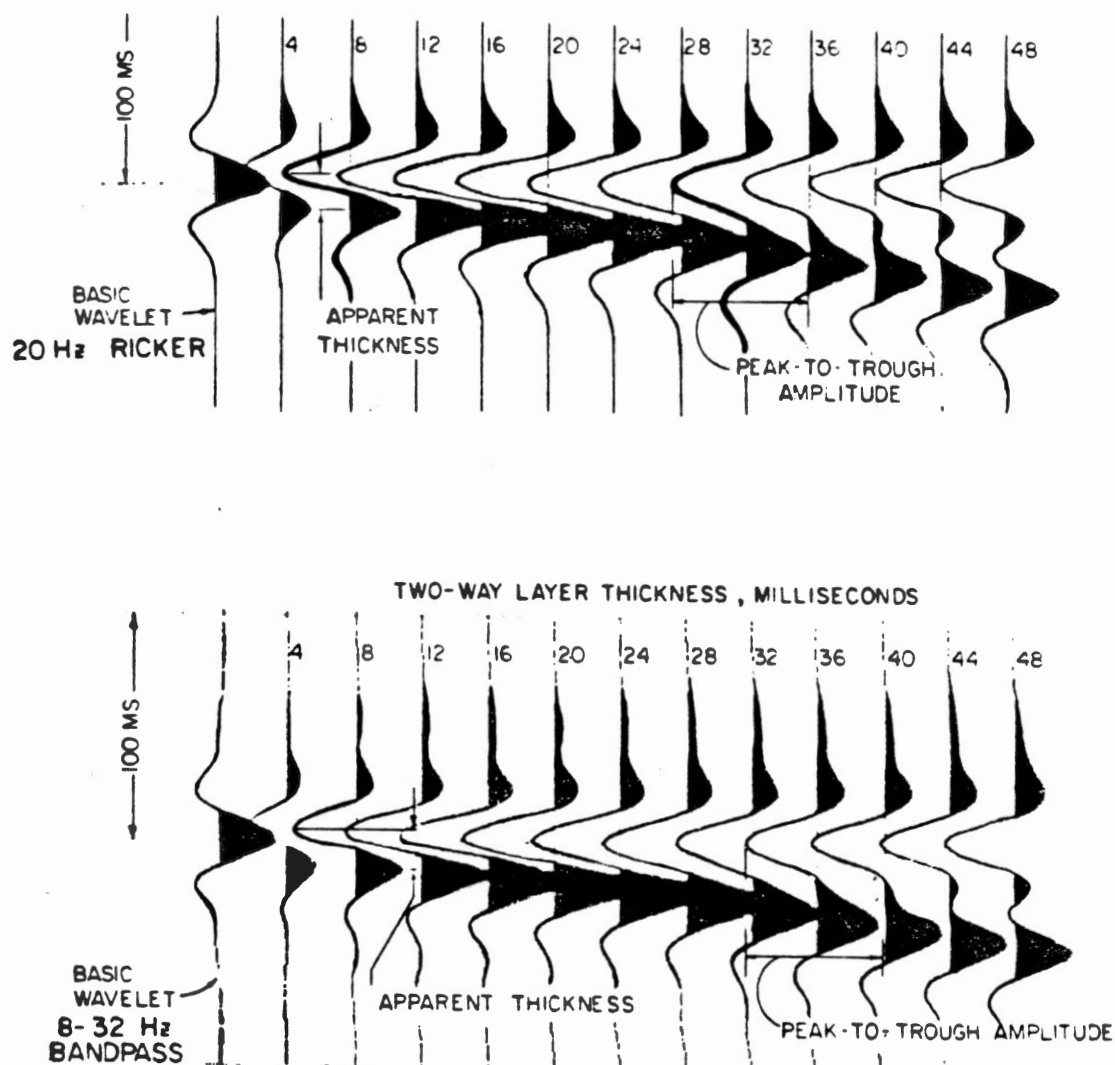


Figure 58. The Limit of Vertical Resolution for a Thin Bed Using Two Different Wavelets (From Meckel and Nath, 1977)

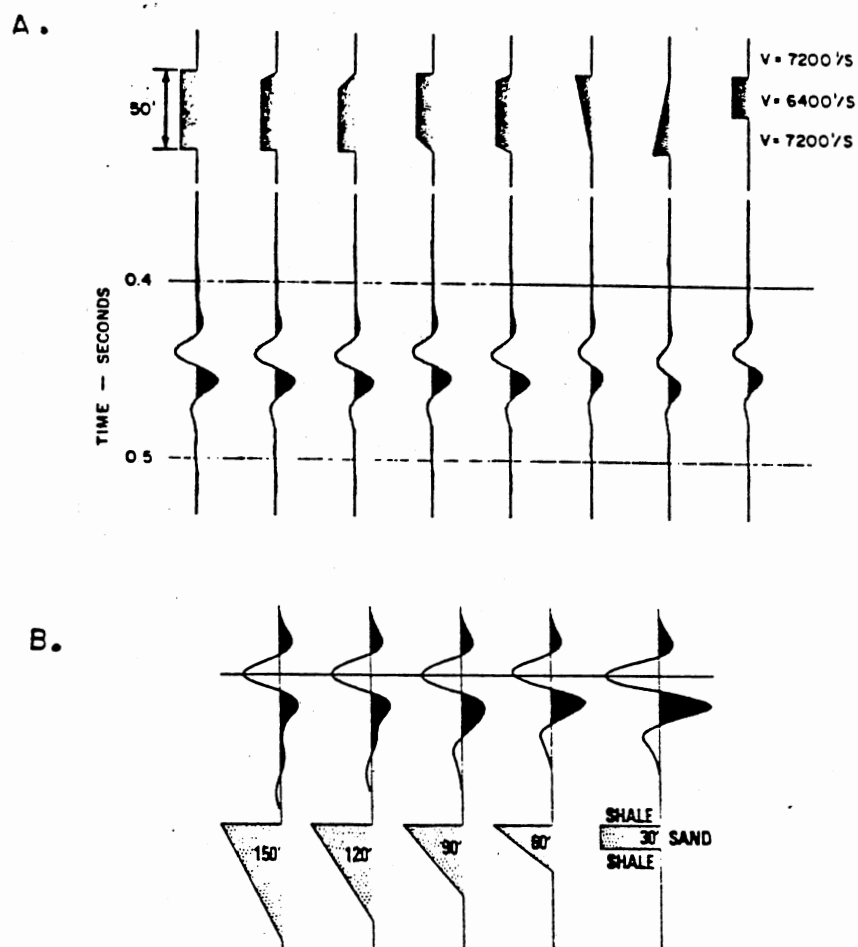


Figure 59. Seismic Response for Different Types of Bed Contacts for:
 A) Thin and B) Thick
 Low Velocity Beds; 10 to 40
 Hz Butterworth Bandpass Wavelet
 (After Meckel and Nath, 1977)

The threshold of resolution depends on: 1) the signal-to-noise ratio, 2) the predominant frequency of the incident wavelet, 3) the form and duration of the incident wavelet, 4) the wavelet shape, and 5) the seismic equipment used (Widess 1977).

The shape, thickness, velocity, and density of a bed, variation in attenuation of the recorded reflections, frequency, amplitude, continuity, vertical and lateral changes in acoustic impedance, wavelet shape and frequency range, Fresnel zone, and fluid content of the bed control the resolution and detection of a bed.

Wavelet Selection and Processing

Wavelet selection is an important step in seismic modeling. Figure 60 illustrates a geologic model of a sandstone layer and three seismic models that were obtained by using three different band-pass wavelets. The sandstone layer has relatively uniform thickness. The upper 60 feet of this sandstone is gas-saturated. The seismic response of this gas-sand is a bright spot (amplitude anomaly). It is impossible to see more stratigraphic detail in the first two seismic models due to low frequency wavelets. In the third model, the gas-sand/water-sand contact can be seen. The contact is seismically visible because of the higher frequency of the wavelet. Since the frequency of this wavelet is too high, the pseudo sand appears below the base of the sand. The wavelet frequency value between the A and

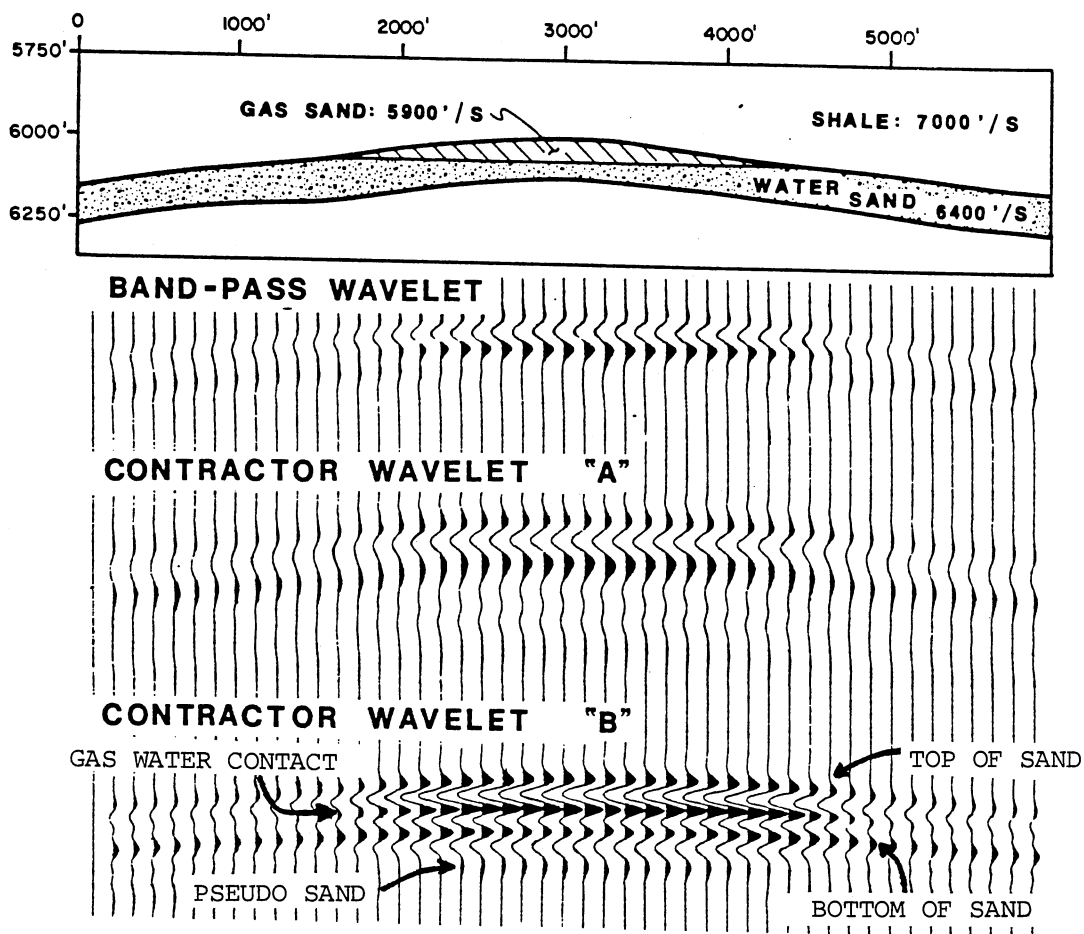


Figure 60. Seismic Response of Sandstone with Gas Cap
Using Three Different Wavelets
(From Schram et. al. 1977)

B values would best simulate the geologic model.

Figure 61 illustrates a geologic model of a horst block and two wave-theory simulated seismic models that show the importance of choosing the correct wavelet. In the first seismic model, a zero-phase wavelet is used. On the contrary, in the second model the nonsymmetrical complex wavelet is used. In the second model, a pinchout is seen at 3.3 seconds. The superposition of the incorrect wavelet and the slightly discordant geometry have caused the pinchout which does not exist.

Figure 62 illustrates four seismic sections which are differently processed, over the same bright spot. Sections a and c are processed conventionally without and with automatic gain control. The sections b and d are wavelet processed without and with automatic gain control. Figure 62-a has a lengthy and complex wavelet which is simplified by wavelet processing (Figure 62-b). This section shows that the reflection character of the bright spot at 1.4 seconds as well as that of the secondary bright spot below 1.55 seconds is simplified. The purpose of automatic gain control is to make the wavelet character more visible at locations other than the amplitude anomaly (bright spot) (Figure 62-d). Thus, the layers that are relatively thin and have low acoustic impedance contrast may be seismically visible. There are two major lobes in figure 62-d. The first one (white lobe) is deflecting to the left, and the second one (black lobe) is deflecting to the right.

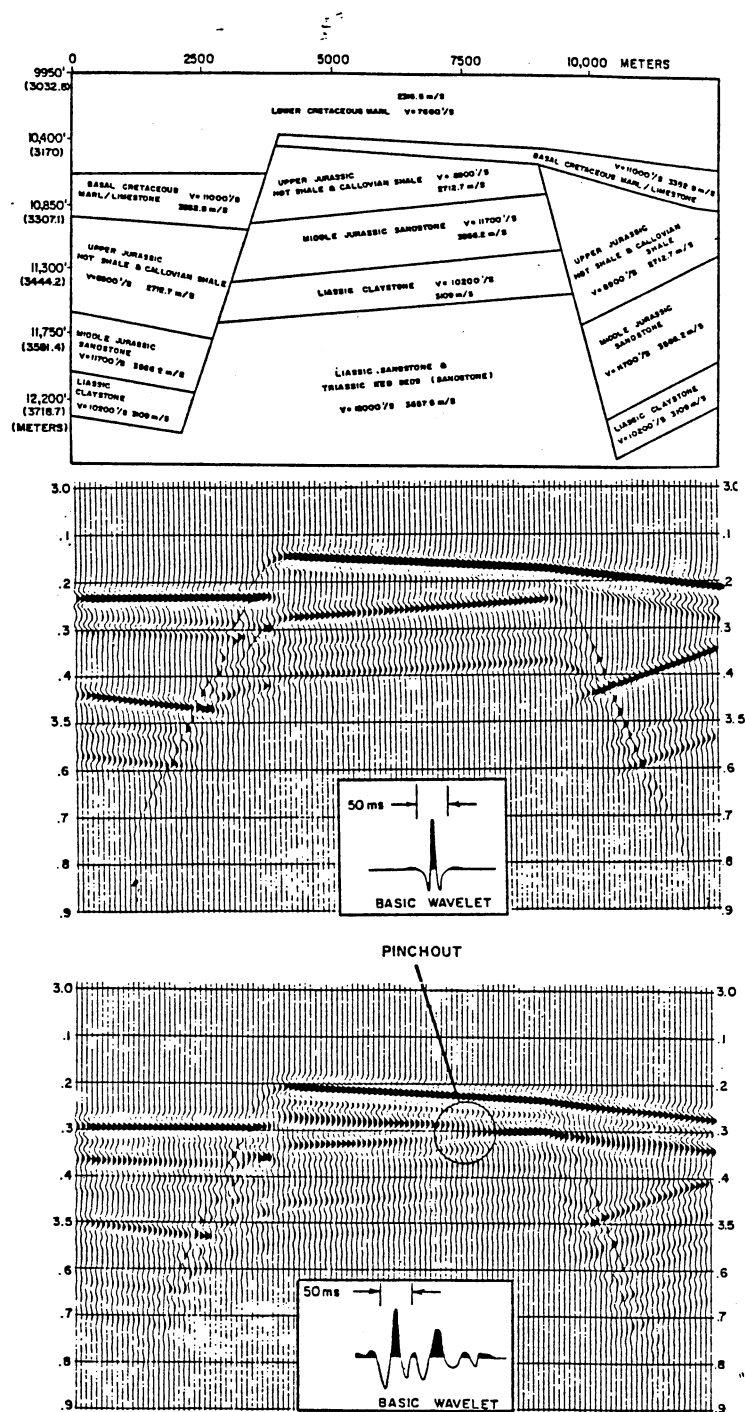


Figure 61. Importance of Choosing the Wavelet
(From Neidel and Poggialiomi, 1977)

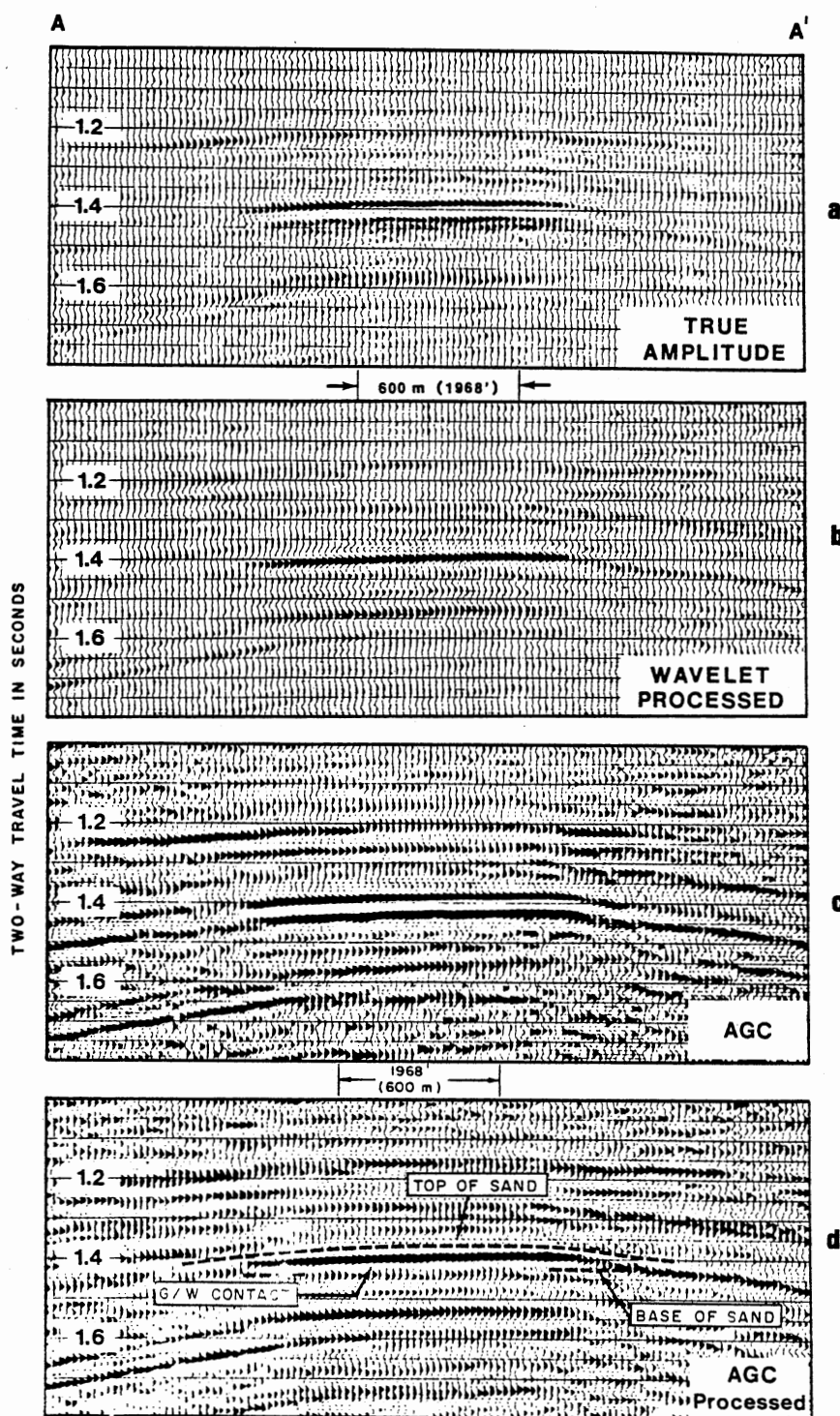


Figure 62. Amplitude and Gain Control Sections
 a-b: Comparison of conventional and wavelet-processed true amplitude sections
 c-d: Conventional and wavelet-processed automatic gain control sections
 (From Schram et. al. 1977)

These lobes are the responses indicating the top and the base of the sand respectively (Schram et al., 1977).

The advantages of wavelet processing are: (1) different wavelets are converted to a basic simple wavelet, (2) a lengthy and complex wavelet is reduced to a short and simple wavelet, (3) better stacked data is obtained because of the improved velocity analysis, (4) a valid relative acoustic impedance section can be generated, (5) borehole acoustic measurements more dependably match seismic measurements, (6) an improved relationship between the seismic section and lithology can be obtained (Hicks, 1983).

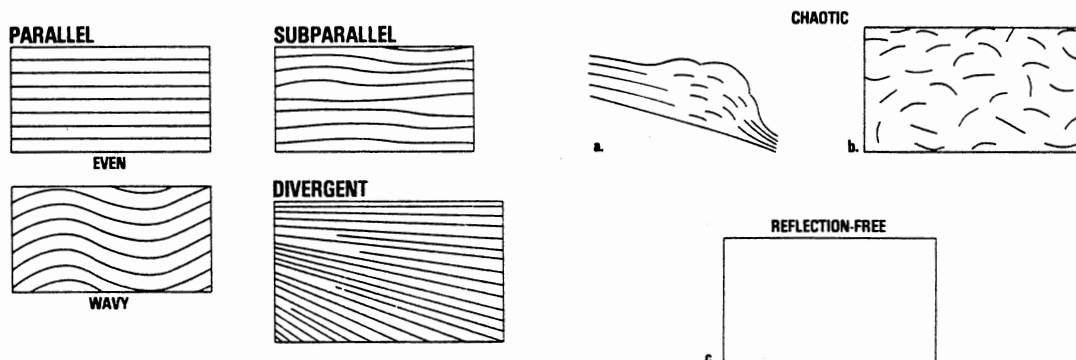
Stratigraphic Interpretation of Seismic Reflection Configurations

Seismic stratigraphic interpretation should contain the distribution of facies and their position within depositional sequences. Depositional facies are bounded by surfaces whose origins are inferred from sedimentary structures, bedding characteristics, and textural variations. Seismic stratigraphic interpretation requires geophysical processing techniques to suppress seismic noise. Otherwise, the seismic response of the features is hidden by the noise.

Seismic facies units are the reflection configurations which result from the seismic response to various depositional facies units (seismic facies units). Seismic facies units are groups of seismic reflections whose

configuration, amplitude, frequency, continuity, and interval velocity differ from adjacent reflection groups.

Major groups of reflection configurations are parallel, subparallel, divergent, chaotic, reflection-free and prograding (Figure 63). Prograding reflection configurations can be subdivided into sigmoid, oblique, complex sigmoid-oblique, shingled, and hummocky clinoform configurations (Mitchum et al., 1977). The interval velocity contains information about fluid content, gross lithology, and lateral lithologic variations. A sufficient knowledge of the arrangement of depositional systems and their seismic expressions is important for making an interpretation of variations on the seismic section.



PROGRADING REFLECTION CONFIGURATIONS

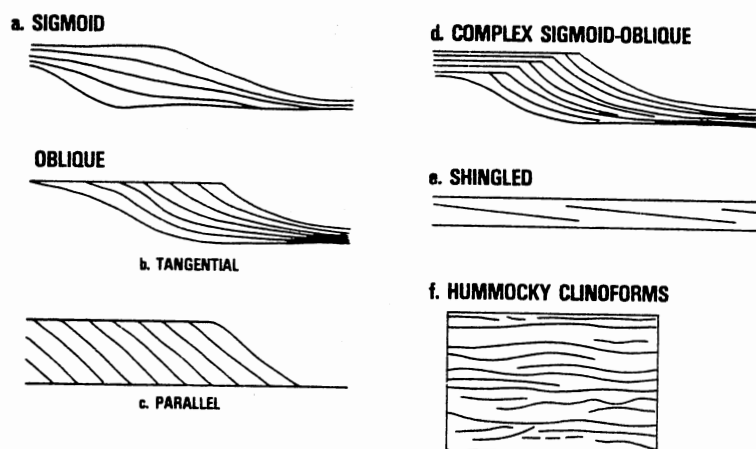


Figure 63. Major Groups of Reflection Configurations
(From Mitchum et. al. 1977)

VITA 2

Yusuf Biyikoglu

Candidate for the Degree of
Master of Science

Thesis: GEOSEISMIC MODELING STUDY OF THE MORROW FORMATION
IN EASTERN DEWEY COUNTY, OKLAHOMA

Major Field: Geology

Biographical:

Personal Data: Born in Ankara, Turkey, November 13, 1949, the son of Kemal and Nadire Biyikoglu. Married to Sadiye on August 24, 1974. Father to Melek and Bilge.

Education: Graduated from the Erzurum High School, Erzurum, Turkey in 1969; received Bachelor of Science degree in Geophysics-Geology in 1974, and Master of Science degree in Geophysics in 1981 from University of Istanbul, Istanbul, Turkey; completed requirements for the Master of Science degree at Oklahoma State University in May, 1988.

Professional Experience: Hydrogeophysicist, State Hydraulic Works, Erzurum, Turkey from June to November 1974; Research Geophysicist, Turkish Navy, Istanbul, Turkey from March 1975 to May 1976; Project Engineer, Chief Engineer, and Site Superintendent, Turkish Iron and Steel Works, Ankara, Turkey from May 1976 to November 1983; Hydrogeologist, MDK Consultants, Inc., Stillwater, Oklahoma since December 1987.

PERIOD	DATE
PENNSYLVANIAN	1944
MISSISSIPPIAN	1944
CHESTERIAN	1944

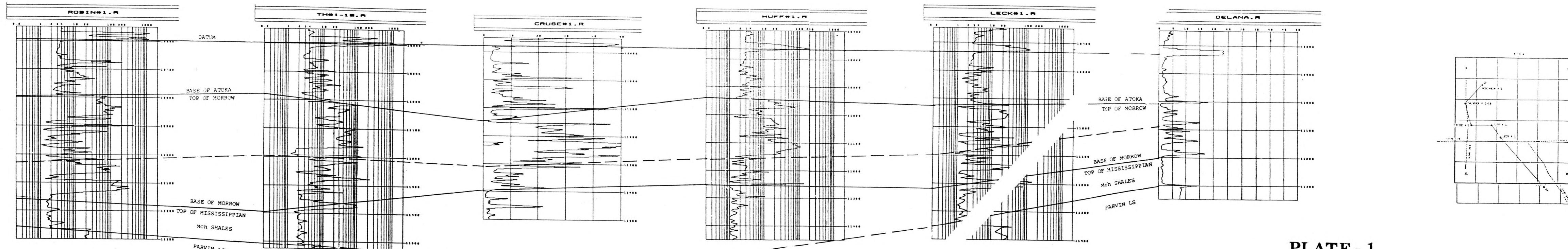


PLATE - 1
STRATIGRAPHIC CROSS SECTION, A1-A2
GEARY FIELD, CANADIAN COUNTY, OK

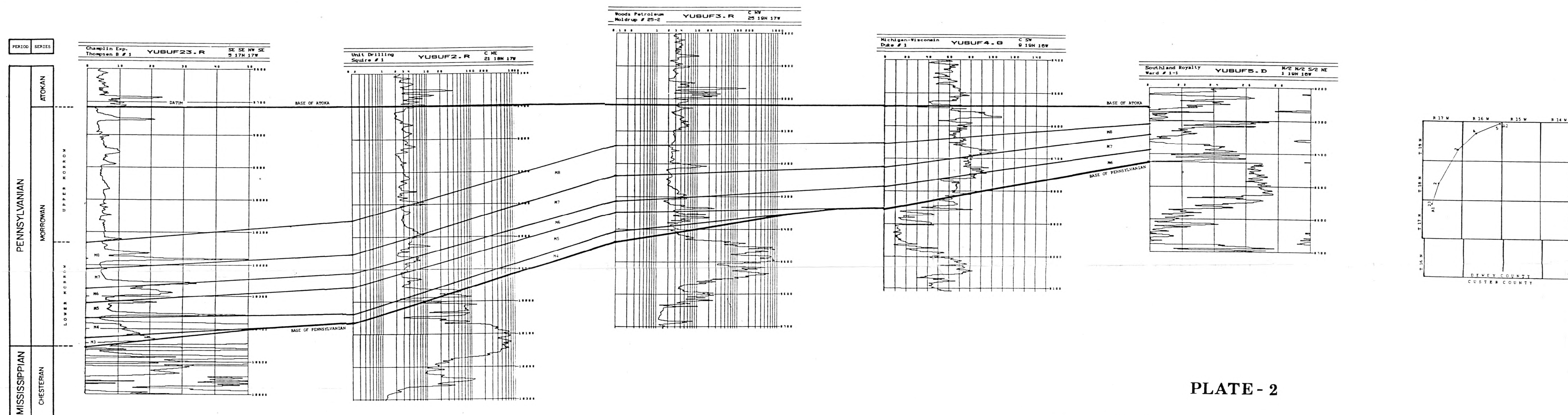
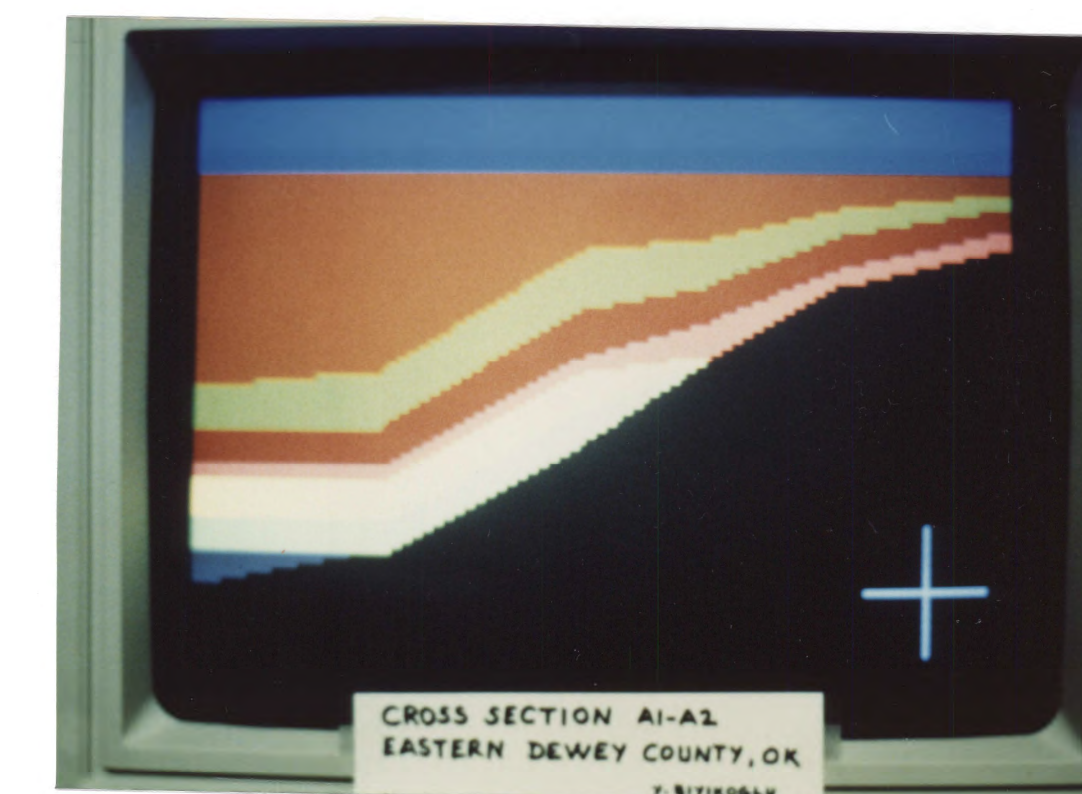


PLATE - 2
STRATIGRAPHIC CROSS SECTION: A1-A2
EASTERN DEWEY COUNTY, OK

MODIFIED FROM BENTKOWSKI, 1985



PERIOD	DATE
PENNSYLVANIAN	1944
MISSISSIPPIAN	1944
CHESTERIAN	1944

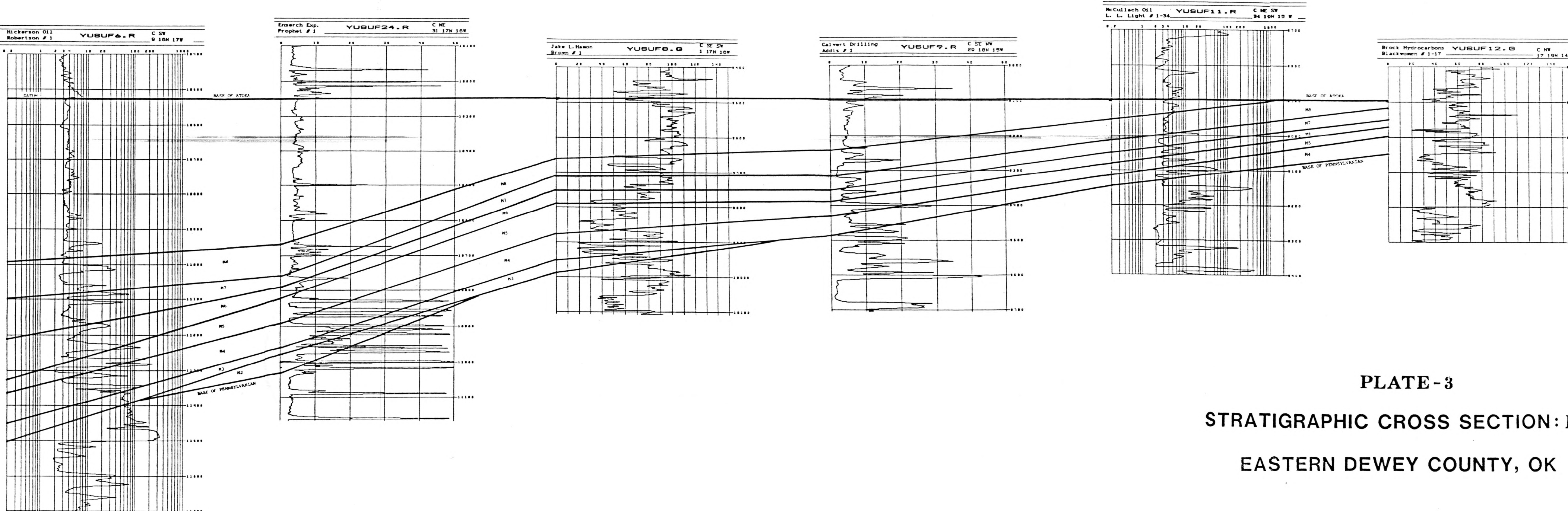
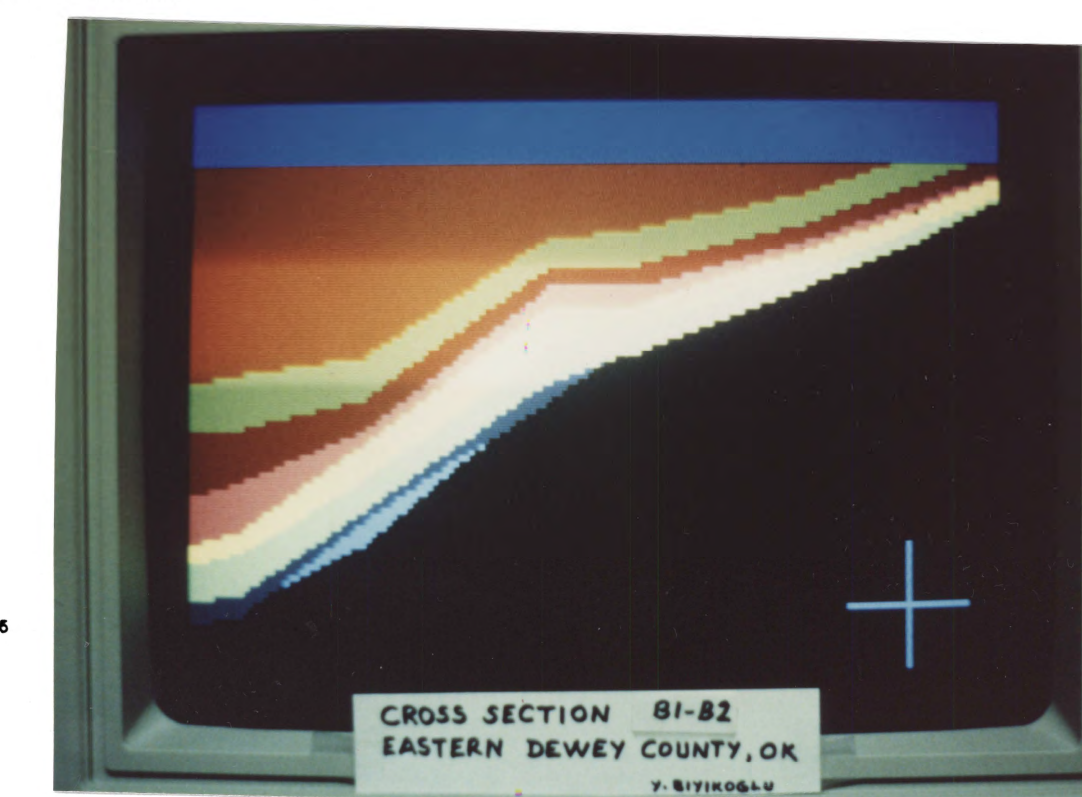


PLATE - 3
STRATIGRAPHIC CROSS SECTION: B1-B2
EASTERN DEWEY COUNTY, OK

MODIFIED FROM BENTKOWSKI, 1985



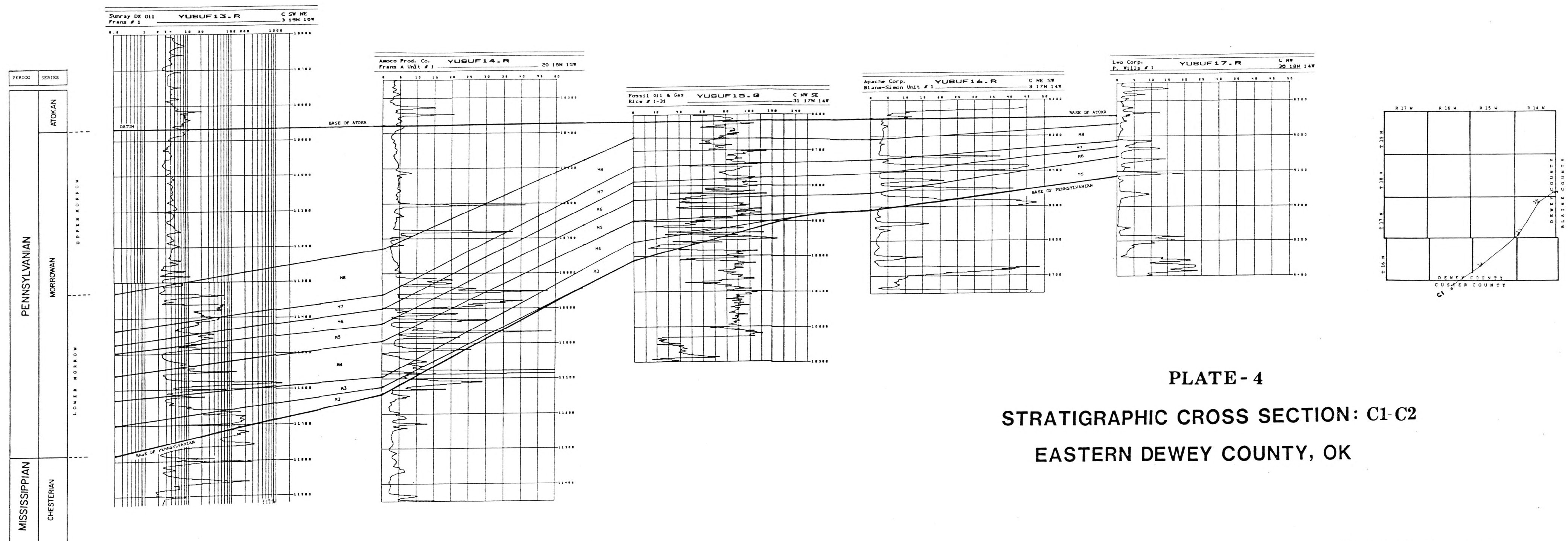


PLATE - 4
STRATIGRAPHIC CROSS SECTION: C1-C2
EASTERN DEWEY COUNTY, OK

MODIFIED FROM BENTKOWSKI, 1988

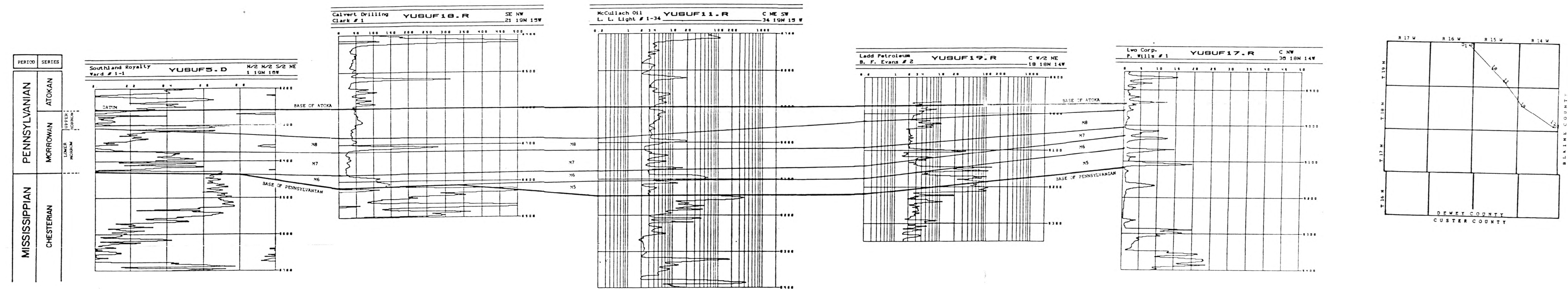
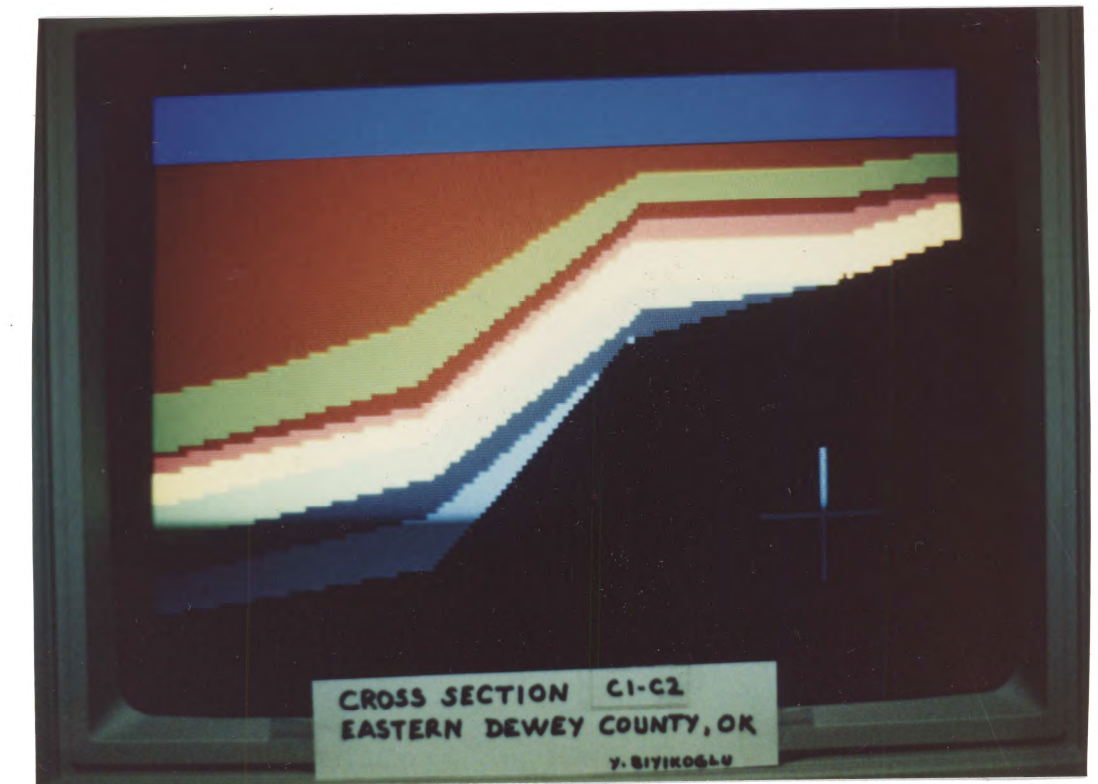


PLATE - 5
STRATIGRAPHIC CROSS SECTION: D1-D2
EASTERN DEWEY COUNTY, OK

MODIFIED FROM BENTKOWSKI, 1988

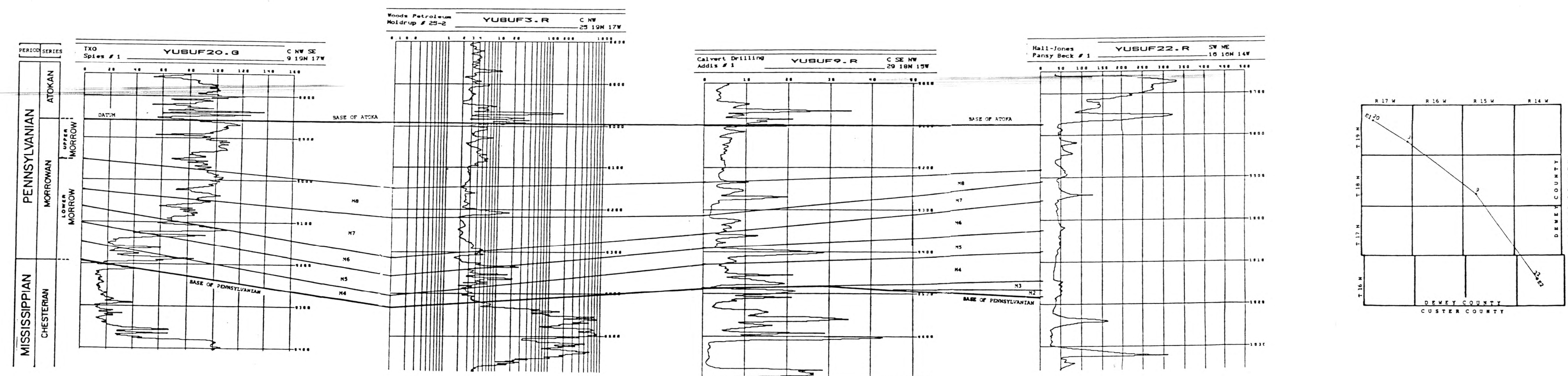
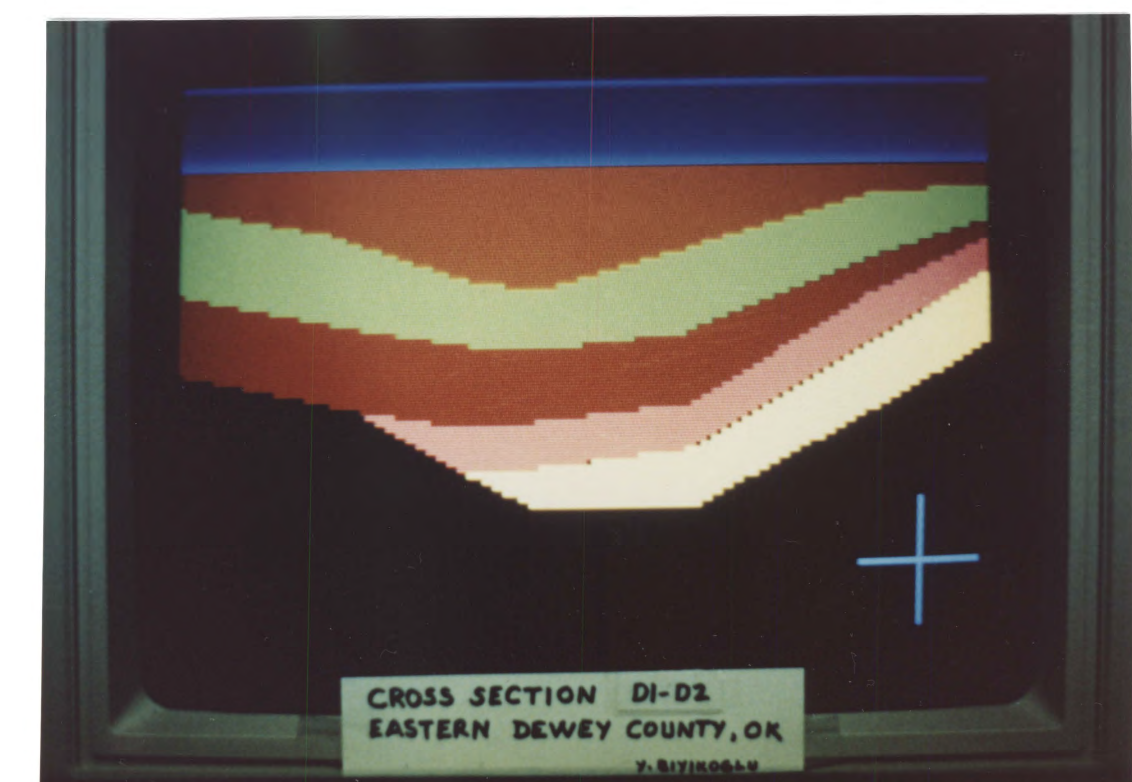
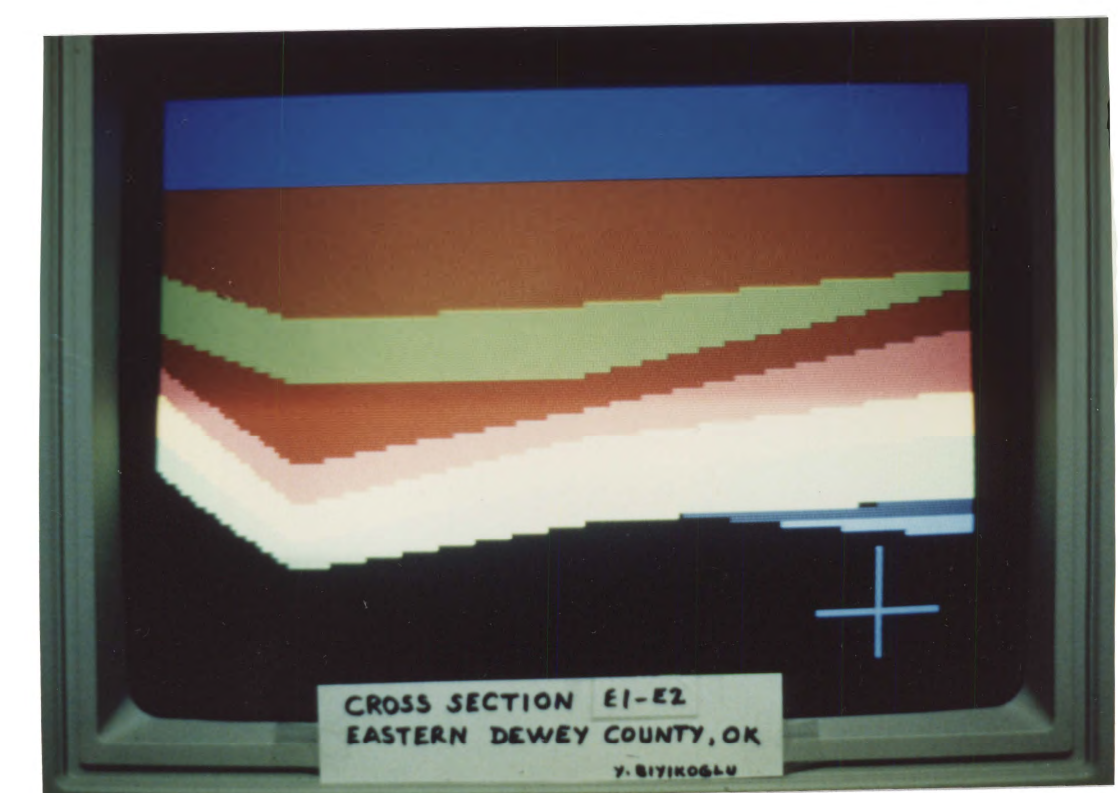


PLATE - 6
STRATIGRAPHIC CROSS SECTION: E1-E2
EASTERN DEWEY COUNTY, OK

MODIFIED FROM BENTKOWSKI, 1988



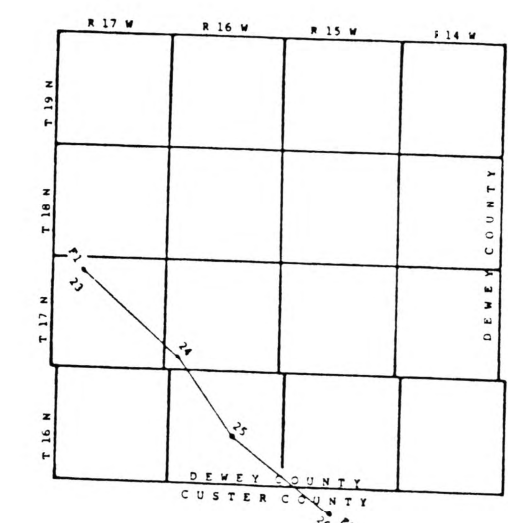
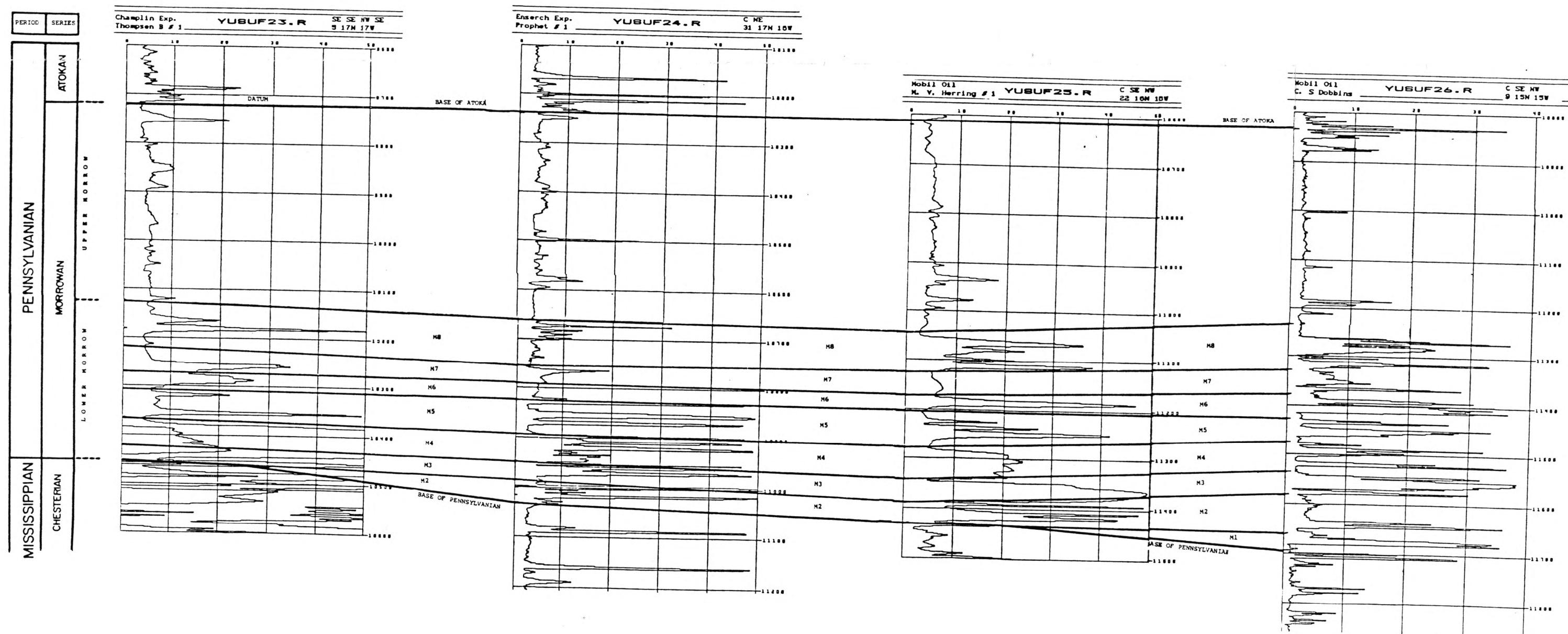


PLATE - 7
STRATIGRAPHIC CROSS SECTION: F1-F2
EASTERN DEWEY COUNTY, OK

MODIFIED FROM BENTKOWSKI, 1986

